UNIVERSITÀ DEGLI STUDI DI MILANO

FACOLTÀ DI MEDICINA E CHIRURGIA

DIPARTIMENTO di FARMACOLOGIA CHEMIOTERAPIA E TOSSICOLOGIA MEDICA

CORSO DI DOTTORATO DI RICERCA IN

FARMACOLOGIA CHEMIOTERAPIA E TOSSICOLOGIA MEDICA
CICLO XXIII

TESI DI DOTTORATO DI RICERCA

Approaches of modulation of therapeutic targets relevant to drug resistance

SETTORE DISCIPLINARE BIO/14

CHIARA GIOMMARELLI
R07808

Tutor
DR. NADIA ZAFFARONI

Coordinatore del dottorato
Prof. ALBERTO PANERAI

ANNO ACCADEMICO 2009/2010

Abstract

An emerging anticancer strategy is to identify molecular targets that when inhibited pharmacologically, result in pleiotropic downstream effects on pathways relevant to the malignant phenotype, with particular reference to the development of resistance.

In recent years, the molecular chaperone Hsp90 has emerged as leading example of such a target-specific therapy. Heat-shock proteins are found at increased levels in many solid tumors and haematological malignancies. Their expression may account for the ability of malignant cells to maintain protein homeostasis even in the hostile hypoxic microenvironment of the tumor. Particularly, Hsp90 has emerged as a target for cancer therapy due to its critical roles in retaining the conformation and the function of its client proteins, many of which are associated with cancer pathology. There are 12 HSP90 inhibitors in clinical trials; all have potencies on the order of 7-35 nM in a cell-based assay and half-lives of 1-3 h in the plasma of rodents. These inhibitors may distribute preferentially to the tumors and may have longer half-lives in the tumors than in the plasma, as in the case of 17-AAG and its active metabolite. However, side effects and poor formulability of 17-AAG restricted its potential of clinical application and motivated many groups to synthesize new compounds. The aim of this project is to identify new Hsp90 inhibitors which could overcome the limitations of available inhibitors and exhibit therapeutic advantages in terms of specificity, therapeutic index and antitumor efficacy. Several compounds have been tested during these years, especially a series of mold metabolites of Ascomycetes, structurally belonging to the class of azaphilones, were found to inhibit the heat shock protein Hsp90. In particular, bulgarialactone B was tested for its binding to Hsp90 using surface plasmon resonance and limited proteolysis assays and for its effects on Hsp90 client proteins expression in a series of human tumor cell lines. This compound showed high affinity for Hsp90, interacting with the 90–280 region of the N-terminal domain and down-regulated the Hsp90 clientproteins Raf-1, survivin, Cdk4, Akt, and EGFR. Bulgarialactone B and other natural azaphilones showed antiproliferative activity in a panel of human tumor cell lines; their conversion into semisyntheticderivatives by reaction with primary amines increased the antiproliferative activity. Preliminary results indicated in vivo activity of bulgarialactone B against an ascitic ovarian carcinoma xenograft, thus supporting the therapeutic potential of this novel series of Hsp90 inhibitors.

Moreover, to identify favourable interactions between Hsp90 inhibitors and target-specific agents, combinations between curcumin and two well-known HDAC inhibitors (vorinostat and panobinostat), have been tested. Curcumin, a natural polyphenol, has been described to exhibit effects on signaling pathways, leading to induction of apoptosis. In this study, we observed that curcumin inhibited Hsp90 activity causing depletion of client proteins implicated in survival pathways. Based on this observation, the study was designed to investigate the cellular effects of curcumin combination with the pan- HDAC inhibitors, vorinostat and panobinostat, which induce hyperacetylation of Hsp90, resulting in inhibition of its chaperone function. The results showed that, at subtoxic concentrations, curcumin markedly sensitized tumor cells to vorinostat- and panobinostat-induced growth inhibition and apoptosis. The sensitization was associated with persistent depletion of Hsp90 client proteins (EGFR, Raf-1, Akt, and survivin). In conclusion, our findings document a novel mechanism of action of curcumin and support the therapeutic potential of curcumin/HDAC inhibitors combination, because the synergistic interaction was observed at pharmacologically achievable concentrations, which were ineffective when each drug was used alone.

Another new therapeutic target is GGT (gamma-glutamyl transferase), the interest in this enzyme is related to recent evidence supporting that it is implicated in tumor progression and in drug resistance to stress-inducing agents (i.e. platinum compounds). The extracellular γ-glutamyltransferase-mediated metabolism of glutathione has been implicated in prooxidant events which may have impact on cellular functions including drug resistance. Therefore the objective of this approach was to investigate the role of GGT in response to various stress-inducing agents. The study was performed in two GGT-transfected melanoma clones to explore the hypothesis that GGT expression in tumour cells is implicated in modulation of cell behaviour under stress conditions. Our results show that GGT-overexpression in melanoma cells was associated with resistance to oxidative stress produced by prooxidant agents such as hydrogen peroxide and ascorbic acid. In GGT-overexpressing cells, ability to tolerate oxidative stress was evidenced by the presence of a moderate level of ROS and lack of DNA damage response following treatment with H2O2. Cellular response to oxidative stress induced by ascorbic acid was detectable only in the clone with low GGT activity which also exhibited an increased susceptibility to apoptosis. The increased resistance of the GGT-overexpressing clone was not related to intracellular GSH content but rather to the increased

expression of catalase and to a reduced efficiency of iron-mediated formation of toxic free radicals. Taken together, these findings are consistent with a contribution of GGT in the mechanisms of drug resistance, because induction of oxidative stress is a relevant event in the apoptotic response to cytotoxic agents.

Again, in an attempt to develop novel strategies for overcoming the mechanisms of cellular protection against oxidative stress, we have explored the efficacy of the combination of two prooxidant agents in the two human melanoma cell clones differently expressing GGT. The γ-glutamyltransferase-overexpressing clone exhibited a low susceptibility to arsenic trioxide-induced apoptosis, associated with low reactive oxygen species induction and increased catalase activity. The combination of arsenic trioxide with subtoxic concentrations of ascorbic acid resulted in a sensitization to apoptotic cell death. The expression of protective mechanisms, in particular catalase activity, accounted for the behavior of the resistant clone. The sensitization achieved by the combination was associated with a cellular response involving the ASK1/p38 axis, which is implicated in the regulation of catalase expression and the activation of apoptotic signals. In conclusion, the results of our study provide evidence that a rational combination of prooxidant agents may be effective in overcoming cellular tolerance to oxidative stress.

Moreover, as a number of recent observations have suggested a potential role for membrane-bound gammaglutamyltransferase (GGT) in tumor progression through redox interactions leading to production of reactive oxygen species, we performed a study to evaluate whether such pro-oxidant activity of GGT can promote oxidative DNA damage, thus contributing to cancer genomic instability. Human GGT-transfected melanoma cells were studied, and DNA damage was measured by using the alkaline comet assay. Our results indicate that higher levels of GGT activity are associated with higher levels of background DNA damage and oxidized bases. This association cannot be explained by differences in cell cycle distribution or apoptotic rates. GGT-over-expressing cells also presented with a markedly higher glucose uptake, a phenomenon potentially leading to higher metabolic rate and oxidative DNA damage. Anyway, when GGT-over-expressing cells were incubated in the presence of GGT substrates and a source of catalytic iron, increased levels of DNA damage and oxidized bases were observed, an effect completely prevented in the presence of GGT inhibitors or various antioxidants. The findings reported indicate that GGT activity is able to promote iron-

dependent DNA oxidative damage, thus potentially representing an important mechanism in initiation/progression of neoplastic transformation.

Index

Introduction

The resistance of many types of cancer to chemotherapies represents the major hurdle in successful cancer treatment. Cancer cells can escape the toxic effect of most commonly used drugs despite their different chemical structure and intracellular targets. The mechanisms underlying the failure of chemotherapeutic drugs have been well studied. Activation of survival/antiapoptotic pathways is a common feature of cancer cells that converge in the development of cellular resistance to cytotoxic agents. The advent of drugs targeting tumor-associated prosurvival alterations of cancer cells has changed the interest of antitumor drug development from cytotoxic drugs to target-specific agents. Although single-agent therapy with molecularly targeted agents has shown limited success in tumor growth control, a promising strategy is represented by the development of rational combinations of target-specific agents and conventional antitumor drugs. The available evidence supports the interest of rationally designed approaches to enhance the efficacy of conventional antitumor treatments through the inhibition of survival pathways and the notion that the concomitant targeting of multiple pathways may be a successful strategy to deal with tumor heterogeneity and to overcome drug resistance of tumor cells [1].

The survival pathways implicated in cellular response to drug treatment are primarily PI3K/Akt and Ras/MAPK, which also mediate the signalling activated by growth factors and play a role in the regulation of critical processes including cell proliferation, metabolism, apoptosis and angiogenesis.

Targeting Hsp90, which acts as a molecular chaperone for survival factors including Akt, may have the potential advantage to simultaneously block multiple oncogenic pathways.

Cancer cells use the HSP90 chaperone machinery to protect an array of mutated and over expressed oncoproteins from misfolding and degradation. Therefore, HSP90 is recognized as a crucial facilitator of oncogene addiction and cancer cell survival. In the past 5 years, the complex nature of HSP90 regulation and the many ways in which it participates in cell physiology have been clarified. Considerable progress has been made in understanding the

dynamic conformational flexibility of HSP90 and in recognizing the contribution made by post-translational modifications to the regulation of the HSP90 chaperone machine.

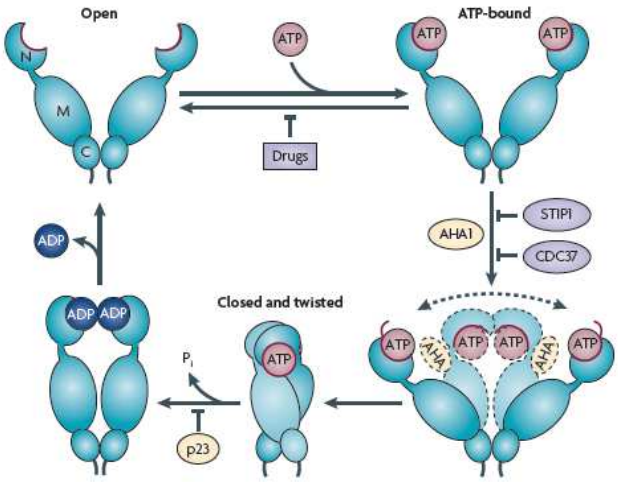

C, carboxy-terminal domain;

M, middle domain;

Pi, inorganic phosphate

Current models propose that ATP binding and hydrolysis, as well as a precisely sequenced interaction with an array of co-chaperones, subtly shift the conformational equilibrium of Hsp90, presumably by lowering the energy barrier between certain conformations, thus providing directionality to the HSP90 cycle. ATP binding to the undimerized (open) amino terminal (N) domain of HSP90 promotes repositioning of a 'lid' segment (red) that leads to transient dimerization of the N domains. Subsequent structural rearrangements result in the 'closed and twisted' conformation of HSP90 that is committed to ATP hydrolysis. Binding of the co-chaperone activator of HSP90 ATPase 1 (AHA1) enhances the rate of ATP hydrolysis-dependent HSP90 cycling by increasing the rate of the conformational alterations that result in the acquisition of ATPase competence. The dashed arrow reflects the difficulty of HSP90 in achieving the ATPase-competent conformation in the absence of AHA1. The co-chaperones STIP1 (also known as p60HOP) and cell division cycle 37 homologue (CDC37), and N domain-binding HSP90 inhibitors, exert an opposite effect to that of AHA1 by preventing the initial structural changes necessary for N domain dimerization. Prostaglandin E synthase 3 (PTGES3; also known as p23) slows the ATPase cycle by stabilizing the closed conformation that is committed to ATP hydrolysis [2].

HSP90 inhibitors currently under clinical evaluation interact with the N domain ATP-binding pocket, prevent ATP binding and stop the chaperone cycle, leading to client protein degradation. There are now 13 HSP90 inhibitors undergoing clinical evaluation, and 23 active HSP90 inhibitor oncology trials. Although there are currently no approved HSP90-targeted drugs, there has been considerable progress on several fronts, and potential routes to approval are becoming apparent. One important advance has been in the drugs themselves. 17-AAG is undergoing Phase III evaluation with an improved formulation that overcomes several toxicities that were common to earlier trials. At the same time, several chemically distinct HSP90 inhibitors with improved properties, including oral biological availability, have recently entered the clinic or will soon undergo clinical evaluation. A second area of advance is in choosing the appropriate indication. Recent preclinical and disease-specific clinical studies have illuminated some key points to consider in the further development of HSP90 inhibitors. Optimal development of HSP90-directed therapeutics will depend also on synthesizing information gained from careful genetic analysis of primary and metastatic tumours with an understanding of the unique environmental context in which the tumour is thriving at the expense of the host.

Pathways involved in ROS-adaptive response may also play a critical role in protecting cells against cytotoxic effects of anticancer agents, thus supporting the hypothesis of a correlation between adaptation/resistance to oxidative stress and resistance to anticancer drugs. One of the major aims is thus to highlight the adaptive mechanisms and their interplay in the intricate connection between oncogenic signaling, oxidative stress, and chemoresistance. Clarification of these mechanisms has tremendous application potential, in terms of developing novel molecular-targeted anticancer therapies and innovative strategies for rational combination of these agents with chemotherapeutic or tumor-specific biologic drugs [3].

A number of recent observations have suggested a potential role for membrane-bound gamma-glutamyltransferase (GGT) in tumor progression and appearance of more aggressive and resistant phenotypes, through redox interactions leading to production of reactive oxygen

species. γ-Glutamyltransferase (GGT) shows a dysregulated expression in several tumour types, but its role in malignant behaviour and tumour progression is still a matter of investigation.

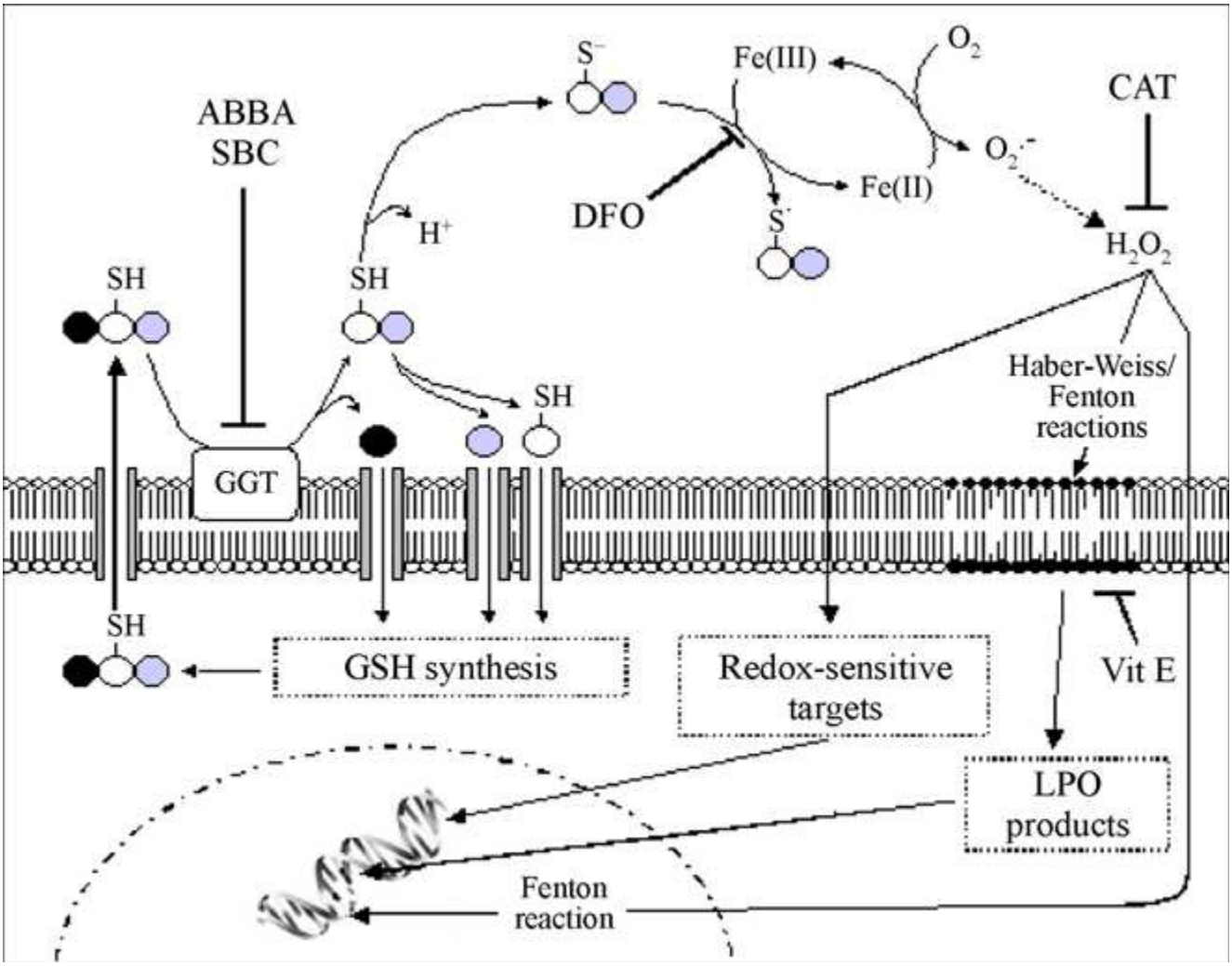

The increased cell resistance against pro-oxidant drugs and other potentially lethal oxidant challenges was generally interpreted as a result of GGT-dependent facilitation of cysteine uptake, a factor favouring the increase of intracellular antioxidant GSH. However, recent studies have documented that GGT-mediated metabolism of extracellular GSH in the presence of extracellular transition metal ions can also exert pro-oxidant effects at the membrane surface level, with generation of reactive oxygen species (ROS). This phenomenon is explained with the high reactivity of GGT-product cysteinyl-glycine, which is in fact able to reduce extracellular transition metal cations (Fe3+ and others) more efficiently than does GSH itself. Such metal ion ‘redox cycles’ was shown to produce ROS and other

free radicals, i.e. reactive species capable of promoting several intra- and extra-cellular biomolecular effects. On this basis, GGT was suggested to be an additional source of (low levels of) endogenous ROS that could contribute to the "persistent oxidative stress" repeatedly described in genomic instability, carcinogenesis and induction of protective systems involved in detoxification and/or resistance to cytotoxic agents [4].

Aims

Since drug resistance is becoming one of the major causes of anti-cancer therapy failure, new pharmacological approaches are welcoming in order to increase the success in the therapy outcome. Inhibition of HSP90 can lead to the simultaneous degradation of a large number of oncogenic proteins thus this protein has become a target of interest for oncology. A major advantage of HSP90 inhibitors is that attacking several pathways necessary for cancer development, they reduce the ability of the tumor to acquire resistance to any single therapeutic pathway. It has also been proposed that HSP90 occurs in an activated form in cancer cells, whereas in normal somatic cells only the latent form is found. This has given rise to the hypothesis that HSP90 inhibitors could be designed to selectively target the activated form and thus more specifically target cancer cells.

However, side effects and poor formulability of currently available Hsp90 inhibitors restricted their potential of clinical application and motivated many groups to synthesize new compounds. Given such a background our aim was to:

1. identify new Hsp90 inhibitors which could overcome the limitations of available inhibitors and exhibit therapeutic advantages in terms of specificity, therapeutic index and antitumor efficacy,
2. identify new drug combinations between Hsp90 inhibitor and conventional therapy to overcome the limitations of drug resistance

Another critical feature of the molecular mechanisms implicated in the drug resistance phenomenon is the oxidative stress balance. A complex intracellular redox buffering network is used by cells to adapt and protect against the dangerous effects of oxidative stress. However, pathways involved in ROS-adaptive response may also play a critical role in protecting cells against cytotoxic effects of anticancer agents, thus supporting the hypothesis of a correlation between adaptation/resistance to oxidative stress and resistance to anticancer drugs. Gamma-glutamyltransferase (GGT) is a key enzyme involved in glutathione metabolism and whose expression is often significantly increased in human malignancies. In

the past years, several studies focused on the possible role of GGT in tumor progression, invasion and drug resistance. The involvement of a pro-oxidant activity of GGT, besides its early recognized contributions to cellular antioxidant defenses, has been repeatedly documented.

GGT-derived pro-oxidants can modulate important redox-sensitive processes and functions of the cell, with particular reference to its proliferative/apoptotic balance, which has obvious and important implications in tumor progression and drug resistance. Given these findings it could be of interest to focus:

1. the role of GGT-mediated oxidative stress in cancer progression and drug resistance, and possibly identify therapeutic stategies to overcome it,
2. whether the pro-oxidant activity of GGT can promote oxidative DNA damage, thus contributing to cancer genomic instability.

Material and Methods

1. Cell lines and culture conditions

The human ovarian carcinoma cell line IGROV-1, the human melanoma cell line JR8, and the human epithelial carcinoma cell line A431 were routinely grown in RPMI 1640 (Lonza, Vierviers, Belgium), supplemented with 10% (v/v) heat-inactivated fetal bovine serum (GIBCO, Invitrogen, Paisley, UK). The human peritoneal mesothelioma cell line STO was kindly provided by Dr. N. Zaffaroni (IRCCS Istituto Nazionale Tumori, Milan) and grown in 50/50 DMEM-Ham's F12 medium (Lonza, Vierviers, Belgium), supplemented with 10% (v/v) heat-inactivated fetal bovine serum and 2mM L-glutamine (L-Gln). All these cell lines were maintained at 37° C in a 5%/95% CO2/air atmosphere.

Two human melanoma cell clones expressing different GGT activity and obtained as previously described [5] were used. Briefly, the c21/GGT clone and the c21/basal clone expressing high (90.78 ± 3.40 mU/mg of cellular protein) and low (0.34 ± 0.13 mU/mg of cellular protein) GGT activity respectively, were obtained by stable transfection of low-expressing GGT activity Me665/2/21 clone (c21) with the full-length cDNA of human GGT. Cells were routinely grown in RPMI 1640 medium, supplemented with 10% (v/v) heat-inactivated foetal bovine serum, 2 mM L-glutamine (L-Gln) and 0.5 mg/ml G418 (Gibco), at 37 °C in a 5%/95% CO2/air atmosphere.

2. Drugs and treatment conditions

All the compounds tested (the series of mold metabolites of Ascomycetes and their semisyntetic derivatives) were obtained as powders from the laboratory of Prof. Merlini (University of Milan) and freshly prepared dissolving powder in dimethylsulfoxide (DMSO) (BDH Prolabo, Milan, Italy) with following dilution in culture medium. Cells were incubated with these drugs for 6, 24 or 72 h (depending on the assay), at 37° C in culture medium supplemented with 10%(v/v) heat-inactivated fetal bovine serum; drug concentrations used for each assay are reported in the Results section. Panobinostat was synthesized as described in the recent US patent application (6,552,065). Vorinostat was provided by BIOMOL International LP (Plymouth Meeting, PA, USA). Curcumin was provided by Sigma Chemical (St. Louis, MO, USA). Stock solutions of all these drugs (10 mg/ml) were prepared in dimethyl sulfoxide (DMSO) (BDH Prolabo, Milan, Italy) and maintained at -20° C. Before each experiment, drugs were diluted in DMSO and used at the concentrations reported in the Results section. 17-AAG was obtained from InvivoGen (San Diego, USA) and it was provided as a

stock solution (5 mM) that we freshly diluted in culture medium before each experiment. Bortezomib was also stocked in 10 mg/ml DMSO solutions, but dilutions were freshly prepared in sterile water. Experiments were performed by incubating cells with drugs for 4, 24, or 72 h at 37° C in culture medium supplemented with 10% (v/v) heat inactivated foetal bovine serum.

Experiments with hydrogen peroxide (H2O2, 3% solution in water; OLCELLI Farmaceutici, Italy), ascorbic acid (AA,1000 mg/5 ml; S.A.L.F., Italy) and arsenic trioxide (As2O3, solutions used for each experiment were freshly prepared following dilution in sterile/distilled water, using a DMSO stock solution of 1 mg/ml (5.05 mM) stored at -20°C) were performed by incubating cells for 2 h at 37° C in RPMI 1640 medium supplemented with 10% (v/v) heat-inactivated foetal calf serum. Cells were then washed and maintained in culture medium for 24 or 72 hours depending on the assay. The exposure time (2 h) was chosen to avoid a marked cytotoxicity of arsenic trioxide and to allow the investigation of drug interaction. In a separate set of experiments, incubations with AA were performed in the presence of glutathione (GSH, 0.5 mmol/L) and glycyl-glycine (glygly, 20 mmol/L), in order to achieve full activation of GGT. Some experiments were performed in the presence of the iron chelators deferoxamine mesylate (DFO; 500 μM) and 2, 2'-bipyridyl (BIP; 500 μM) and the antioxidant catalase (200 U/ml).

For basal levels of DNA damage, cells were harvested 24 h after seeding. Where indicated, the GGT competitive inhibitor l-2-amino-4-boronobutanoic acid (20 μM; ABBA) was sterile filtered and added to incubation media. ABBA was kindly provided by Dr. R.E. London (Natl. Inst. Environ. Health Sci., NC, USA); in preliminary experiments a 20 μM concentration of ABBA caused a strong inhibition of GGT activity but no significant effects on cell proliferation (data not shown). For stimulation of GGT activity, complete culture medium was replaced with RPMI medium containing GSH (2 mmol/L), ADP-chelated FeCl3 (2–0.2 mmol/L) and glycyl-glycine (20 mmol/L). Incubations were started by adding ADP-Fe3+ to incubation mixtures, in the presence or absence of glycyl-glycine. The latter served as acceptor for transpeptidation and was added to stimulate GGT activity. Incubations were performed for 60 min at 37 ◦C in a 5%/95% CO2/air atmosphere. At the end of this time, cells were washed two times and harvested for comet assay. In separate sets of experiments, inhibition of GGT activity was obtained by adding to incubation mixtures GGT competitive inhibitors serine/boric acid (20/20mM) complex (SBC) or ABBA (20 μM). Where indicated, soluble GGT

(100mU/mL), deferoxamine mesylate (DFO; 3 mM), erythrocyte CuZn/SOD (500 U/mL), thymolfree liver catalase (400 U/mL), α-tocopherol (200 μmol/L), butylated hydroxytoluene (BHT; 200 μmol/L) or Trolox C (1 mmol/L) were added to incubation mixtures.

3. Anti-proliferative assay

Cell sensitivity to all the tested compounds was determined by a growth inhibition assay. Briefly, cells were seeded in 12-well plates (50,000 or 40,000 cells/well, depending on the cell line), 24 h before experiments. Cells were exposed to the drugs for 72 h to allow approximately three replications in the control cells. In a separate set of experiments, after 24 h of treatment, cells were incubated in drug-free medium for 72 h. Cell sensitivity to hydrogen peroxide, ascorbic acid and arsenic trioxide was determined after 2 h of exposition to the drugs. Then cells were washed, medium was changed, and cultures were grown up to 72 h.

Adherent cells were then trypsinized and counted with a cell counter (Beckam Coulter, Fullerton, CA, USA). IC50 values, derived from dose–response curves, were defined as drug concentrations required for 50% inhibition of cell growth.

4. Protein expression analysis

Total cell lysates were prepared rinsing cells twice with ice-cold PBS supplemented with 0.1 mM sodium orthovanadate, then lysing them in hot sample buffer as previously described [23]. After determination of protein concentration (BCA Protein Assay Reagent, Pierce, Thermo Fisher Scientific, Rockford, IL, USA), whole-cell extracts were separated by SDS polyacrylamide gel electrophoresis (PAGE) and transferred onto nitrocellulose membranes. Detection of proteins was accomplished using horseradish peroxidase-conjugated secondary antibodies and a chemiluminescence reagent purchased through Amersham Biosciences (Rockford, IL). Primary antibodies used in this study are: anti-Raf-1 (sc-133) and anti-Cdk4 (sc-601) (Santa Cruz Biotechnology, CA, USA), anti-EGFR (Upstate Biotechnology, Millipore, Billerica, MA,USA), anti-Survivin and anti-p23 and anti-Hsc70 (Abcam,Cambridge, UK), anti-Akt (Transduction Laboratories,Lexington, USA), anti-PARP-1 (Calbiochem, MerckChemicals, Nottingham, UK), anti-Cleaved Caspase-3 (Asp175) (Cell Signaling Technology, Inc., MA, USA), anti-p53 (Dako, Glostrup, Denmark), anti-Bcl-2 (Dako, Denmark), anti-Bax (BD Pharmingen, USA), anti-γ-H2AX (Upstate Biotechnology, USA), anti-RPA-2 (NeoMarker, USA), anti-cytochrome C (BD Pharmingen), anti-

phospho-p53(Ser15) (Cell Signaling Technology, USA) anti-RPA-2 (NeoMarker, Thermo Fisher Scientific, Fremont, CA, USA), anti-cytochrome C (BD Pharmingen), anti-phospho-p53(Ser15), anti-phospho-p38 (Thr180/Tyr182) and anti-phospho-ASK1 (Thr845) (Cell Signaling Technology, Danvers, MA, USA), anti-LC3 B I/II (Abcam, Cambridge, UK) anti-Actin and anti-Tubulin (Sigma Chemical Co., St. Louis, MO, USA). Quantification of western blot analyses was obtained by Image Quant 5.2 program.

For determination of cytochrome C release from mitochondria, melanoma cells were exposed to equitoxic concentrations of arsenic trioxide (1 μM and 5 μM for c21/basal and c21/GGT, respectively) and ascorbic acid (0.03 mM and 0.06 mM, respectively), alone or in combination, for 2 h. Floating and adherent cells were harvested and cytosolic extracts were prepared as described previously. Briefly, to maintain the integrity of mitochondria, cells were disrupted by a Dounce homogenizer (30 strokes) in ice-cold lysis buffer (20 mM HEPES-KOH, pH 7.5, 10 mM KCl, 1.5 mM MgCl2, 1 mM EDTA, 1 mM EGTA, 250 mM sucrose, 0.5 mM phenyl-methyl-sulfonyl fluoride, 10 μg/ml leupeptin, 10 μg/ml aprotinin and 10 μg/ml trypsin inhibitor), then samples were centrifuged at 20,000 g for 20 min. Supernatants were stored at –70°C until gel electrophoresis. Cytosolic protein extracts (80 μg) were separated on a 15% SDS-PAGE gel and processed for Western blot analysis.

5. Co-immunoprecipitation and immunoblot analysis

Following the designated treatments, cells were lysed in NET buffer [50 mmol/L Tris (pH 7.4), 150 mmol/L sodium chloride, 0.1% NP40, 1 mmol/L phenylmethylsulfonyl fluoride, 1 mmol/L EDTA, 2.5 lg/mL leupeptin, 5 lg/mL aprotinin] first for 30 min on ice and then for 30 min at 4 °C in rotation on a wheel. Nuclear and cellular debris were cleared by centrifugation (10,000g, 10 min, and 4 °C). Total cellular proteins were then quantified using the BCA protein assay. Cell lysates (500 μg) were incubated with the Raf-1 or Hsp90 polyclonal-specific monoclonal antibodies (Santa Cruz Biotechnology Inc., CA, USA) for 2 h at 4 °C. Protein A-sepharose (Sigma–Aldrich, Germany) (90 μL), previously prepared in TNT solution (20 mM Tris–HCl pH 7.4, 150 mM NaCl, 1% Triton X-100) was added to the lysates and incubated overnight at 4 °C. The immunoprecipitates (separated by centrifugation 15,000g, 2 min, 4 °C) were washed twice in NET buffer and twice in PBS with 1% aprotinin and 1 mmol/L PMSF. Proteins were eluted with the SDS sample loading buffer before the immunoblot analyses with specific antibodies against Raf-1, Hsp90 or Hsp70 (Santa Cruz

Biotechnology Inc., CA, USA), p23 or Hsc70 (Abcam). Quantification of western blot analyses was obtained by Image Quant 5.2 program.

6. Determination of apoptosis

Apoptosis was determined by TUNEL assay (Roche) 72 h after the start of the treatment. The time of exposure to drugs depend on the assay and is indicated in the Results section. Treated cells were fixed in 4% paraformaldehyde (RT, 45 min), washed and resuspended in ice-cold PBS. The in situ cell death detection kit (Roche, Germany) was used according to the manufacturer's instructions, and samples were analyzed by flow cytometry (FACScan; Becton-Dickinson, Franklin Lakes, NJ, USA).

7. Fluorescence polarization assay

GM-FITC, supplied by Invivogen (06C23-MT, California 92192, USA), was previously dissolved in DMSO to obtain 10 mM stock solutions and kept at -20 °C until use. HSP90, purchased from Stressgen (cat. No. SPP-776, Victoria BC, Canada), was previously dissolved in assay buffer (HFB) to form 2.2 μM stock solutions and kept at -80 °C until use. The compounds were previously dissolved in DMSO to obtain stock solutions and kept at -20 °C. The day of experiment, the compounds were prepared by serial dilutions in assay buffer (HFB) containing 20 mM HEPES (K) pH 7.3, 50 mM KCl, 5 mM MgCl2, 20mMNa2MoO4, and 0.01% NP40. Before each use, 0.1 mg/mL bovine gamma globulin and 2 mM DTT were freshly added. Fluorescence polarization (FP) was performed in Opti-Plate™-96F well plates (Perkin Elmer, Zaventem, Belgium) using a plate reader (Wallac Envision 2101 multilabel reader, Perkin Elmer, Zaventem, Belgium) To evaluate the binding affinity of the molecules, 50 μL of the GM-FTC solution (5 nM) were added to 30 nM of HSP90 in the presence of 5 μL of the test compounds at increasing concentrations. The plate was mixed on a shaker at 4 °C for 4 h, and the FP values in mP (millipolarization units) were recorded.

The IC50 values were calculated as the inhibitor concentration where 50% of the tracer is displaced; each data point is the result of the average of triplicate wells, and was determined from a plot using nonlinear least-squares analysis. Curve fitting was performed using Prism GraphPad software program (GraphPad software Inc., San Diego, CA).

8. Surface plasmon resonance analyses

SPR analyses were performed using a Biacore 3000 optical biosensor equipped with research-grade CM5 sensor chips (Biacore AB). Using this platform, two separate recombinant Hsp90 surfaces, a BSA surface and an unmodified reference surface, were prepared for simultaneous analyses. Proteins (100 lg/ml in 10 mM sodium acetate, pH 5.0) were immobilized on individual sensor chip surfaces at a flow rate of 5 μl/min using standard amine-coupling protocols [7] to obtain densities of 8–12 kRU. Compound 2 and radicicol were dissolved in 100% DMSO to obtain 4 mM solutions, and diluted 1:200 (v/v) in PBS (10 mM NaH2PO4, 150 mM NaCl, pH 7.4) to a final DMSO concentration of 0.5%. Compounds concentration series were prepared as twofold dilutions into running buffer: for each sample, the complete binding study was performed using a six-point concentration series, typically spanning 0.05–10 μM, and triplicate aliquots of each compound concentration were dispensed into single-use vials. Included in each analysis were multiple blank samples of running buffer alone [8]. Binding experiments were performed at 25°C, using a flow rate of 50 μL/min, with 60 s monitoring of association and 200 s monitoring of dissociation. Simple interactions were adequately fit to a single-site bimolecular interaction model (A+B =AB), yielding a single KD. Sensorgram elaborations were performed using the Biaevaluation software provided by Biacore AB [9].

9. Limited proteolysis

Limited proteolysis experiments were performed at 37 °C, PBS 0.1% DMSO, at a 3 μM recombinant human Hsp90α concentration using trypsin, chymotrypsin and endoprotease V8 as proteolytic agents; 30 μL of solution were used for each experiment. Binary complexes Hsp90/inhibitor were formed by incubating the protein with a 10:1 M excess of the individual inhibitor at 37°C for 15 min prior to proteolytic enzyme addition. Each complex was digested using a 1:100 (w/w) enzyme to substrate ratio. The extent of the reactions was monitored on a time-course basis by sampling the incubation mixture after 5, 15, and 30 min of digestion. Samples were desalted by ziptip C4 (Millipore) and the proteolytic fragments were analyzed by MALDITOF/MS using a MALDI-MX micro (Waters). In order to optimize sensitivity and accuracy of the mass measurements, three different m/z ranges were explored for each sample: a first range, from m/z 500 to 3,500 was analyzed in reflector mode; the other two ranges, from m/z 3,500 to 20,000 and from m/z 20,000 to 95,000, were analyzed in linear

mode. Each m/z range was calibrated using a suitable peptide or protein mixture. Mass data were elaborated using the Masslynx software (Waters). Preferential hydrolysis sites on Hsp90 under different conditions were identified on the basis of the fragments released during the enzymatic digestions. When comparative experiments were carried out on Hsp90 in the presence or in the absence of inhibitors, differences in the susceptibility of specific cleavage sites were detected, from which protein regions involved in the conformational changes could be inferred [10].

10. Yeast Hsp82 protein expression and purification

Escherichia coli strain BL21-CodonPlus (DE3)-RIL (Stratagene; La Jolla, CA) was transformed with the plasmid pET28-Hsp82/NdeI containing the full-length Hsp82 gene of Saccharomyces cerevisiae, with an N-terminal His6 tag for purification. Transformed cells were selected on LB agar, containing 50 μg/mL kanamycin and 40 μg/mL chloramphenicol, and a preliminary analysis on individual colonies was performed to evaluate their overexpressing ability. A 4 L culture of the clone with the highest Hsp82 expression was grown in the presence of kanamycin until A600 reached 1.2, and then expression of His-tagged Hsp82 was induced by the addition of 1 mM isopropyl-1-thio-b-D-galactopyranoside. Cells were then grown for 3 h and harvested by centrifugation at 7000 rpm for 30 min, at +4 °C. Harvested cells were washed in ice-cold 1X PBS, weighed and then stored at -70 °C. Frozen cells were thawed and then re-suspended and lysed in B-PER_ Bacterial Protein Extraction Reagent (Pierce; Rockford, IL), containing phenylmethylsulfonyl fluoride (PMSF). The lysate was centrifuged at 27,000g for 15 min at +4 °C and supernatant was ultra-centrifuged at 100,000g for 45 min at +4 °C. Supernatant was then loaded, at a flow rate of 1 mL/min, onto a Ni–NTA column (HisTrap™ HP Columns, GE Healthcare) prepacked with NiSepharose and activated according to manufacturer's instructions. The column was washed with potassium phosphate buffer (pH 7.4) containing 30 mM imidazole. A linear gradient of imidazole in potassium phosphate buffer was finally applied to the column for Hsp82 elution. The collected fractions were pooled, then subjected to gel filtration on Superdex 200 resin (GE Healthcare) in 20 mM Tris–HCl, pH 7.5, containing 300 mM KCl and 1 mM EDTA, and finally stored at -80 °C in the presence of glycerol (10% final concentration).

11. Determination of yeast Hsp90 ATPase activity

Inhibition of the intrinsic ATPase activity of full-length recombinant yeast Hsp82 was measured by a modified enzymatically coupled ATPase assay, in which the amount of inorganic phosphate released by HSP90-dependent ATP hydrolysis is utilized by maltose phosphorylase, which phosphorylates maltose and then cleaves the disaccharide to produce glucose and glucose-1-phosphate. Glucose is a substrate for glucose oxidase, which uses atmospheric oxygen to produce gluconolactone and hydrogen peroxide. Finally, horseradish peroxidase consumes hydrogen peroxide by the oxidation of the colorless N-acetyl-3, 7-dihydroxyphenoxazine (Amplex Red) to provide the Resorufin product, which has unique absorption spectra at 563 nm. For every molecule of ATP, that is, hydrolyzed by yeast Hsp90, one molecule of Amplex Red is ultimately oxidized to Resorufin. Inhibition of yeast Hsp82 ATPase activity by test compounds was tested, following 3 h incubation in the presence of 500 Lm ATP, in 96-well cell culture cluster clear plates by using a commercially available kit (PiPer™ Phosphate Assay kit; Molecular Probes, Eugene, OR), according to manufacturer's instructions. To determine IC50 values, several appropriate concentrations of test compounds were evaluated depending on their relative potency. Each assay plate was run with a positive control which consisted of three wells containing the well-known Hsp90 inhibitor 17-DMAG, at a final concentration of 20 μM.

12. Animals

Experiments were carried out using female athymic Swiss nude mice, 8–10 weeks old (Charles River, Calco, Italy). Mice were main- tained in laminar flow rooms keeping temperature and humidity constant. Mice had free access to food and water. Experiments were approved by the Ethics Committee for Animal Experimentation of the Istituto Nazionale Tumori of Milan according to institutional guidelines.

13. Intraperitoneally growing tumor

The human IGROV-1 ovarian carcinoma was adapted to grow ip and maintained by serial ip passages of ascitic cells into healthy mice. Ascitic tumor cells 2.5 x 10^6 in 0.2 mL of saline were ip injected. Mice developed hemorrhagic ascites and diffuse peritoneal carcinomatosis and died by 15–30 days. Survival was the end point of the study and the median day of death (median survival time: MST) was calculated for each group. Antitumor activity was assessed as T/C%, that is, the ratio of MST in

treated over control mice x 100. Treatment started the day after tumor cell injection, delivering 2 ip every day for four days a week for two weeks (qdx4/wx2w) at a dose of 25 mg/kg.

14. Determination of GGT activity

Confluent cell monolayers were harvested with hypotonic lysis buffer (10mM Tris–HCl, pH 7.8) and disrupted by a tight-fitting glass–glass Dounce homogenizer (30 strokes, 4 ◦C). Determination of GGT activity was performed according to Huseby and Strømme [11] using γ-glutamyl-p-nitroanilide as substrate and glycylglycine as transpeptidation acceptor. The amounts of p-nitroaniline formed were measured by reading the absorbance at 405nm and using a molar extinction coefficient of 9200mol/L cm. One unit of GGT activity was defined as 1μmol of substrate transformed/mL/min. The results were expressed as mU/mg protein.

15. Reactive oxygen species (ROS) determination

Intracellular production of ROS was measured using the H2O2-sensitive compound 2′, 7′-dichlorofluorescin diacetate (DCFH-DA, Molecular Probes, Invitrogen Ltd, Paisley, UK). After diffusion into viable cells, DCFH-DA is converted by intracellular esterase to 2′, 7′-dichlorofluorescin (DCFH) which reacts quantitatively with ROS within the cell thus producing the fluorescent dye 2′, 7′-dichlorofluorescin (DCF). The latter remains trapped within the cells and can be measured as an index of intracellular ROS production. Cells were seeded in Petri dishes (100,000 cells/ml) and 24 h after the 2 h treatment with H2O2, arsenic trioxide or/and ascorbic acid (depending on the assay, as explained in the Results section) cells were incubated with DCFH-DA (10 μM, in DMSO) at 37°C for 20 min. Adherent and floating cells were collected and washed twice with phosphate-buffered saline (PBS). DCF fluorescence was detected using a flow cytometer (FACScan, Becton Dickinson, Franklin Lakes, NJ, USA); for each sample 10,000 events were collected.

16. Determination of catalase activity

The Amplex Red Catalase Assay Kit, used for the determination of catalase activity, was purchased from Molecular Probes (Invitrogen Ltd, Paisley, UK). In this assay, catalase first reacts with H2O2 to produce water and oxygen, then the Amplex Red reagent reacts with any unreacted H2O2 in the presence of horseradish peroxidase to produce the highly fluorescent oxidation product, resorufin. Catalase activity was determined 6 and 24 h after 2 h treatment. Briefly, cells were rinsed twice with ice-cold PBS containing 0.1 mM sodium orthovanadate and then lysed in hot sample buffer (0.125 M

Tris-HCL pH 6.8, 25 mM NaF, 1 mM phenyl-methyl-sulphonyl fluoride, 10 μg/ml trypsin inhibitor, 10 μg/ml pepstatin, 5% sodium dodecyl sulphate, 12.5 μg/ml leupeptin and 100 kIU aprotinin) [6]. Catalase activity was determined spectrophotometrically (550 nm) according to manufacturer's instructions and data were normalized to total protein content.

17. Cell cycle analysis

For cell cycle analysis, cells were washed 24 h after drug treatment, fixed in ice-cold 70% ethanol, and stored at –20°C. Subsequently, samples were rehydratated with PBS and cellular DNA was stained with 10 μg/ml propidium iodide in PBS, containing ribonuclease A (RNase A) (66 kU/ml). Cell cycle distributionwas determined by flow cytometry and data were analyzed using the CellQuest® software (Becton Dickinson, Franklin Lakes, NJ, USA); for each sample 40,000 events were collected.

18. Detection of BrdU incorporation in DNA synthesizing cells

Twenty-four hours after drug exposure, cells were treated with 10 μM bromodeoxyuridine (BrdU) for 1 h. Adherent cells were trypsinized and fixed in ice-cold ethanol 70%. Cells were then incubated with 2N HCl for 30 min and resuspended in 1 ml 0.1 M disodiumtetraborate (Na2B4O7*10H2O), for 10 min. Following washing with PBA (PBS containing 1% bovine serum albumin) for 10 min, cells were incubated first with the anti-BrdU antibody (Becton Dickinson, Franklin Lakes, NJ, USA) for 30 min and then with the anti-mouse IgG FITC (Sigma Chemical Co., St. Louis, MO, USA) for 30 min. Cells were washed twice in PBA and resuspended in 1 ml PBS containing propidium iodide (5 μg/ml) and RNase A (66 kU/ml). DNA content was then analyzed with a FACScan flow cytometer.

19. Single-cell gel electrophoresis (comet assay)

DNA damage was measured using the alkaline comet assay as described by Duarte et al. [12]. Briefly, cells were harvested by trypsinisation and suspended in 0.6% low melting point agarose. Eighty microliters of the agarose gel (containing approximately 10^4 cells) were dispensed onto glass microscope slides previously coated with 1% normal melting point agarose. The agarose was allowed to set on ice under a coverslip and the slides left overnight in ice-cold lysis buffer (100mM disodium EDTA, 2.5M NaCl, 10mM Trizma® base, adjusted to pH 10 with NaOH 10M and containing 1% Triton X-100 (v/v) added fresh). Slides were washed with distilledwater and then placed in a horizontal electrophoresis tank containing ice-cold alkaline electrophoresis solution (300mM NaOH, 1mM disodium EDTA) for 20 min to allow DNA unwinding. Electrophoresis was conducted for

20min (30 V, 300mA) at 4 ◦C. Slides were neutralised with 0.4M Tris–HCl, pH 7.5 for 20 min and washed with double-distilled water, then allowed to dry. All procedures were carried out under subdued light to minimise background DNA damage. For staining, slideswere re-hydrated in distilled water, incubated with a freshly made solution of 2.5μg/mL propidium iodide for 20 min, washed again for 30 min and allowed to dry. Comets were visualised with a fluorescence microscope (Leica) at 200× magnification using a 20× objective. Images were captured by an on-line Leica DFC320 camera and subsequently analyzed with the CometScoreTM software (TriTek Corporation).

A total of 100 cells were analyzed per sample, 50 per duplicate slide. The percentage of DNA in the tail of the comet (% tail DNA) was calculated for each cell by the CometScoreTM software.

20. Fpg-modified comet assay

Oxidative DNA damage was evaluated by Fpg-modified comet assay as previously described [13]. This assay uses the formamidopyrimidine-DNA-glycosylase (Fpg) enzyme (New England Biolabs), a glycolase that recognizes and specifically cleaves the oxidized bases principally 8-oxoguanine from DNA, producing apurinic sites which are then converted into breaks by the associated AP-endonuclease activity. These additional breaks can be detected by comet assay and give a measure of oxidative DNA damage. The comet assay was carried out as described above, with the exception that after lysis the slideswerewashed three times for 15 min with the enzyme reaction buffer (40mM HEPES, 0.1M KCl, 0.5mM EDTA, 0.2mg/mL bovine serum albumin, adjusted to pH 8 with KOH 1 M). After this time, slides were incubated with 100 μL of Fpg enzyme. Enzyme dilution (1:103 from a stock solution of 8000 U/mL) was prepared just before use, according to the manufacturer's instructions. Control slideswere treated with 100 μL of enzyme reaction buffer only. Slides were placed horizontally in humidity chamber at 37 ◦C for 45 min. DNA unwinding and electrophoresis was then performed as described above.

21. Glucose uptake

For determination of glucose uptake complete culture medium was replaced with Hanks' buffer, pH 7.4, containing 2μCi of 2-deoxy-D-[1-3H]glucose (Amersham Biosciences, UK), and cells were incubated for 30min at 37 ◦C in a 5%/95% CO2/air atmosphere. GLUT inhibitor cytochalasin B (20μM) was added to a subset of wells to determine specific carrier-mediated glucose uptake. The medium was then removed and the cells were washed twice with ice-cold PBS. Lysiswas induced by

adding 600μL of 0.1N NaOH. Aliquots of 450μL of lysates were then mixed with a liquid scintillator (Beckman Ready Safe cocktail) and the radioactivity was measured by liquid scintillation counting (Beckman LS-6500 Multi Purpose Scintillation counter). Finally, the remaining part of samples was used for determination of protein content. In a separate set of experiments, c21/GGT cells were pre-treated for 24 h with GGT competitive inhibitor ABBA (20μM) before incubation with radiolabeled glucose. Data are expressed as glucose uptake in the absence of cytochalasin B minus uptake in the presence of cytochalasin B.

22. Other determinations

For GSH determinations, aliquots of incubation mixtures were collected, acidified with 5-sulfosalicylic acid (1%, w/v) and stored to −20 ◦C until GSH determinations that were performed according to Baker et al. [14].

23. Statistical analysis

All the reported values represent the mean ± standard deviation (SD) of at least three independent experiments performed in duplicate. Where necessary, data were statistically compared by t test.

More exhaustive statistical analysis of data was performed, were necessary, by ANOVA, with Newman–Keuls test for multiple comparison.

Results and Discussion

Section A: Hsp90

Chapter A1: Natural and semisynthetic azaphilones as a new scaffold for Hsp90 inhibitors

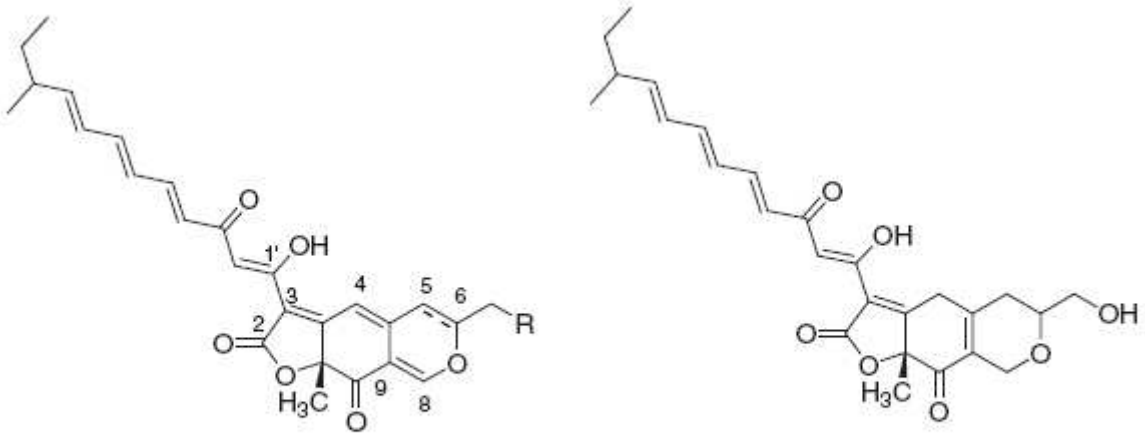

R = H C_5-C_6 single bond Bulgarialactone A (**1**)
R = OH C_5-C_6 single bond Bulgarialactone B (**2**)
R = H C_5-C_6 double bond Bulgarialactone C (**3**)

Bulgarialactone D (**4**)

During a target-oriented screening of natural compounds aimed at stabilizing and enhancing the function of p53, a transcription factor which regulates the cell cycle and thus functions as a tumor suppressor, we found that a fungal metabolite, named bulgarialactone B (2), did not change the wild-type p53 protein level but induced partial down-regulation of the mutant p53, which is known to be stabilized by Hsp90. This result prompted us to investigate the activity of bulgarialactone B as a potential Hsp90 inhibitor. Structurally, bulgarialactone B features a highly oxygenated tricyclic core linked to a 13-C unsaturated chain containing a β-diketone. It is a member of a large group of fungal pigments known as azaphilones, mainly isolated from perfect and imperfect stages of Ascomycetes, such as Aspergillus, Penicillium, Hypoxylon, and Monascus spp.

As a first step of this study, we investigated the cellular and biochemical profile of compound 2.

The antiproliferative assays were performed on a panel of human tumor cell lines following 72 h exposure. The IC50 values of 2, reported in Table 1, indicated variable antiproliferative effects on the tested cell lines in a range of micromolar concentrations.

Successively, compound 2 was tested for its effects on Hsp90 client protein expression in the same cell lines used in the antiproliferative assay (Fig. 1). Following 24-h exposure to a concentration corresponding to IC80 (around 2 X IC50; i.e., ca. 10 μM), the examined client proteins (Raf-1,

survivin, Cdk4, Akt, and EGFR) were down-regulated. The effect was marginal in melanoma JR8 cells. In contrast, protein depletion was almost complete in the ovarian carcinoma cell line, IGROV-1. The p53 protein was partially down-regulated only in A431 cells carrying a mutant p53 protein. This effect was consistent with the stabilization of the mutant form by Hsp90.

Table 1
Antiproliferative activity in different cell lines, ATPase activity inhibition and binding to Hsp90 (IC_{50}, μM ± SD) of azaphilones 1–13

Compd	Antiproliferative activity (μM) Cell lines				Hsp90-ATPase activity inhibition	Binding Hsp90 (FP)
	NCI-H460	A431	JR8	IGROV-1		
1	18.7 ± 0.4	6.87 ± 0.82	11.45 ± 1.71	4.12 ± 0.53	>50	>100
2	50	5.53 ± 0.71	6.42 ± 0.87	4.65 ± 0.64	9.87 ± 0.71	61.7 ± 0.85
4	>50	17.60 ± 1.9	–	–	>50	>100
5	21.3 ± 3.1	1.20 ± 0.11	5.70 ± 0.95	0.80 ± 0.11	14.5 ± 0.93	35.4 ± 1.3
6	30 ± 0.2	7.05 ± 0.89	5.64 ± 0.79	5.08 ± 0.64	26.3 ± 3.5	>100
7	>50	17.77 ± 2.5	30.64 ± 3.9	>30	>50	>100
8	>50	13 0.89	130.89	102.8 8	22.9 ± 3.3	0.27 ± 0.01
9	>50	28.2 ± 3.4	>30	28.2 ± 3.5	9.2 ± 1.2	0.040 ± 0.001
10	>50	>28	>28	>28	>50	>100
11	–	26 ± 3.7	26 ± 3.2	26 ± 3.5	>50	>100
12	>50	>25	–	–	>50	>100
13	>50	>25	–	–	>50	>100

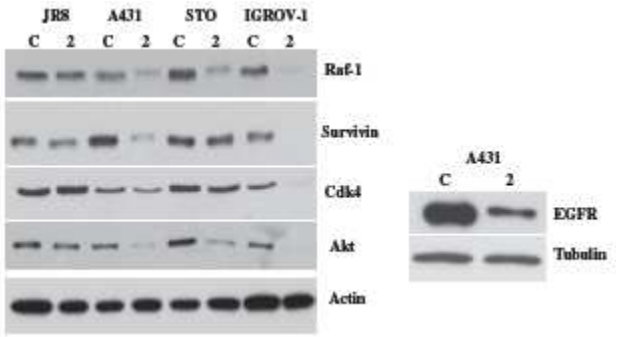

Figure 1. Analysis of Hsp90 client protein levels (survivin, Cdk4, Akt, Raf-1) in tumor cells treated with (2). Total cellular extracts were obtained 24 h after treatment (11 μM, IC_{80}). Actin is shown as a control for protein loading. EGFR levels were analyzed only in A431 cells and tubulin is shown as a control for protein loading.

In an effort to confirm the Hsp90/compound 2 binding and to identify the binding site, we used surface plasmon resonance (SPR) analyses and the limited proteolysis–mass spectrometry technique. SPR allows verifying the affinity of compounds toward the protein, and to assess how they associate with and dissociate from the protein in real time, giving a more detailed view of their interaction with Hsp90. SPR experiments were performed using radicicol (Chart 1), a well-known Hsp90 inhibitor, as a positive control. Our data demonstrated the high affinity of 2 for Hsp90, comparable with that measured for radicicol (Table 2), both in terms of thermodynamic (KD) and kinetic (kd) dissociation constants. The limited proteolysis approach is based on the evidence that exposed, weakly structured, and flexible regions of a protein can be recognized by a proteolytic enzyme. Trypsin, chymotrypsin, and endoprotease V8 were selected as conformational probes in order to provide structural information on different regions of Hsp90. The fragments released from the protein were identified by MALDI-TOF/MS analyses, leading to the assignment of cleavage sites (Table 2).

Table 2
Study of the interaction with Hsp90

Compd	K_D[a] (nM)	k_d[a] (s^{-1})	Protected sites[b]
Radicicol	3.04 ± 0.82	0.011 ± 0.003	75, 94, 215
2	1.30 ± 0.53	0.017 ± 0.82	94, 215, 245, 277

[a] SPR data.
[b] limited proteolysis data.

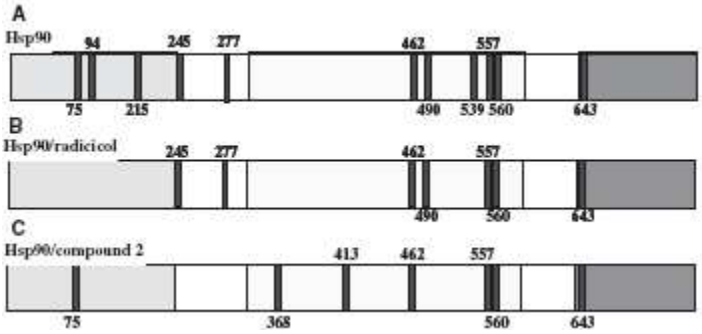

Figure 2. Schematic representation of the results obtained from limited proteolysis experiments on recombinant Hsp90. The preferential cleavage sites detected performing enzymatic digestions on recombinant Hsp90 (A), on the Hsp90/radicicol complex (B), or on the Hsp90/compound 2 complex (C), are in dark gray. The Hsp90 N-terminal domain is highlighted in light gray, the middle domain is boxed and the C-terminal domain is highlighted in gray.

The differences in the proteolytic patterns were analyzed to identify the protein regions involved in the molecular interactions. In Figure 2A, the preferentially hydrolyzed positions observed on isolated Hsp90 are shown: widespread cleavage sites within the entire protein structure have been identified. Comparing our data with the predicted secondary structure organization of Hsp90, it can be deduced that most of the identified cleavage sites are located in unstructured portions, thus confirming the efficiency of the approach. To further validate the method, the radicicol/Hsp90 complex was investigated, since the radicicol binding region has been deeply characterized by crystallography.The results achieved in the radicicol/Hsp90 complex are shown in Figure 2B. Comparison between the proteolysis patterns observed on Hsp90 with or without radicicol indicates significant protection of the N-terminal domain from enzymatic hydrolysis. This result is in agreement with the radicicol/Hsp90 interaction involving the ATPase located in the N-terminal domain of Hsp90. Limited proteolysis analysis of the compound 2/Hsp90 complex produced the fragmentation pattern summarized in Figure 2C. These data demonstrate that most of the N-terminal domain sites as well as those located in the protein portion interconnecting this domain to the middle domain were protected following complex formation, thus suggesting an interaction involving the 90–280 region of Hsp90.

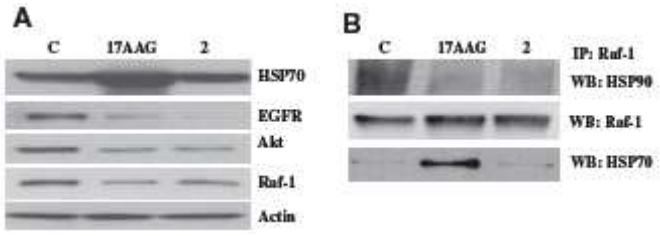

Figure 3. (A) Analysis of Hsp90 client protein levels and Hsp70 in A431 cells. Total cellular extracts were obtained 24 h after treatment (11 μM, IC_{80}). Actin is shown as a control for protein loading. EGFR levels were analyzed only in A431 cells and tubulin is shown as a control for protein loading.
(B) Coimmunoprecipitation of Raf-1/Hsp90 4 h after 17-AAG or (2) treatment, in A431 cells. Cells were treated with equitoxic (IC_{80}) concentrations of 17AAG (0.1 μM) or 2 (11 μM). Cell lysates were than harvested and immunoprecipitated with anti-Raf-1 rabbit polyclonal antibody. Immunoprecipitates were immunoblotted for Hsp90 Blots were stripped and probed for Raf-1.

In contrast to the effects of ansamycin inhibitors of Hsp90 (e.g., 17AAG), compound 2 did not induce up-regulation of Hsp70. The lack of modulation of Hsp70 could reflect a different binding mode of 2 to Hsp90, which did not involve the shift of client association from Hsp90 to Hsp70 prior to proteasome-mediated degradation. In A431 cells treated with 2 for 4 h, a coimmunoprecipitation experiment performed with anti-Raf-1 antibody revealed a reduced amount of Hsp90 bound to the client protein, as could be expected from an Hsp90 inhibitor (Fig. 3A). The effect was comparable to that of 17AAG at equitoxic concentrations. However, this short treatment did not induce a shift of the binding of Raf-1 from Hsp90 to Hsp70, because the level of coprecipitated Hsp70 with Raf-1 was undetectable (Fig. 3B). The lack of up-regulation of Hsp70 in treated cells has been observed with other putative inhibitors of Hsp90 (e.g., epigallocatechin [15] and curcumin [16]).

This finding would suggest a mechanism of interaction different from that of geldanamycins, that target the ATP-binding site of Hsp90. This interpretation was also supported by proteolysis experiments (Fig. 2). If interaction with other cochaperones contributes to the modulation of Hsp90 function by the novel agents remains to be explored.

In the above experiments, aimed at a biochemical analysis of protein expression modulation (Fig. 1), the exposure time was only 24 h, because prolonged exposure resulted in the partial detachment of cells. Indeed, at 48 h, marked cleavage of poly (ADPribose) polymerase and activation of caspase-3 were found in cells treated with 2, supporting apoptosis induction (Fig. 4).

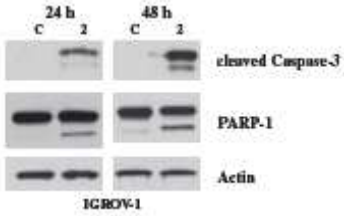

Figure 4 Biochemical analysis of apoptosis-related factors in IGROV-1 cells.
Cleaved Caspase-3 and PARP-1 expression levels were analyzed by Western blot and total cellular extracts, used for this analysis, were obtained both 24 h and 48 h after treatment with 2 (11 μM).

The promising results obtained by testing compound 2 prompted us to investigate the activity of other azaphilones as potential Hsp90 inhibitors. We therefore tested the natural compounds 1–13 for their cytotoxic activity against a variety of human tumor cell lines; they were also tested for their ability to inhibit Hsp90 ATPase activity and for binding affinity in the FP assay (Table 1). The most potent compounds of this series were 1, 2, and 5, characterized by IC50 values ≤10 μM against several cell lines. The potency of these compounds was substantially lower than that of geldanamycin or its analogue 17-AAG (IC50 in A431 cells, 0.2 ± 0.04 and 0.07 ± 0.01 μM, respectively). In the case of compound 2, the reduced potency was consistent with a low affinity for Hsp90 in the competitive

binding assay (IC50 61.7 ± 0.85 vs 1.095 ± 0.05 for 17AAG). Interestingly, the two pyranyl compounds 8 and 9, with a saturated side-chain, exhibited strong binding to Hsp90. This was paralleled by the twofold increase of binding going from 2 to 5. However, this strong binding was not reflected in the antiproliferative potency. A plausible explanation for this discrepancy could be the unfavorable cellular pharmacokinetics. The series of natural deflectins (10–13), characterized by an angular lactone fused to a dihydroisochromenone ring, were found to be almost inactive. In an attempt to identify the structural requirements involved in the Hsp90 inhibitory activity, the semisynthetic compounds 14–19 were prepared exploiting the well-known reactivity of azaphilones with amines. The IC50 values of compounds 14–19, reported in Table 3, indicated that these agents were generally more potent than compounds of the previous series (1–13).

Table 3
Antiproliferative activity on different cell lines, ATPase activity inhibition and binding to Hsp90 (IC_{50}, μM ± SD) of compounds 14–19

Compd	Antiproliferative activity (μM) Cell lines					Hsp90 ATPase activity inhibition	Binding Hsp90 (FP)
	NCI-H460	A431	JR8	IGROV-1	STO		
14a	4.3 ± 0.1	0.30	4.80	0.20	3.57	5.75 ± 0.75	27.7 ± 0.65
14b	11.0 ± 4.2	3.30	6.00	1.90	9.47	13.11 ± 0.87	2.29 ± 0.06
14c	17.3 ± 0.3	4.48	15.46	2.32	5.77	–	6.83 ± 0.04
14d	10.2 ± 1.7	1.54	8.59	1.72	2.06	6.10 ± 0.68	27.4 ± 0.38
14e	30 ± 7.5	4.24	9.02	2.86	4.0	19.9 ± 1.24	37.5 ± 0.59
15	21.3 ± 3.1	1.20	5.70	0.80	4.36	14.5 ± 0.93	35.4 ± 1.3
16	>20	3.98	5.16	2.92	2.92	8.9 ± 0.5	0.28 ± 0.06
17	3.4 ± 0.06	2.67	4.0	3.46	2.28	–	0.004 ± 0.0001
18	–	>18	–	>18	>10	>50	>50
19	6.7 ± 0.2	2	–	–	4.5	>50	>100

Among the open-ring analogues (14a–e), compound 14a, containing a benzyl substituent on the nitrogen, was the most potent in the antiproliferative assay. These compounds showed moderate binding to Hsp90, comparable to that of 2. On the contrary, compounds 16 and 17, containing the same tricyclic system and the same benzyl substituent on N-7, exhibited increased Hsp90 binding, the highest value (IC50 4 nM) being shown by the monascorubrin derivative 17. Figure 5 shows the analysis of client protein expression modulation.

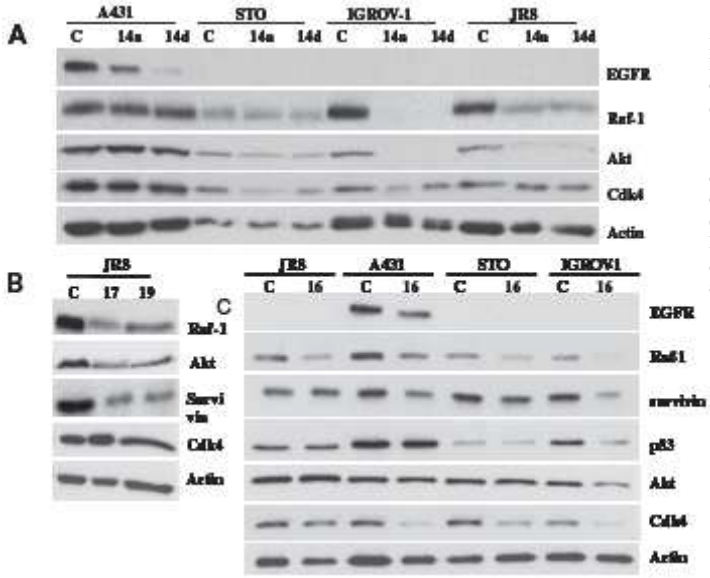

Figure 5. Comparison of biochemical effects on Hsp90 client proteins. (A) Hsp90 client expression levels after 24 h treatment with (14a) or (14d). Total cellular extracts were obtained 24 h after treatment with equitoxic (IC_{80}) doses of (14a, 2.7 μM for A431 cells; 10.7 μM for JR8 cells, 2.3 μM for IGROV-1 and 11.6 μM for STO cells) or (14d, 8.6 μM for A431; IGROV-1 and STO cells; 16 μM for JR8 cells). Actin is shown as a control for protein loading. (B) Hsp90 client expression levels after 24 h treatment with (17) or (5) in JR8 cells. Total cellular extracts were obtained 24 h after treatment with equitoxic (IC_{80}) doses of (17, 6.36 μM) or (5, 9.3 μM). Actin is shown as a control for protein loading. (C) Hsp90 client expression levels after 24 h treatment with (16). Total cellular extracts were obtained 24 h after treatment (16, 9.8 μM, IC_{80}). Actin is shown as a control for protein loading.

The effects on the examined proteins were variable among cell lines. Compounds 14a and 14d caused marked depletion of Raf-1 and Akt in IGROV-1 and JR8 cells (Fig. 5A). In contrast to the marginal effect of 2, compounds 14a, 14d, 15, and 17 were very effective in causing depletion of client proteins in JR8 cells (Fig. 5A and B). Compound 14d caused almost complete depletion of EGFR in A431 (Fig. 5A). The effects of 14a and 16 on EGFR expression in A431 cells were less marked at equitoxic concentrations (IC80) (Fig. 5A and C). For compound 14a, coimmunoprecipitation with anti-Raf-1 antibody, performed after 4-h exposure, revealed reduced binding of Raf-1 to Hsp90 (not shown). However, the depletion was dose dependent and the variable effects on the client protein levels were likely determined by the relative sensitivity of the various cell lines (Fig. 6).

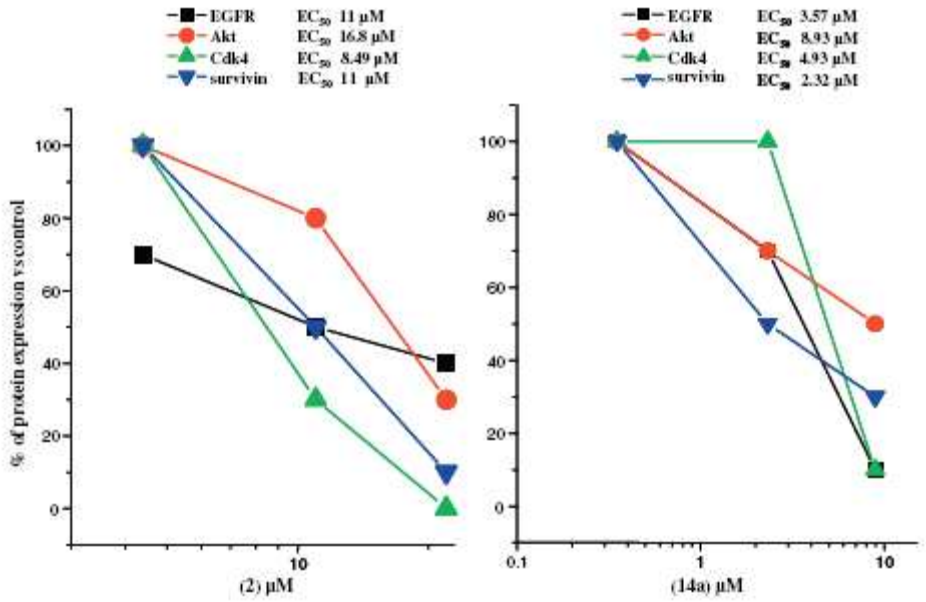

Figure 6. Dose–response of the biochemical effect of (2) and (14a) on Hsp90 client proteins in A431 cells.
Total cellular extracts were obtained 24 h after treatment with (2) (4.4, 11, 22 μM) or (14a) (0.3, 2.32, 8.93 μM). Protein expression levels of EGFR, Akt, Cdk4 and survivin were analyzed by Western blot. The quantification of Western blot analyses was obtained with the Image Quant 5.2 software and results (relative expression normalized to the tubulin, as loading control) are presented as % of protein expression, as compared to the control. IC_{50} values of the down-regulation of each protein level are reported in the plots.

Compound 17 shows a strong binding to the enzyme (FP test), confirmed by the SPR analysis (KD 47.8 ± 0.5 nM). However, the limited proteolysis experiment for 17 (Fig. 7) indicates a pattern similar to that of control, that is, no protection of the sensitive regions.

Figure 7

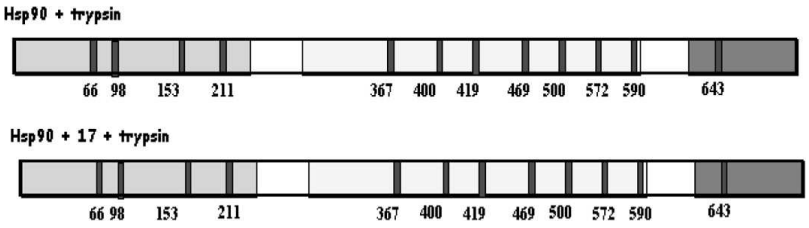

It is therefore possible that compound 17 interacts with the protein in rather rigid regions (beta leaflets or, more likely, helical regions), about which the limited proteolysis approach cannot give enough information. Again, the deflectin derivative 19 showed no appreciable Hsp90 binding, like the parent natural compounds, thus confirming the detrimental effect of an angular structure. The lack of close correlation between affinity for Hsp90, as determined in the FP assay, and cellular effects, in terms of cell growth inhibition and of client protein depletion, could reflect an unfavorable cellular pharmacokinetics or interaction with other proteins which may limit the Hsp90 binding inside the cell. Indeed, the compounds related to bulgarialactone (e.g., 9 and 17) are characterized by a reactive conjugate system that could react with amines and thiols, present at high concentrations inside the cell (e.g., GSH). Preliminary in vivo antitumor activity studies supported the therapeutic potential of this new series of compounds. In particular, intraperitoneal administration of 2 to athymic nude mice bearing ovarian carcinoma xenografts growing intraperitoneally as ascitic tumors resulted in a substantial increase in survival (Fig. 8).

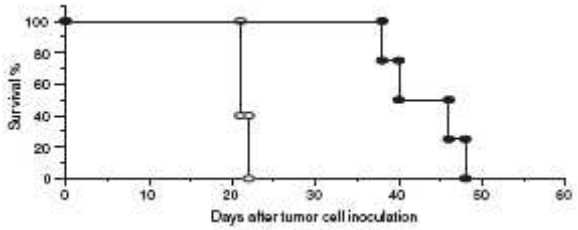

Figure 8. Effect of 2 on survival of mice bearing ip ovarian carcinoma tumor IGROV-1. (s) Control mice; (d) mice treated ip daily with 2 (25 mg/kg) for 4 days/week for 2 weeks.

Chapter A2: The enhancement of antiproliferative and proapoptotic activity of HDAC inhibitors by curcumin is mediated by Hsp90 inhibition

A2.1: Down-regulation of Hsp90 client proteins by curcumin

The analysis of protein expression was performed in two cell lines, the squamous cell carcinoma A431 and mesothelioma STO cells after 24 h-exposure to IC80 of curcumin (5 μM). The two cell lines exhibited a comparable sensitivity to curcumin in the anti-proliferative assay Curcumin and HDAC inhibitors (Fig. 1).

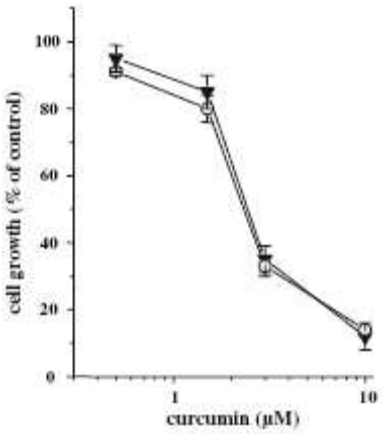

Fig. 1 Antiproliferative effect of curcumin on A431 and STO cells. Cells were treated for 72 h with curcumin and cell growth was evaluated 72 h after the treatment by cell counting. Inverted filled triangle A431 cells (IC_{50}, 2.2 μM); open circle STO cells (IC_{50},2.1 μM). Data are the mean of three independent experiments

As shown in Fig. 2a, EGFR, Raf-1, Survivin, and Cdk4 protein expression were strongly downregulated by curcumin treatment, whereas the effect was less marked for Akt. This effect was consistent with previous observations indicating a delayed depletion of Akt produced by other Hsp90 inhibitors [17].

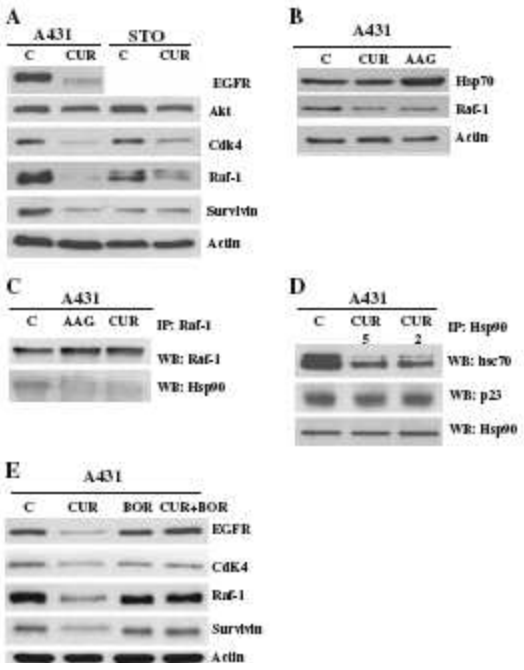

Fig. 2 a Effect of curcumin on Hsp90 client protein levels in A431 and STO cells. Total cellular extracts were obtained 24 h after treatment with curcumin (5 μM, IC_{80}). Actin is shown as a control for protein loading. C Control, CUR curcumin. b Comparison of the effects of curcumin and 17-AAG on protein levels of Hsp70. Cells were treated as described in (a), with curcumin (5 μM) or 17-AAG (0.1 μM). c Coimmunoprecipitation of Raf-1/Hsp90 in A431 cells treated with 17-AAG or curcumin for 1 h. Cells were treated with equitoxic concentrations of 17-AAG (0.1 μM, IC_{80}) or curcumin (5 μM). Cell lysates were than harvested and immunoprecipitated with anti-Raf-1 rabbit polyclonal antibody. Immunoprecipitates were immunoblotted for Hsp90. Blots were stripped and probed for Raf-1. C Control, AAG 17-AAG, CUR curcumin. d Coimmunoprecipitation of Hsp90/hsc70 and Hsp90/p23 in A431 cells treated with curcumin. Cells were treated with two concentrations of curcumin (2 and 5 μM; i.e., IC_{50} and IC_{80}) as described above. Immunoprecipitated obtained by anti-Hsp90 antibody were immunoblotted for hsc70 or p23. C Control, CUR2 curcumin 2 μM, CUR5 curcumin 5 μM. e Effect of bortezomib (BOR) on the depletion of Hsp90 client proteins induced by curcumin (CUR) in A431 cells. Total cellular extracts were obtained 24 h after treatment (curcumin 5 μM, bortezomib 0.001 μM). Actin is shown as a control for protein loading. C Control

However, in contrast to the geldanamycin derivative, 17-AAG, curcumin did not cause increased expression of Hsp70 (Fig. 2b). To investigate the mechanism of down-regulation of Hsp90 clients, co-immunoprecipitation of Raf-1/Hsp90 was performed in A431 cells. After 4 h exposure to curcumin (5 μM) or equitoxic concentration of 17-AAG (0.1 μM), a lower amount of Hsp90 was found in complex with Raf-1 (Fig. 2c). Thus, in spite of a different potency, the effects of the two agents were comparable at equitoxic concentrations. An additional characterization of the effect of curcumin on the association between Hsp90 and cochaperones was performed in an immunoprecipitation assay with anti-Hsp90 antibody (Fig. 2d). The results showed that anti-proliferative concentrations of curcumin reduced the interaction of Hsc70 (but not of p23) with Hsp90. The inhibition of Hsp90–client interaction is expected to result in client protein degradation mediated by the ubiquitin–proteasome system [18, 19]. The combination of bortezomib, a well-known proteasome inhibitor, with curcumin prevented protein depletion induced by curcumin (Fig. 2e), thus supporting that the observed curcumin-induced protein down-regulation occurred via the ubiquitin–proteasome pathway.

A2.2: Curcumin-Hsp90 interaction

The competitive binding fluorescence polarization assay gave an IC50 of 6.2 ± 0.12 lM for curcumin, 1.09 ± 0.05 lM for 17-AAG, and 0.058 ± 0.001 for radicicol. Thus, the different anti-proliferative potencies of curcumin and 17-AAG (IC50 values, 2.4 and 0.06 μM, respectively) were consistent with their binding affinities to Hsp90. We used the limited proteolysis–mass spectrometry technique for the structural analysis of drug–Hsp90 interaction [20]. This approach is based on the evidence that exposed, weakly structured, and flexible regions of a protein can be recognized by a proteolytic enzyme. The differences in the proteolytic patterns occurring on the protein when it underwent digestion in the presence or in the absence of putative ligands allow identification of the protein regions involved in the molecular interactions [21]. Results achieved in the experiment performed on Hsp90, on the Hsp90/curcumin complex, and on the Hsp90/radicicol complex are summarized in Fig. 3 and in Table 1.

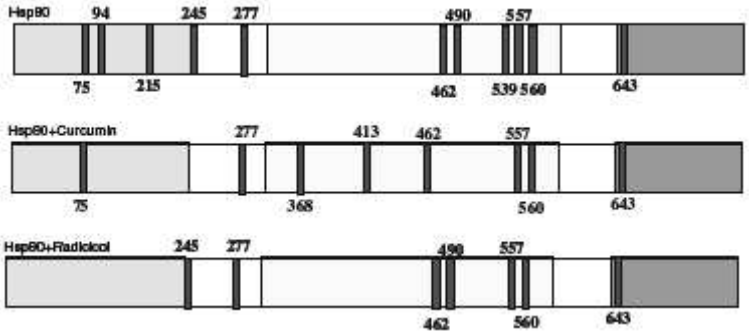

Fig. 3 Schematic representation of the results obtained from limited proteolysis experiments on recombinant Hsp90. The preferential cleavage sites detected performing enzymatic digestions on recombinant Hsp90, on the Hsp90/curcumin complex, and on the Hsp90/radicicol complex are in dark grey. The Hsp90 N-terminal domain is highlighted in light grey, the middle domain is boxed and the C-terminal domain is highlighted in grey

Table 1 Curcumin and radicicol interaction with Hsp90

Compound	K_D (nM)[a]	K_d (s^{-1})[a]	Protected sites[b]	Exposed sites[b]	Putative interaction region
Radicicol	3.04 ± 0.85	0.0113 ± 0.0005	75, 94, 215	–	N-terminal domain
Curcumin	6.68 ± 3.28	0.0090 ± 0.0008	94, 215, 245	368, 413	N-terminal domain

[a] Dissociation constants obtained by SPR analysis

[b] Proteolytic pattern obtained by limited proteolysis and mass spectrometry analysis

A comparison between the proteolysis patterns observed on free Hsp90 and Hsp90/curcumin complex demonstrated that the sites 94, 215, and 245, cleaved in the experiments performed on the isolated proteins, were protected following the complex formation, thus suggesting an interaction involving the Hsp90 N-terminal domain. However, binding of the protein with curcumin also produced an higher susceptibility to enzymatic hydrolysis of same sites located into the middle domain, suggesting a possible long-range effect of the curcumin on the protein tertiary structure. The experiments performed on the Hsp90/radicicol complex indicated a significant protection of the N-terminal domain from enzymatic hydrolysis. This result is in agreement with the radicicol/Hsp90 interaction involving the ATPase portion located into the N-terminal domain of Hsp90 [22]. We used surface plasmon resonance to measure kinetic and thermodynamic parameters of ligand–protein complex formation [23]. An SPR-based binding assay as implemented with Biacore technology was, therefore, used to investigate the drug–protein interactions. The values of the constants (Table 1) indicated that curcumin exhibited an high affinity for Hsp90, even if it was lower than that measured for radicicol. However, the difference in the thermodynamic dissociation constants (KD) observed for these two compounds mainly depend on the stability of the respective protein complexes, as inferred by the lower kinetic constant (Kd) determined for curcumin in respect of that of radicicol.

A2.3: Cellular effect of the combination of curcumin with HDAC inhibitors

In combination studies, we used vorinostat and panobinostat, two hydroxamic acid-based compounds, which are well-known pan-histone deacetylase inhibitors including HDAC6. The cell growth inhibition studies were performed using subtoxic concentrations of curcumin (IC10–20) (Fig. 4).

Under these conditions, the combined treatment resulted in a marked enhancement of the anti-proliferative activity of either vorinostat or panobinostat as shown by the dose response curves. Based on these observations, further experiments of drug interaction were performed with subtoxic concentrations of all agents (IC20), i.e. curcumin (1.5 μM), panobinostat (11.5 nM), and vorinostat (15 nM). Apoptosis response was examined after 72 h exposure by TUNEL analysis (Fig. 5a).

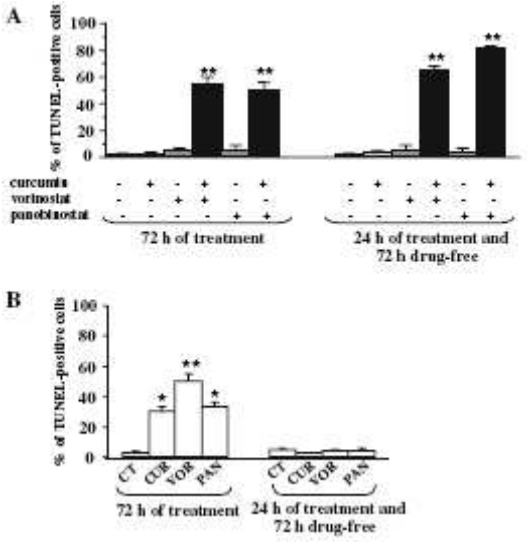

Fig. 5 a Effect of curcumin on apoptosis induced by HDAC inhibitors in A431 cells. Cells were exposed for 72 h to subtoxic concentrations of panobinostat (11.5 nM) or vorinostat (15 nM), alone or in combination with curcumin (1.5 μM). b Apoptotic cell death caused by cytotoxic concentrations of single agent treatment. Cells were exposed for 72 h to cytotoxic concentrations of panobinostat (100 nM), vorinostat (1 μM) and curcumin (5 μM). At the end of the treatment, apoptosis was detected by TUNEL assay and determined by FACS analysis. In a parallel experiment, cells were treated for 24 h and apoptosis was detected after 72 h following drug removal. Data from three independent assays were analyzed by t test (control vs treatment): *P≤0.05, **P≤0.005

When tested at these concentrations, single drug treatment induced only a marginal extent of apoptosis, whereas the combination treatment markedly enhanced apoptotic response to around 50%. A similar enhancement was observed following a shorter exposure (24 h) and 72 h incubation in drug-free medium. On the contrary, when apoptosis was assessed after 72 h exposure to cytotoxic concentrations of single drug (IC80), a consistent number of apoptotic cells was found; but the shorter exposure followed by drug removal, indicated the reversibility of the effect of these agents, as no significant apoptosis was found (Fig. 5b). These results confirm that, differently from single treatment, the sensitization resulting from the drug interaction did not require prolonged exposure, suggesting an irreversible effect specific of the combined treatment.

A2.4: Effect of the combination of curcumin and HDAC inibitors on levels of Hsp90 client proteins

In order to investigate the molecular basis of the synergistic interaction between curcumin and HDAC inhibitors, the effects of single agents and their combination on Hsp90 client proteins were examined by western blot analysis using the same (subtoxic) concentrations of previous experiments.

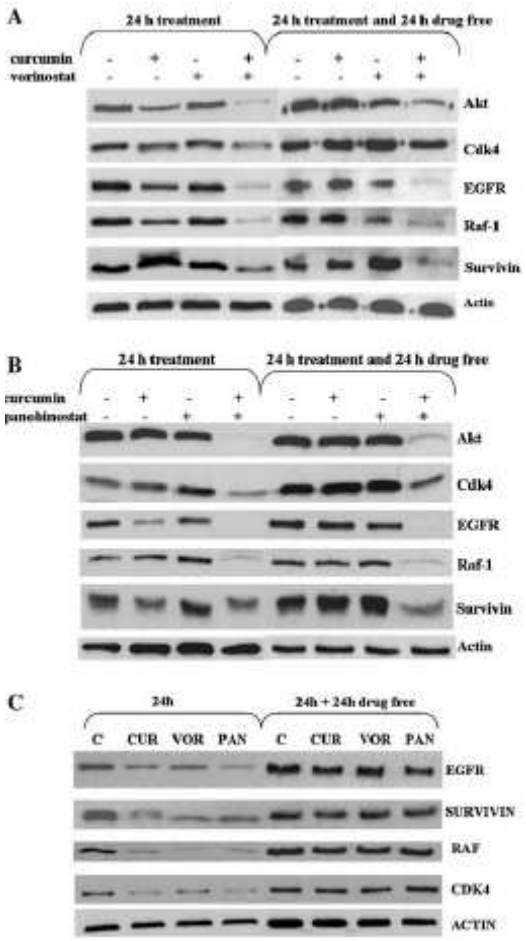

Fig. 6 Effects of combination of curcumin/vorinostat (a) or curcumin/panabinostat (b), or single agent treatment (c) on cellular levels of Hsp90 client proteins. a,b Cells were exposed to each drug alone or in combination for 24 h and processed as indicated in legend to Fig. 2.
Subtoxic concentrations of each drug were used (i.e. curcumin 1.5 μM, vorinostat 15 nM, panobinostat 11.5 nM). The analysis was also performed after incubation of the drug-treated cells in drug-free medium for 24 h. c Cells were exposed to cytotoxic concentrations (IC_{80}) of each drug (i.e. curcumin 5 μM, vorinostat 1 μM, panobinostat 0.1 μM) for 24 h and processed as indicated in the legend to Fig. 2. The analysis was also performed after incubation of the drug-treated cells in drug-free medium for 24 h. Actin is shown as a control for protein loading

Figure 6 shows that, under these conditions, single agents did not produce appreciable changes of protein expression. In contrast, the combinations of curcumin with either HDAC inhibitors caused depletion of the well-established client proteins, in particular Akt, EGFR, and Raf-1. The downregulation of Cdk4 and survivin was less marked and may reflect a different kinetics of depletion as suggested by the effect of the combination on survivin 24 h after treatment.

The reduction of the Hsp90 client protein levels was persistent even 24 h after drug removal, with the exception of Cdk4. The persistence of the client down-regulation was typical of the combined treatments; indeed, when cells were treated with single agents (IC80) and incubated in drug-free medium for 24 h, the biochemical effects were lost (Fig. 6c).

To better document the involvement of Hsp90 inhibition in down-regulation of client proteins, we have performed a coimmunoprecipitation analysis after 4 h exposure, i.e. under conditions where a substantial depletion of client proteins is not expected (Fig. 7).

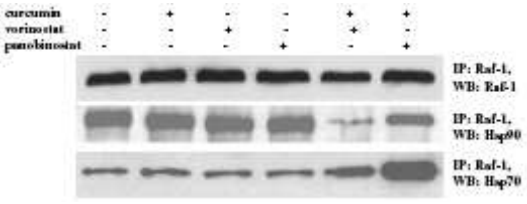

Fig. 7 Coimmunoprecipitation of Raf-1/Hsp90 in A431 cells treated with curcumin, vorinostat, panobinostat alone or in combination. A431 cells were exposed to subtoxic concentrations of panobinostat (11.5 nM), vorinostat (15 nM), and curcumin (1.5 μM) alone or in combination, for 4 h. Cell lysates were than harvested and immunoprecipitatedwith anti-Raf-1 rabbit polyclonal antibody. Immunoprecipitates were immunoblotted for Raf-1. Blotswere stripped and probed for Hsp90 and Hsp70

Again in contrast to a negligible effect of single agents, the combination treatment reduced the amount of Hsp90 bound to Raf-1, an effect most evident with the combination of curcumin and vorinostat. This observation was consistent with an enhanced inhibition of Hsp90 function, resulting in a reduced association of Hsp90 with Raf-1. The combined treatment resulted in a concomitant increase in the binding of Raf-1 to Hsp70. The shift of the binding from Hsp90 to Hsp70 has been described as an event preceding proteasome-mediated degradation of the client proteins [24, 25, and 26].

Section B: GGT

Chapter B1: Cellular response to oxidative stress and ascorbic acid in melanoma cells overexpressing γ- glutamyltransferase

B1.1: Biochemical characterisation of cell clones

The study was performed on two human melanoma clones, characterised by a marked difference in GGT activity (Table 1), the c21/GGT clone exhibiting a high GGT activity (90.8 ± 3.4 mU/mg protein), in contrast to the low activity of the c21/basal clone (approx. 180 times lower). In spite of the substantial difference in GGT activity and expression (not shown), the GSH content was marginally higher in the c21/basal clone. Interestingly, the content of GSSG was appreciably increased in the GGT-overexpressing clone and the increased GSSG/GSH ratio supports conditions of oxidative stress. Cell doubling time was not modified by transfection procedures, and was approximately 24 h in both clones.

Table 1 – Melanoma clones characterisation

	c21/GGT	c21/basal
GGT activity (mU/mg protein)	90.78 ± 3.4	0.344 ± 0.13
GSH content (nmol GSH eq./mg protein)	51.25 ± 10.75	67.56 ± 8.6
GSSG content	1.05 ± 0.12	0.33 ± 0.32
GSSG/GSH ratio (%)	2.05	0.49
Doubling time (h)	24 ± 0.8	24 ± 1.2

B1.2: Cell response to H2O2-induced oxidative stress

We have investigated whether the overexpression of GGT could influence the antiproliferative activity of hydrogen peroxide. The effects of H2O2 were investigated both in standard cell culture conditions and in medium supplemented with GSH (500 μM) and glycyl-glycine (20 mM), in order to achieve full activation of GGT.6 As shown in Fig. 1, when cells were exposed for 2 h to hydrogen peroxide under standard conditions, a different response was observed, with an IC50 value for c21/GGT cells (2.3 mM) about 50 times higher than that observed for c21/basal cells (0.05 mM). Similar differences were observed when clones were exposed to H2O2 in conditions of full GGT activation (data not shown). On the basis of these results, two equitoxic hydrogen peroxide concentrations (4.6 mM and 100 μM for c21/GGT and c21/basal clone, respectively, causing approx. 70% inhibition of cell growth in standard culture medium) were chosen for subsequent experiments.

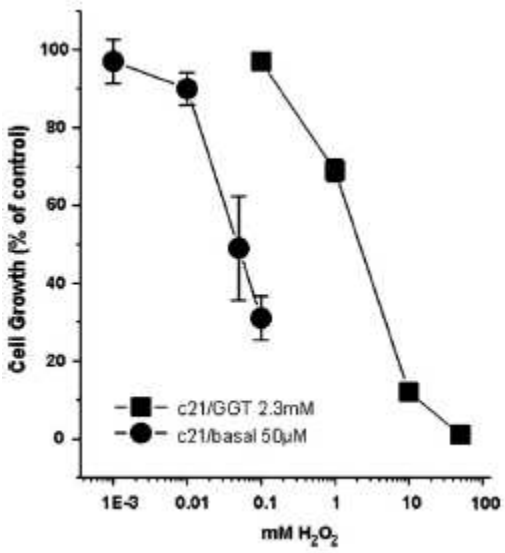

Fig. 1 – Cytotoxic effect of H_2O_2 on c21/GGT and c21/basal clone. Cells were treated for 2 h with H_2O_2 and cell viability was evaluated 72 h after the treatment by cell counting. Data are the mean of three independent experiments.

B1.3: Effects of H2O2 on intracellular ROS production

Analysis of ROS production was performed 24 h after the end of H2O2 treatment. As shown in Fig. 2, in spite of the higher concentration of H2O2 applied, in the c21/GGT clone the extent of intracellular ROS production was lower than in c21/basal cells.

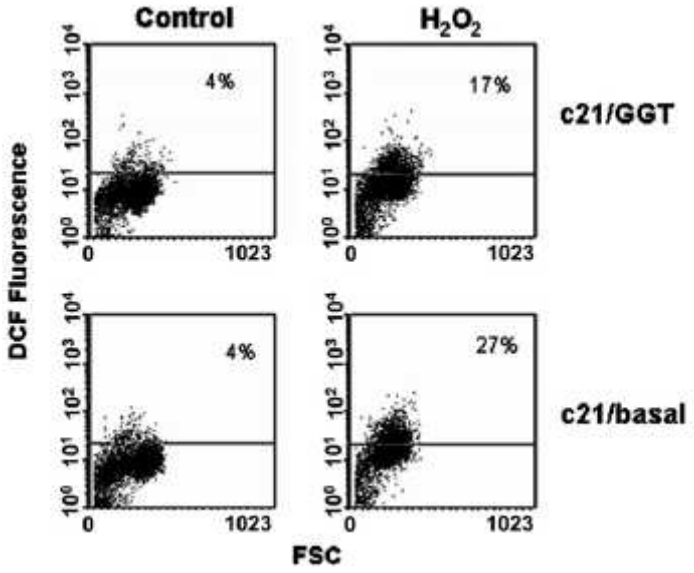

Fig. 2 – ROS induction 24 h after a 2 h H_2O_2 exposure. Cells treated with H_2O_2 (4.6 mM and 100 µM for c21/GGT and c21/basal clone, respectively) were incubated with 10 µmol/L DCFH-DA. The DCF fluorescence was detected by FACScan flow cytofluorimeter. One representative experiment out of three was reported. The percentages of DCF-positive cells

B1.4: Effects of H2O2 on cell cycle

As shown in Fig. 3, equitoxic concentrations of H2O2 caused different effects on cell cycle distribution in the two clones. 24 h after a 2 h-exposure to H2O2, an accumulation in G2 phase was observed for c21/GGT cells, while the c21/basal clone showed an arrest in S phase concomitant with a decreased percentage of cells in G1 phase.

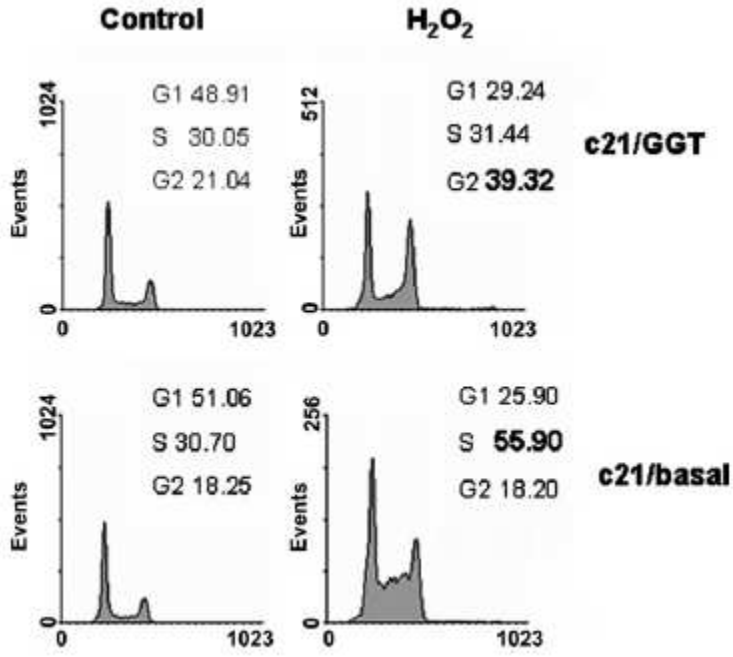

Fig. 3 – Cell cycle distribution after H_2O_2 exposure. Cells treated with the same equitoxic concentrations of H_2O_2 used for ROS induction analyses were examined for cell cycle distribution 24 h after the end of treatment. The percentages of cells in G1, S or G2 phases are reported in each histogram.

To elucidate the reasons for the differences observed, we examined the activation of three selected proteins involved in DNA damage/repair response, i.e. histone γ–H2AX, phospho-p53 (Ser15) and RPA-2. As assessed by western blot analysis (Fig. 4), exposure to equitoxic concentrations of H2O2 induced a higher induction of γ–H2AX phosphorylation and phospho-p53 (Ser15) in c21/basal than in c21/GGT cells, whereas RPA-2 was not activated in either clones.

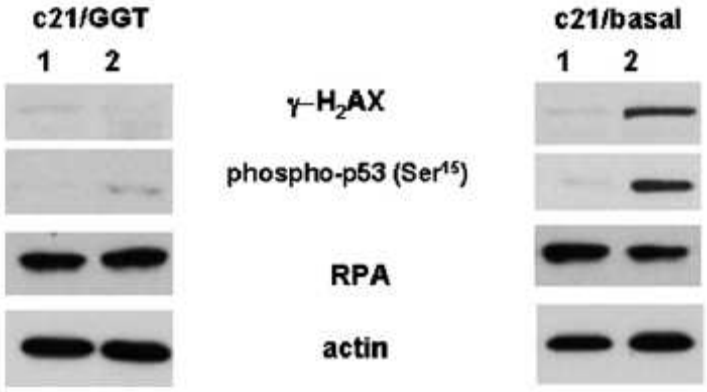

Fig. 4 – Induction of DNA damage response in c21/GGT and c21/basal cells exposed to equitoxic H_2O_2 concentration for 2 h. After 24 h from the end of treatment, cells were lysed and processed for Western blotting. 1 = control, 2 = H_2O_2 treatment (4.6 mM for c21/GGT and 100 μM for c21/basal clone). Loading control is shown by actin.

B1.5: Effects of ascorbic acid on cell proliferation

Exposure to AA for 2 h was able to exert an antiproliferative effect, which was two times higher in c21/basal than in c21/GGT cells (Fig. 5).

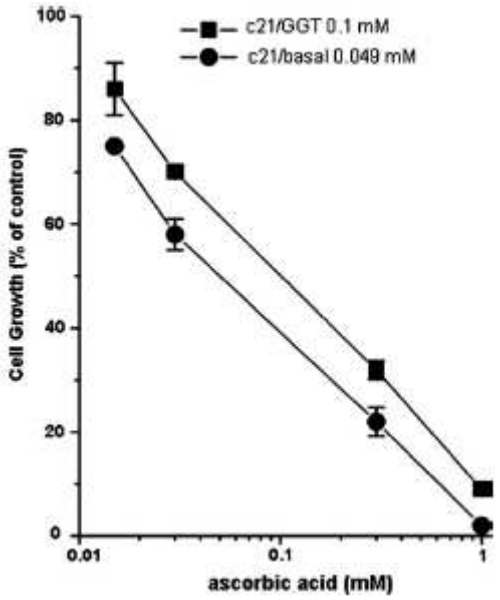

Fig. 5 – Antiproliferative effect of ascorbic acid. Dose dependent effect 72 h after a 2 h ascorbic acid treatment of c21/GGT and c21/basal cells, in GGT activating condition. Data are the mean of three independent experiments.

Again, the differences observed between the two clones were similar in standard culture conditions and in the medium enriched with GSH and glycyl-glycine to activate GGT, even if in the latter condition AA citotoxicity was higher (Table 2).

Table 2 – Comparison of sensitivity of c21/GGT and c21/basal cells to ascorbic acid in standard culture medium and in GGT activating condition

	IC_{50} (mM)	
	c21/GGT	c21/basal
Standard culture medium	0.4 ± 0.06	0.2 ± 0.07
GGT activating condition	0.1 ± 0.05	0.049 ± 0.001

On the basis of these results, two equitoxic concentrations of AA (0.06 mM and 0.03 mM for c21/GGT and c21/basal, respectively, causing approximately 30% inhibition of cell growth in GGT activating condition) were chosen for subsequent experiments.

B1.6: Iron-mediated antiproliferative effects of H2O2 and ascorbic acid

The involvement of redox-active iron in oxidative stress processes is a well established mechanism. To explore the possible role of iron in H2O2 and AA cytotoxicity, we evaluated the cellular response to these oxidative agents after lowering extra- and/or intracellular free (ionic) iron concentrations. In order to remove extracellular iron, incubation mixtures were pre-treated with the iron chelator DFO, 1 h at 37 °C, before cell treatments. As shown in Fig. 6A-B, pre-treatment with DFO resulted in a reduced antiproliferative activity of H2O2 and AA in both clones.

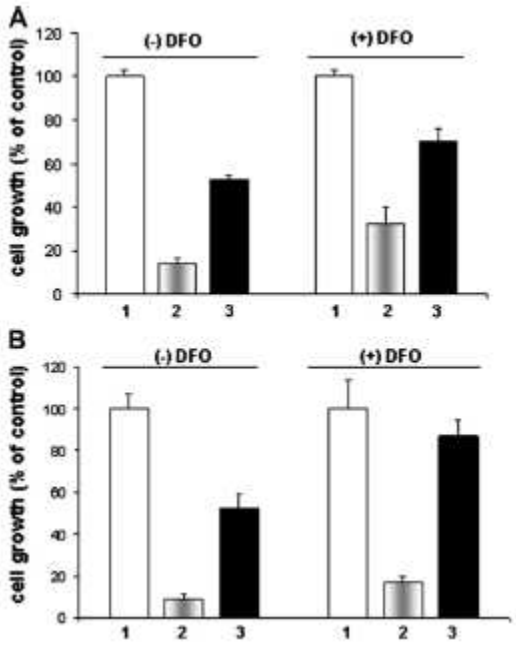

Fig. 6 – Cellular sensitivity of c21/GGT (A) and c21/basal (B) cells to H_2O_2 and ascorbic acid in the presence or absence of DFO. Cells were treated for 2 h with a medium pre-incubated with ascorbic acid or H_2O_2 in the presence/absence of DFO (500 μM; 1 h, 37 °C). 1 = control; 2 = H_2O_2 (4.6mM and 100 μM for c21/GGT and c21/basal, respectively); 3 = AA (0.06 mM and 0.03 mM for c21/GGT and c21/basal, respectively).

Interestingly, when the same incubation mixtures were pre-treated with bipyridyl, an iron chelator capable of entering the cell and chelating both extra- and intracellular free iron, the antiproliferative effect of H2O2 and AA was almost completely prevented (Fig. 7A-B).

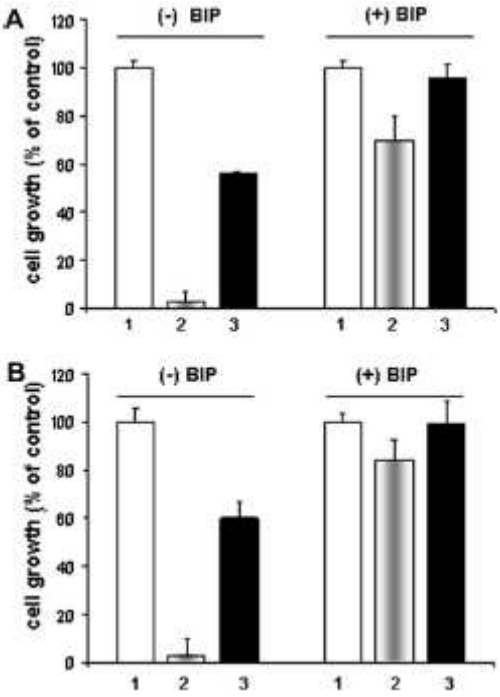

Fig. 7 – Cellular sensitivity of c21/GGT (A) and c21/basal (B) cells to H_2O_2 and ascorbic acid in the presence or absence of bipyridyl (BIP). Cells were treated for 2 h with a medium preincubated with ascorbic acid or H_2O_2 in the presence/absence of bipyridyl (500 μM; 1 h, 37 °C). 1 = control; 2 = H_2O_2 (4.6mM and 100 μM for c21/GGTand c21/basal, respectively); 3 = AA (0.06 mM and 0.03 mM for c21/GGT and c21/basal, respectively).

The crucial role played by redox-active iron was further confirmed in experiments carried out at equimolar concentrations of AA. Indeed, in the presence of bipyridyl the sensitivity of c21/basal cells to AA was markedly reduced, down to a value similar to that observed in c21/GGT cells (from 65% to 40% dead cells, Fig. 8A).

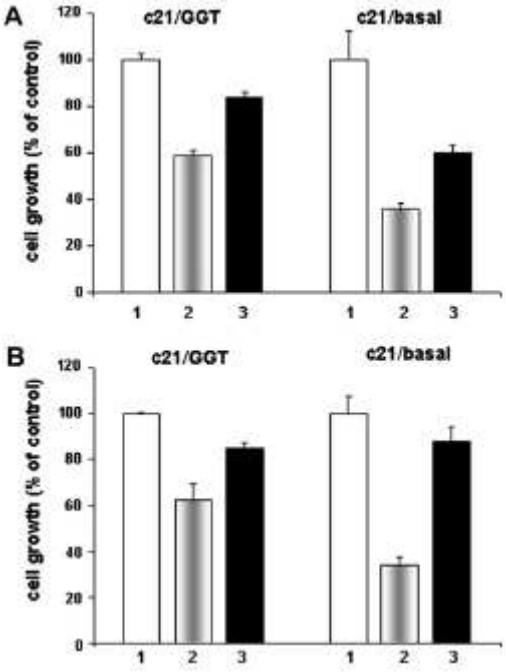

Fig. 8 – Cellular sensitivity of c21/GGT and c21/basal clone to ascorbic acid 0.06 mM in the presence or absence of bipyridyl (BIP) (A) or in the presence or absence of catalase 200 U/ml (B). (A) Cells were treated for 2 h with a medium pre-incubated with ascorbic acid (equimolar concentration, 0.06 mM) in the presence/absence of bipyridyl (500 μM; 1 h, 37 °C). 1 = control; 2 = AA 0.06 mM; 3 = AA (0.06mM in the presence of bipyridyl 500 μM). (B) Cells were treated with a medium containing ascorbic acid (equimolar concentration, 0.06 mM) or ascorbic acid and catalase 200 U/ml. 1 = control; 2 = AA 0.06 mM and 3 = AA (0.06 mM in the presence of catalase 200 U/ml).

B1.7: Suppression of AA antiproliferative effects by exogenous catalase

Further experiments were performed to assess the involvement of hydrogen peroxide in AA antiproliferative effect. As shown in Fig. 8B, after pre-treatment with catalase (200 U/ml, 1 h, 37 °C) sensitivity to AA was significantly reduced in both clones, and the difference between clones was abolished.

B1.8: AA treatment causes induction of apoptosis and ROS production

Fig. 9 shows the results obtained with TUNEL assay 72 h after treating clones for 2 h with equitoxic concentration of AA. Ascorbic acid was able to cause a marked apoptotic cell death in c21/basal clone (27% TUNEL positive cells) while no appreciable effect was detectable in c21/GGT cells (3% TUNEL positive cells). Deeper analysis of the apoptotic behaviour of the two clones showed that cytochrome c release was induced by AA treatment in both clones (Fig. 10A), whereas cleavage of CPP32 was detectable only in c21/basal clone (Fig. 10B). No differences were observed either for Bax or Bcl-2 protein levels (Fig. 10B). Fig. 11 shows intracellular ROS induction in the two clones under the same experimental conditions used in TUNEL assay. DCF fluorescence induced by AA in c21/basal was at least six times higher than in c21/GGT cells.

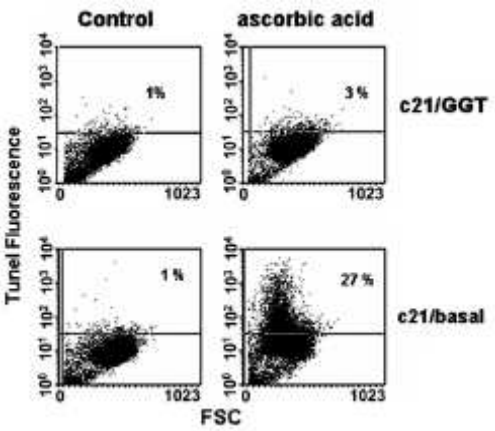

Fig. 9 – Apoptosis induced by ascorbic acid. Cells were exposed for 2 h to 0.06 mM and 0.03 mM ascorbic acid corresponding to equitoxic value in c21/GGT and c21/basal cells, respectively. Apoptosis was detected by TUNEL assay 72 h after the end of the treatment and determined by FACS analysis. Numbers in the dot-plots indicate the percentage of Tunel positive cells.

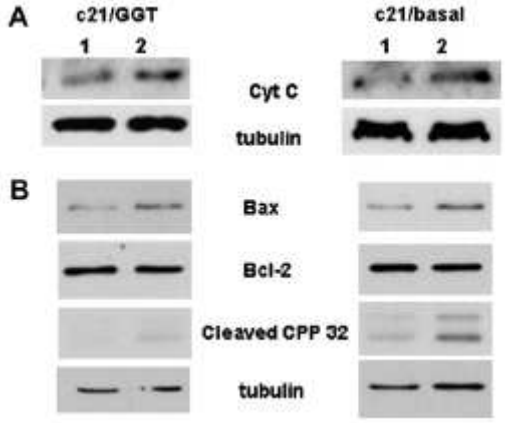

Fig. 10 – Effect of ascorbic acid treatment on the apoptotic pathway. (A) Effect of ascorbic acid on cytochrome C release.
The two cell lines were exposed to equitoxic concentration of ascorbic acid and the cytosolic extracts were prepared 24 h after the drug exposure. (B) Bax, Bcl-2 and CPP32 cleavage levels. Total cellular extracts were obtained 24 h after cell treatment. Tubulin is shown as a control for protein loading. Lane 1: control; lane 2: ascorbic acid.

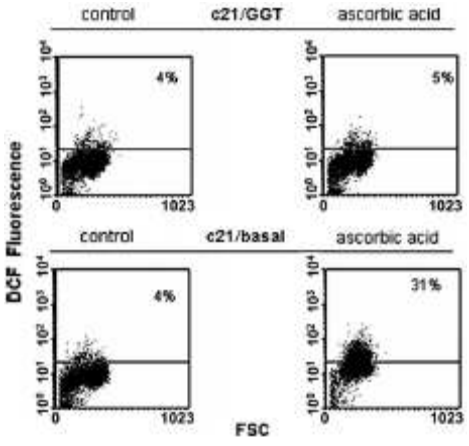

Fig. 11 – ROS induction by ascorbic acid. Cells were exposed for 2 h to 0.06 mM and 0.03 mM ascorbic acid for c21/GGT and c21/basal cells, respectively. After 24 h, ROS levels were detected by DCFH-DA assay and determined by FACS analysis.

B1.9: AA treatment activates DNA damage response and cell cycle arrest

DNA damage and cell cycle progression were investigated 24 h after AA treatment. The results showed an activation of DNA-damage responsive histone γ-H2AX and phospho-p53 (Ser15), which was more marked in c21/basal cells (Fig. 12). Cell cycle analysis indicated an accumulation of both clones in S phase (Table 3), suggesting the activation of a DNA damage checkpoint.

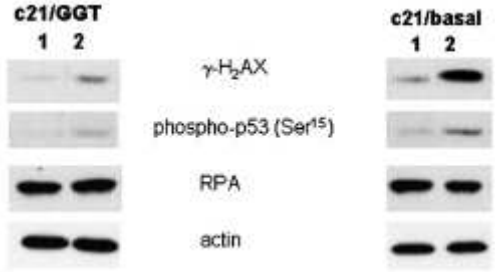

Fig. 12 – Induction of DNA damage response in c21/GGT and c21/basal cells exposed to equitoxic ascorbic acid concentration for 2 h. Protein expression of phospho-p53 (Ser_{15}), RPA, γ-H_2AX, and actin (loading control) after ascorbic acid treatment. 1 = Control, 2 = ascorbic acid treatment (0.06 mM and 0.03 mM for c21/GGT and c21/basal respectively).

Table 3 – Cell cycle distribution of c21/GGT and c21/basal cells after treatment with equitoxic concentration of ascorbic acid (one experiment representative of three is shown)

	c21/GGT			c21/basal		
	G1	S	G2	G1	S	G2
Control	52.3	28.04	19.66	47.69	29.22	23.1
Ascorbic acid	29.17	48.46	22.37	32.97	53.82	13.21

B1.10: Constitutive catalase activity in c21/GGT cells

In order to elucidate the cellular basis for lower presence of ROS after H2O2 and AA treatment in c21/GGT cells, two major cellular enzymes involved in hydrogen peroxide catabolism, catalase and glutathione peroxidase, were investigated. Basal catalase activity was actually two times higher in c21/GGT than in c21/basal cells (Fig. 13). This difference reflected the expression of the enzyme as documented by Western blot analysis. Treatment with H2O2 induced a further increase of catalase activity, more evident in c21/basal cells. A marked induction of catalase activity (56%) was caused by AA treatment only in c21/basal cells. In all conditions studied, catalase activity was anyway higher in c21/GGT cells. In both clones, no substantial modifications were found in catalase expression after treatments. With regard to glutathione peroxidase basal activity, no differences were found between the two clones (8.5 ± 1.1 and 8.4 ± 0.8 mU/mg of protein for c21/GGT and c21/basal cells, respectively).

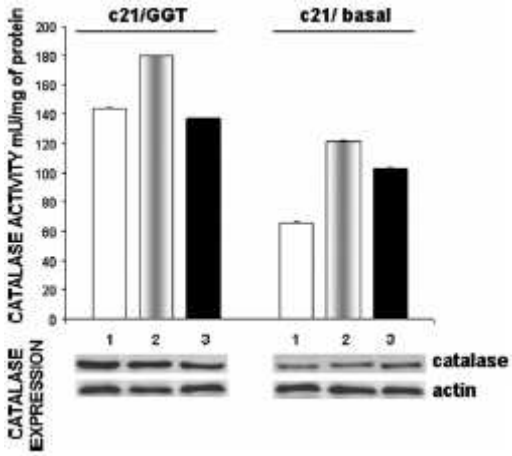

Fig. 13 – Catalase activity and expression. Cells were exposed for 2 h to H_2O_2 or to ascorbic acid, and catalase activity and expression were determined 24 h after treatment (see Materials and Methods for details). Actin is shown as loading control. One representative analysis out of three is shown. 1, control; 2, H_2O_2 (4.6 mM and 100 μM for c21/GGT and c21/basal cells, respectively); 3, Ascorbic Acid (0.06 mM and 0.03 mM for c21/GGT and c21/basal cells, respectively).

Chapter B2: γ-Glutamyltransferase-dependent resistance to arsenic trioxide in melanoma cells and cellular sensitization by ascorbic acid

B2.1: Sensitivity of melanoma cells to arsenic trioxide and ascorbic acid

The c21/basal cells exhibited an increased sensitivity to arsenic trioxide (IC50, 0.57 μM) as compared to the GGT overexpressing c21/ GGT clone (IC50, 2.6 μM) (Fig 1). This finding was consistent with our previous observation that the c21/GGT clone is more resistant to oxidative stress-inducing agents (e.g., H2O2) [27]. The differential sensitivity to arsenic trioxide paralleled the extent of ROS produced by the drug. As observed following treatment with H2O2 or ascorbic acid [27], the induction of oxidative stress by arsenic trioxide was more marked in the c21/basal cells (ROS level 29%) than in c21/GGT cells (ROS level 11%) (Fig. 2).

Subtoxic concentrations of ascorbic acid (in the range of 0.015-0.030 mM, causing about 10% cell growth inhibition) sensitized c21/GGT cells to arsenic trioxide, because the combination resulted in a substantially increased growth inhibition (Fig. 1B). In contrast, in the c21/basal cells, which were more sensitive to both agents, the combination resulted in an additive inhibitory effect (Fig. 1A). In the following experiments, the comparison of drug effects was performed using equitoxic concentrations of each agent, i.e. concentrations producing comparable antiproliferative effects in the two clones determined 72 h following exposure. Equitoxic concentrations of arsenic trioxide (IC70) used in the following experiments were 1 μM and 5 μM for c21/basal and c21/GGT, respectively. Ascorbic acid was used at a less toxic concentration (around IC40), i.e., 0.03 mM and 0.06 mM in c21/basal and c21/GGT, respectively. Early events associated with drug effects (cell cycle perturbation and biochemical modulation) were examined within 24 h of drug exposure to avoid any influence of indirect effects of cellular response.

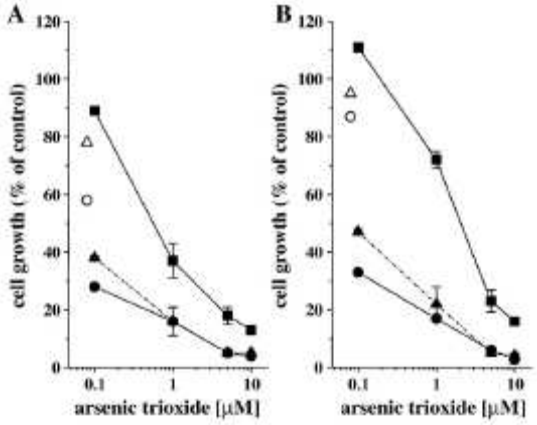

Fig. 1. Antiproliferative effect of arsenic trioxide alone or in combination with ascorbic acid on c21/basal (A) and c21/GGT (B) clones. Cells were treated for 2 h with arsenic trioxide alone (10, 5, 1 and 0.1 μM) or in combination with subtoxic concentrations of ascorbic acid (0.015 mM and 0.03 mM); cell growth inhibition was determined by cell counting 72 h after drug treatment. The results represent the mean±SD of three independent experiments. Arsenic trioxide (■); arsenic trioxide + ascorbic acid 0.015 mM (▲); arsenic trioxide + ascorbic acid 0.03 mM (●); ascorbic acid 0.015 mM (△); ascorbic acid 0.03 mM (○).

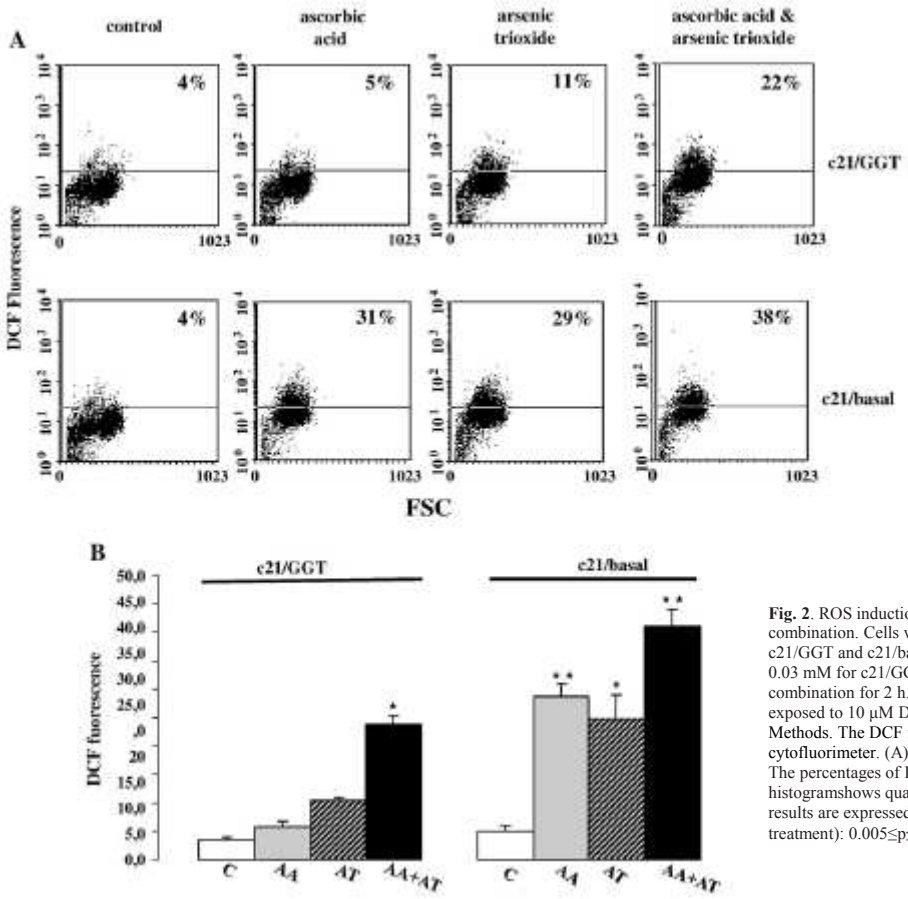

Fig. 2. ROS induction by ascorbic acid and arsenic trioxide, alone or in combination. Cells were exposed to arsenic trioxide (5 μM and 1 μM for c21/GGT and c21/basal cells, respectively) and ascorbic acid (0.06 mM and 0.03 mM for c21/GGT and c21/basal cells, respectively), alone or in combination for 2 h. After 24-h incubation in drug-free medium, cells were exposed to 10 μM DCFH-DA for 10 min as specified in Materials and Methods. The DCF fluorescence was detected by FACScan flow cytofluorimeter. (A) One representative experiment out of three is reported. The percentages of DCF-positive cells are reported in each dot plot. (B) The histogramshows quantifications of all the experiments performed and the results are expressed as mean±SD. Data were analyzed by t test (control vs. treatment): $0.005 \leq p \leq 0.001$ (*), $p \leq 0.001$ (**).

B2.2: Induction of oxidative stress and modulation of catalase activity

ROS induction analysis (Fig. 2) shows that ascorbic acid (0.06 mM, i.e. ~ IC40) enhanced the oxidative stress induced by arsenic trioxide (5 μM, i.e. ~ IC70) in cells overexpressing GGT (c21/GGTcells), where at this concentration ascorbic acid alone was ineffective in inducing oxidative stress. In c21/basal cells exposed to the combination of the two agents at equitoxic concentrations (0.03 mM ascorbic acid and 1 μM arsenic trioxide), only an additive enhancement was observed.

To investigate the response of the two clones to oxidative stress, the levels of catalase, which is a key player in antioxidant defenses, were assessed 6 h (Fig. 3A) and 24 h (Fig. 3B) after drug treatments. At both time points the basal catalase activity in c21/GGT cells was double than that of c21/basal cells. In GGT overexpressing cells, the catalase activity and ROS levels (5%, Fig. 2) were not changed by ascorbic acid treatment and only a slight reduction of enzyme activity was evident after arsenic trioxide treatment (ROS level 11%, Fig 2). Combined treatment resulted in a substantial reduction of catalase activity with an increased ROS level (22%, Fig. 2), both at 6 and 24 h after treatment. A different response was found in c21/basal cells, with an early marked increase in the

enzyme activity after single-drug treatment. The combined treatment did not produce changes in enzyme activity. The drug-induced changes of catalase activity did not closely reflect enzyme expression (Figs. 3C and 3D).

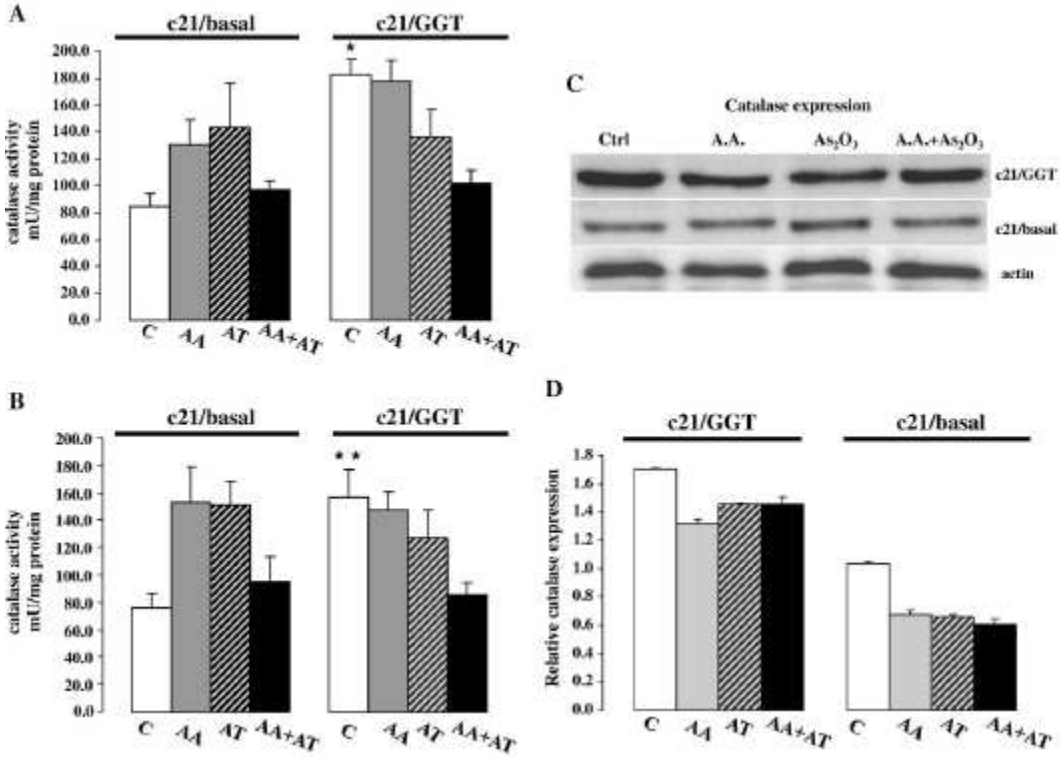

Fig. 3. Catalase activity. Catalase activity was determined spectrophotometrically 6 h (A) or 24 h (B) after-2 h exposure to arsenic trioxide and ascorbic acid, alone or in combination. The histograms show the results of three independent experiments. Enzyme activity for each sample is normalized and indicated as mU/mg of total protein content. C) control, AA) ascorbic acid (0.06 mM and 0.03 mM for c21/GGT and c21/basal cells, respectively), AT) arsenic trioxide (5 μM and 1 μM for c21/GGT and c21/basal cells, respectively), AA + AT) ascorbic acid and arsenic trioxide. The t test was used to compare control data of c21/basal vs. c21/GGT: $0.005 \leq p \leq 0.001$ (*), $p \leq 0.001$(**). (C) Western blot analysis of catalase expression performed 24 h after the 2 h treatment. (D) The histogram shows data from three independentWestern blot analyses of catalase, indicated as mean±SD, normalized to actin as loading control.

B2.3: Potentiation of arsenic trioxide-induced apoptosis by ascorbic acid in GGT overexpressing cells

In c21/GGT cells no apoptosis induction was found 72 h after a 2 h treatment with 0.06 mM ascorbic acid (Fig. 4). The extent of TUNEL positive cells was appreciably increased with the combination of ascorbic acid and arsenic trioxide, as compared to the effect of single agent treatment. In the c21/basal cells, which were more susceptible to apoptosis after single-agent treatment, the combined treatment resulted in an additive induction of apoptosis, without evidence of sensitization.

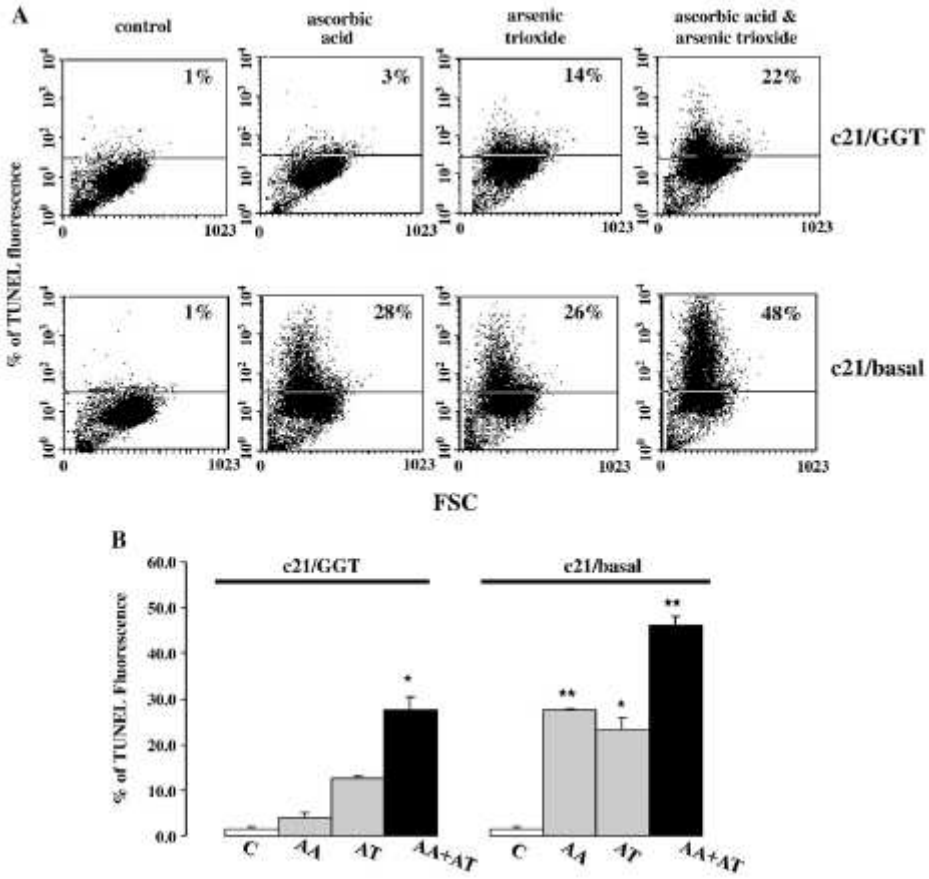

Fig. 4. Apoptosis induced by arsenic trioxide and ascorbic acid, alone or in combination. Cells were exposed for 2 h to the same concentrations of ascorbic acid and arsenic trioxide, alone or in combination, as in Fig. 3. Apoptosis was detected by TUNEL assay 72 h after the end of treatment and determined by FACS analysis. (A) The numbers in the dot plots indicate the percentage of TUNEL-positive cells. (B) Quantification of three independent assays; each result is expressed as mean±SD. Data were analyzed by t test (control vs. treatment): $0.005 \leq p \leq 0.001$ (*), $p \leq 0.001$ (**).

In order to gain insight into the cell-death mechanism, we assessed proteins and enzymes involved in the apoptotic process 24 h after drug exposure. As shown in Fig. 5, Bcl-2 level was not modified by single agent treatments in both cell systems, whereas the combination slightly downregulated the Bcl-2 protein only in c21/GGT cells.

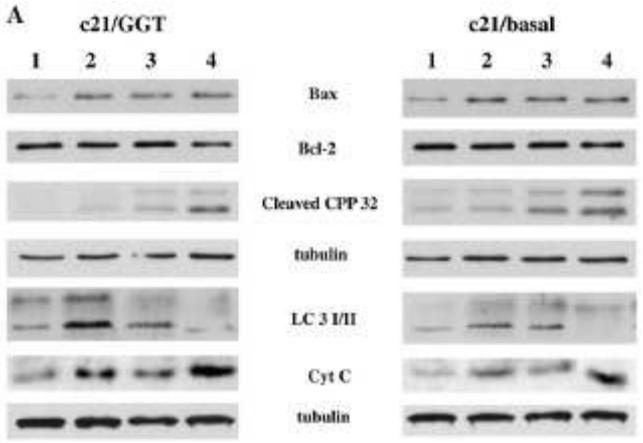

Fig. 5. Drug effect on apoptosis-related factors.Western blots were performed with total cellular extracts obtained 24 h after cell treatments using the same concentrations as in Fig. 3.
(A) Tubulin was used as a control for protein loading. Lane 1: control; lane 2: arsenic trioxide; lane 3: ascorbic acid; lane 4: ascorbic acid and arsenic trioxide. (B) Histograms show the quantification of Western blot analyses obtained with the Image Quant 5.2 software. Results (mean±SD) are reported as relative expression normalized to the tubulin used as loading control. T test were performed (control vs. treatment) and p values are indicated as follows: (*) $0.001 \leq p \leq 0.0005$, (**) $p \leq 0.0005$, (***) $p \leq 0.00001$.

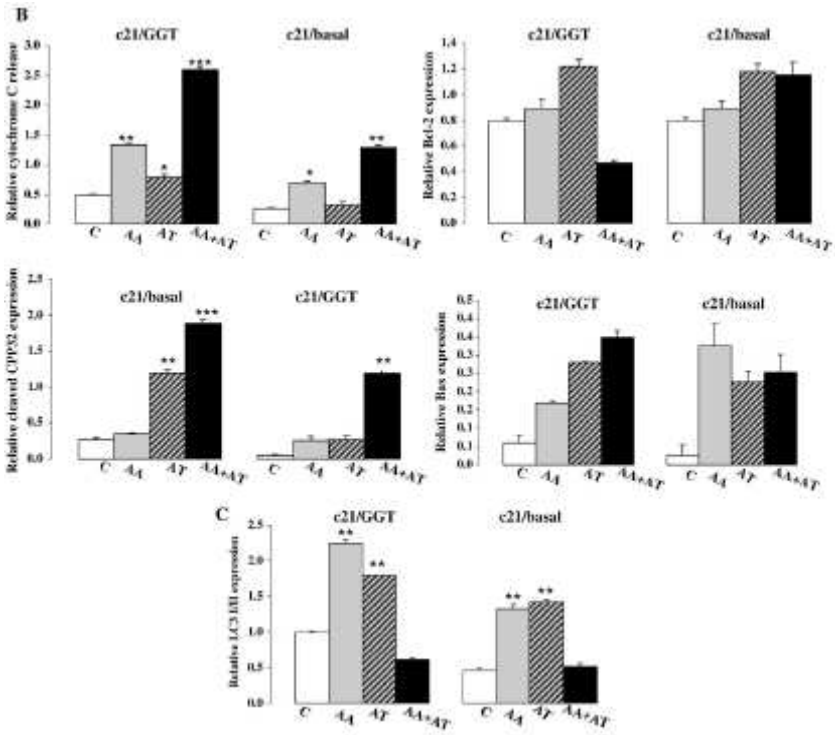

Sensitization to apoptosis by the drug combination in c21/GGT cells was also supported by CPP-32 cleavage. Indeed, whereas single-agent treatments caused only a marginal cleavage, the combination resulted in an evident effect. Sensitization was less evident in the more sensitive c21/basal cells. Cyt C release in c21/GGTcells was far more evident after the combined treatment than after the single-agent treatment. Again, the effect of the combination was less marked in the c21/basal cells.

Since macroautophagy is an accepted mechanism of cellular recovery which may confer resistance to cellular injuries, such as oxidative stress, the LC-3 I/II level was determined as a reliable marker of autophagosome formation. The active form LC-3 II was evident in both clones after single-agent treatment, but it was not detectable after combined treatment.

B2.4: Response to DNA damage

Cell cycle analysis performed 24 h after a 2-h treatment with the same equitoxic concentrations of ascorbic acid and arsenic trioxide as in previous assessments, indicated cell accumulation in S phase after each treatment, both in c21/GGT and c21/basal cells (Fig. 9). As shown in Fig. 6, BrdU incorporation analysis indicated that cells accumulated in S phase after drug treatments were not synthesizing DNA, thus supporting the activation of an efficient DNA damage checkpoint in both cell systems.

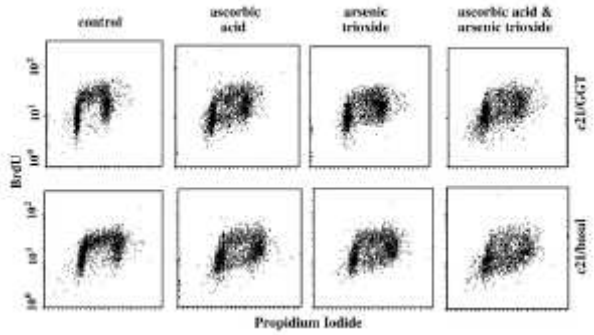

Fig. 6. Bromodeoxyuridine (BrdU) incorporation analysis in c21/GGT and c21/basal cells. Cells were exposed for 2 h to arsenic trioxide (5 μM and 1 μM for c21/GGT and c21/basal cells, respectively) and ascorbic acid (0.06 mM and 0.03 mM for c21/GGT and c21/basal cells, respectively), alone or in combination. Twenty-four h after 2 h drug treatment cells were exposed to BrdU for 1 h and then processed for analysis, as described in Material and Methods. One representative experiment of three is shown.

Western blot analysis of the proteins involved in DNA damage response documented the phosphorylation of histone γ−H2AX and p53 (Fig. 7). However, in c21/basal cells these modulations already occurred with single-agent treatment, which was in keeping with cell sensitivity. In contrast, the activation of these DNA damage markers in c21/GGT cells was evident only after combination treatment. A lack of activation of RPA-2 was consistent with the type of DNA lesions induced by the oxidative stress (i.e., single-strand breaks).

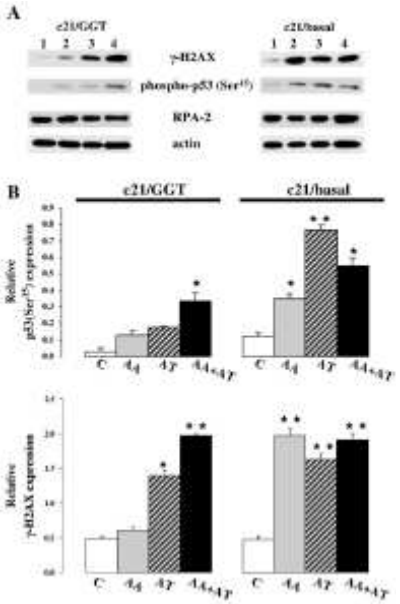

Fig. 7. Induction of DNA damage response in c21/GGT and c21/basal cells exposed to ascorbic acid and arsenic trioxide, alone or in combination. Twenty-four h after 2 h drug treatment, cells were lysed and processed for Western blotting. (A) Lane 1: control; lane 2: ascorbic acid treatment (0.06 mM for c21/GGT and 0.03 mM for c21/basal clone); lane 3: arsenic trioxide (5 μM for c21/GGT and 1 μM for c21/basal clone); lane 4: ascorbic acid and arsenic trioxide. Actin was used as loading control. (B) Histograms show the quantification of Western blot analyses using the ImageQuant 5.2 software. Data (mean±SD) are reported as relative expression normalized to the actin used as loading control. Data were analyzed by t test (control vs. treatment): $0.005 \leq p \leq 0.001$ (*), $p \leq 0.001$ (**).

B2.5: Different modulation of ASK-1 pathway in the two melanoma cell clones

Since the stress-activated protein kinase p38 is known to be involved in the regulation of catalase expression following oxidative stress [28], we examined the phosphorylation status of p38 and ASK1, which is an upstream regulator of this stress-activated pathway (Fig. 8). The c21/basal clone showed an evident phosphorylation of ASK-1 both under single-agent and combined treatment, whereas for the c21/GGT clone the activated (phosphorylated) form was increased only following combination treatment. Phosphorylation of p38 was higher in the c21/GGT clone than that in the c21/basal clone,

both in basal control conditions and after single-agent treatment whereas combined treatment resulted in a lack of p38 activation in both melanoma clones. Modulation of p21 levels appeared to parallel the pASK-1 one.

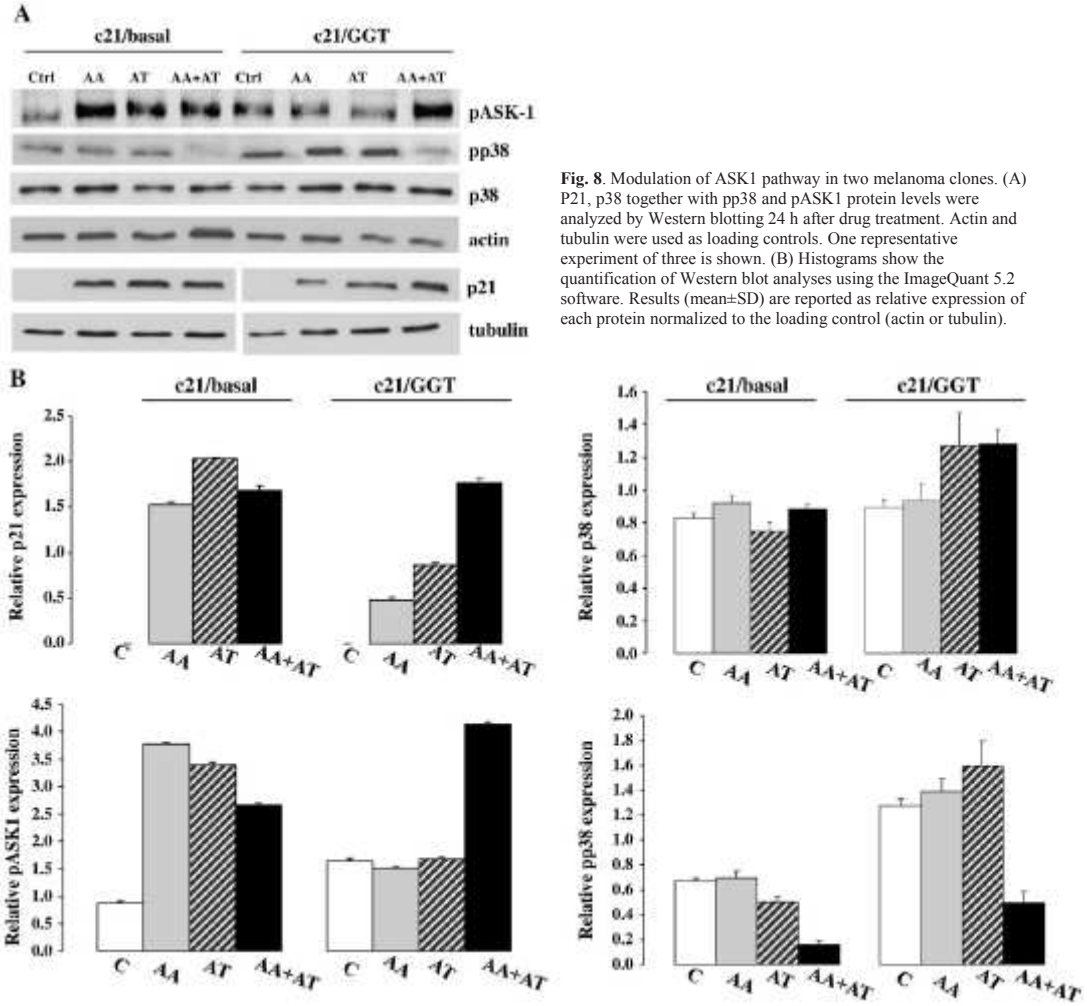

Fig. 8. Modulation of ASK1 pathway in two melanoma clones. (A) P21, p38 together with pp38 and pASK1 protein levels were analyzed by Western blotting 24 h after drug treatment. Actin and tubulin were used as loading controls. One representative experiment of three is shown. (B) Histograms show the quantification of Western blot analyses using the ImageQuant 5.2 software. Results (mean±SD) are reported as relative expression of each protein normalized to the loading control (actin or tubulin).

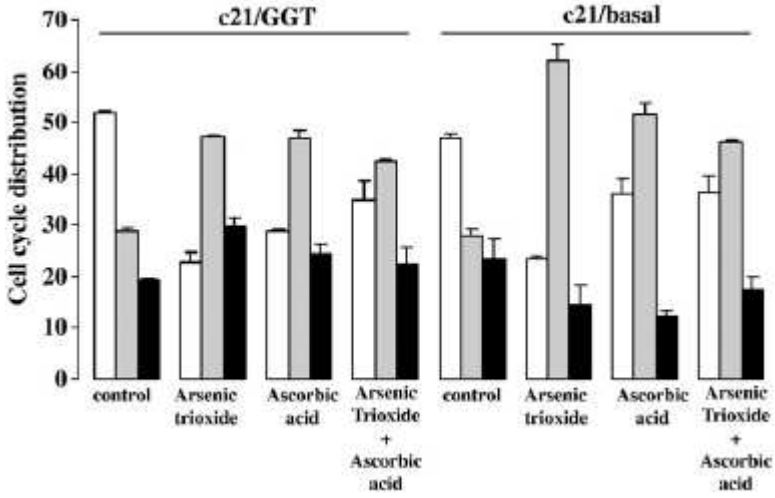

Fig. 9. Cell cycle distribution analysis. Twenty-four h after a 2 h exposure to ascorbic acid and arsenic trioxide, alone or in combination, cell cycle distribution was determined by flow cytometry and data were analyzed with the Cell Quest® software.
The histogram shows the distribution of cells in G1 (white column), S (grey column) or G2/M (black column) phase. The results are expressed as mean ± SD from three independent experiments.

Chapter B3: Membrane gamma-glutamyl transferase activity promotes iron-dependent oxidative DNA damage in melanoma cells

B3.1: Basal levels of DNA damage and oxidized bases

Two distinct human melanoma cell clones were used: the c21/basal clone, exhibiting low GGT activity (~0.3mU/mg protein), and the c21/GGT clone, presenting with high enzyme activity (~90mU/mg protein). To evaluate the potential role of GGT in inducing DNA damage, basal levels of DNA damage were analyzed in both melanoma clones by alkaline comet assay. Under normal culture conditions, c21/GGT cells showed higher levels of basal DNA damage as compared to c21/basal cells, and this difference was accompanied by higher levels of oxidized bases, as detected by Fpg treatment (Fig. 1A and B).Interestingly, when cells were treated with the GGT-specific inhibitor ABBA, the difference in basal DNA damage between the two clones was suppressed (Fig. 1C).

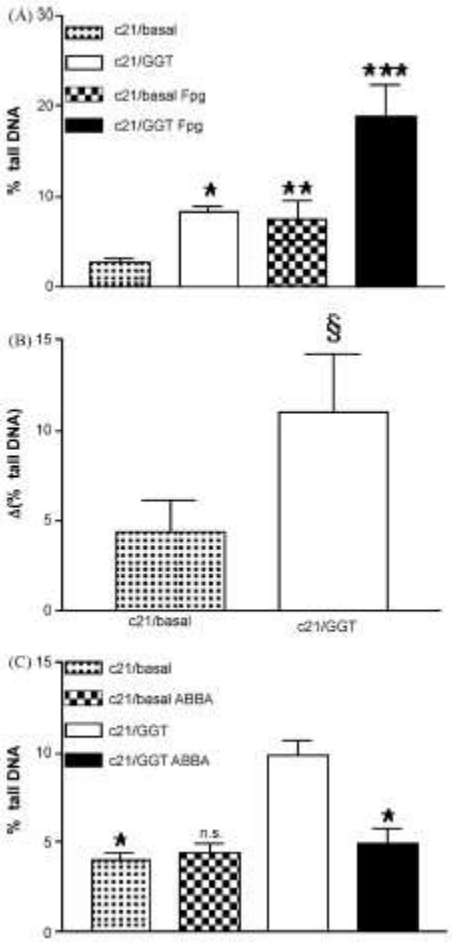

Fig.1. Basal levels of DNA damage and oxidized bases in c21/basal and c21/GGT cells. Cells were collected after 24 h from seeding and processed for the comet assay. Where indicated cells were incubated with GGT competitive inhibitor ABBA.
Data in Fig. 1B were obtained by subtracting the level of DNA damage observed for no treated samples from Fpg treated ones. Each value represents the mean±S.D. from three independent experiments. Data were analyzed by one-way ANOVA with Newman–Keuls multiple comparisons test. (A) (*) $p < 0.001$, (**) $p < 0.05$ compared with "c21/basal"; (***) $p < 0.001$ compared with "c21/GGT"; (B) (§) $p < 0.05$; *(C)* (*)$p < 0.001$ compared with "c21/GGT"; (n.s.) not statistically different from"c21/basal".

B3.2: Cell proliferation and apoptosis

The possibility that the differences observed might depend on different proliferation or apoptotic rates between the two clones was investigated. No differences in cell cycle distributions between the two clones were observed by flow cytometry, neither in basal conditions nor after a 24 h treatment with GGT-inhibitor ABBA (Fig. 2A). Moreover, when apoptosis was analyzed by TUNEL assay, in basal conditions both clones presented with very low, negligible percentages of apoptotic cells and inhibition of GGT by ABBA did not produce any effect (Fig. 2B).

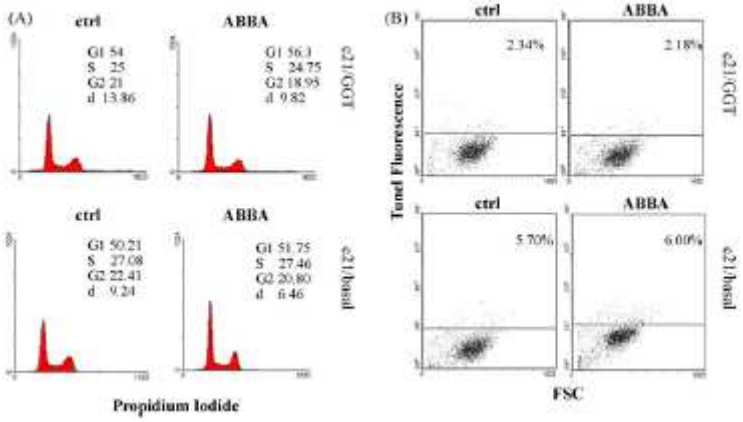

Fig. 2. Cell cycle distribution and apoptotic rate in basal and ABBA treated melanoma clones. Cells were incubated for 24 h in the presence/absence of GGT competitive inhibitor ABBA. (A) Cell cycle distribution was determined by flow cytometry. The percentages of cells in G1, S or G2 phases are reported in each histogram. (B) Apoptosis was detected by TUNEL assay. Numbers in the dot-plots indicate the percentage of tunel positive cells. One representative experiment out of three was reported.

B3.3: GGT expression and oxidative metabolism

A correlation has been reported to occur between DNA oxidative damage and cell metabolic rate [29]. Previous studies in our laboratories showed that the in vivo growth rate of tumors obtained from c21/GGT cells (after transplantation in immunodeficient mice) was higher than tumors derived from c21/basal cells [5]. Interestingly, c21/GGT cells presented with a higher glucose uptake than c21/basal (Fig. 3A)—an observation in agreement with their significantly higher proliferation rate in vitro (data not shown). Higher glucose uptake in c21/GGT cells was partially prevented by a 24 h pre-treatment with GGT-inhibitor ABBA (Fig. 3B).

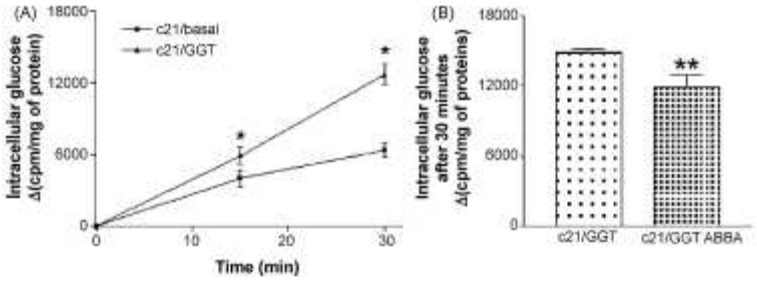

Fig. 3. Deoxy-glucose transport in melanoma clones. (A) Time course of glucose uptake in melanoma clones; (B) effect of a 24 h ABBA pre-incubation on c21/GGT glucose uptake. Data are expressed as glucose uptake in the absence of cytochalasin Bminus uptake in the presence of cytochalasin B. Each value represents the mean±S.D. from five independent experiments. Data were analyzed by two-way ANOVA (A) or Student's *t* test (B). (*) $p < 0.0001$; (**) $p < 0.001$.

B3.4: Stimulation of GGT activity and DNA damage

The possibility that the differences observed in basal DNA damage could be related to the pro-oxidant activity of GGT was investigated in more detail. As can be seen in Fig. 4A and B, when the c21/GGT clone was incubated in the presence of substrate GSH, transpeptidation acceptor glycyl-glycine ("GGT stimulation"), and ADP-chelated iron, a marked increase in DNA damage levels was observed (Fig. 4A) along with a marked acceleration of GSH consumption (Fig. 4B). In the absence of glycyl-glycine such effects were markedly lower. Conversely, when GGT activity was stimulated in c21/basal cells, no differences in GSH hydrolysis or DNA damage –despite the presence of ADP-chelated iron – were observed (Fig. 4C and D). On the other hand, when purified GGT was exogenously added to incubation mixture, GSH consumption and increased DNA damage were concomitantly observed (Fig. 4C and D).

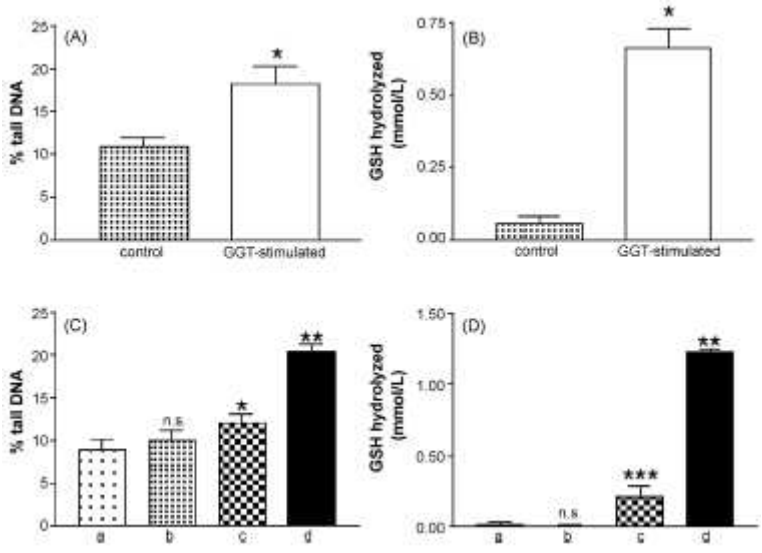

Fig. 4. Effects of GGT stimulation on DNA damage and GSH hydrolysis in melanoma clones. (A and B) c21/GGT cells were incubated in RPMI medium containing GSH, ADP-chelated $FeCl_3$ in the presence ("GGT-stimulated") or absence ("control") of transpeptidation acceptor glycyl-glycine. Each value represents the mean±S.D. from five independent experiments. Data were analyzed by Student's *t* test; (*) $p < 0.0001$. (C and D) c21/basal cells were incubated in RPMI medium containing GSH, ADP-chelated $FeCl_3$ in the presence or absence of transpeptidation acceptor glycyl-glycine and purified GGT. a) Control; b) control with glycyl-glycine added; c) control with purified GGT added; d) control with glycyl-glycine and GGT added. Each value represents the mean±S.D. from three independent experiments. Data were analyzed by one-way ANOVA with Newman–Keuls multiple comparisons test. (*) $p < 0.05$ compared with "a"; (**) $p < 0.001$ compared with "b"; (***) $p < 0.001$ compared with "a"; (n.s.) not statistically different from "a".

In agreement with what was observed in the case of basal DNA damage levels, significantly higher levels of oxidized bases (oxidized purines) were detected by Fpg treatment in GGT-stimulated c21/GGT cells (Fig. 5A and B).

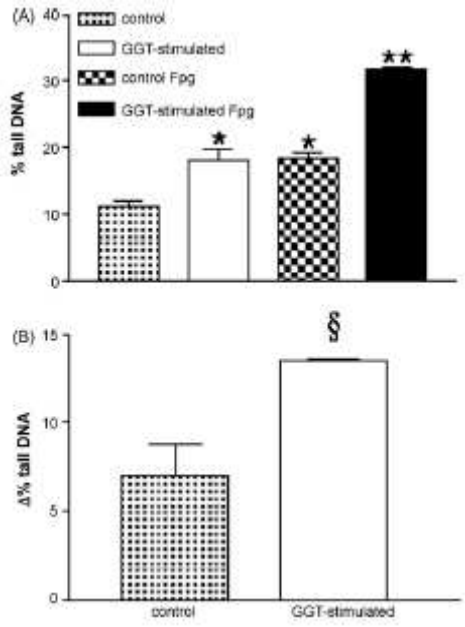

Fig. 5. Effect of GGT stimulation on bases oxidation in c21/GGT cells. c21/GGT cells were incubated in RPMI medium containing GSH, ADP-chelated $FeCl_3$ in the presence ("GGT-stimulated") or absence ("control") of transpeptidation acceptor glycyl-glycine. Data in Fig. 4B were obtained by subtracting the level of DNA damage observed for no treated samples from Fpg treated ones. Each value represents the mean±S.D. from three independent experiments. Data were analyzed by oneway ANOVA with Newman–Keuls multiple comparisons test. (*) $p < 0.001$ compared with "control"; (**) $p < 0.001$ compared with "GGT-stimulated" and "control Fpg"; (§) $p < 0.01$.

The relationships between GSH hydrolysis and DNA damage were further investigated by plotting GSH consumption data against DNA damage levels. Data were analyzed in order to isolate the effects truly depending on the sole GGT activity, i.e. by subtracting control GSH hydrolysis from GSH hydrolyzed in conditions of GGT stimulation. Fig. 6 shows the graph obtained by plotting "net" GSH hydrolysis values in c21/GGT cells vs. "net" DNA damage levels.

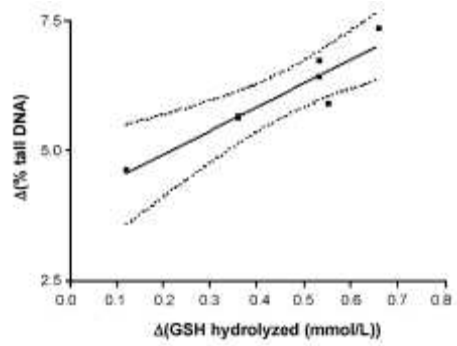

Fig. 6. Direct relationship between GSH hydrolysis and DNA damage in c21/GGT clone. Data were obtained from different experiments performed on c21/GGT clone by subtracting GSH hydrolyzed and percentage of tail DNA values in "GGTstimulated" samples from "control" ones. $R_2 = 0.867$.

As can be seen, a strong correlation between the two parameters was found (R2 = 0.867), further confirming the role of enzyme activity in iron-dependent DNA damage. Such a role was also supported by data independently obtained with two GGT inhibitors, ABBA and serine–boric acid complex (SBC). As shown in Fig. 7, both ABBA and SBC concomitantly inhibited GSH hydrolysis and DNA damage in GGT-stimulated c21/GGT cells.

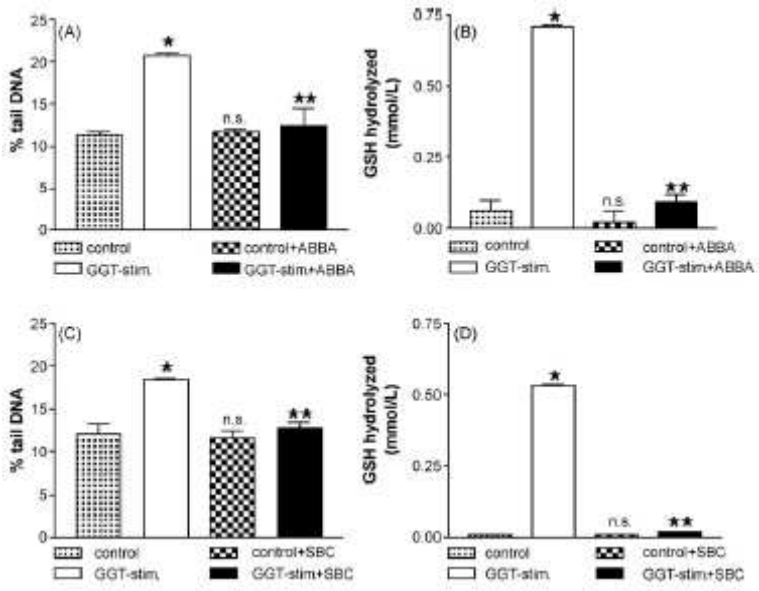

Fig. 7. Effects of GGT inhibitors ABBA (A and B) and SBC (C and D) on GGT-induced DNA damage and GSH hydrolysis in c21/GGT clone. c21/GGT cells were incubated in RPMI medium containing GSH, ADP-chelated $FeCl_3$ in the presence ("GGT-stimulated") or absence ("control") of transpeptidation acceptor glycyl-glycine. Where indicated GGT competitive inhibitors ABBA or SBC were added to incubation mixtures. Each value represents the mean±S.D. from three independent experiments. Data were analyzed by one-way ANOVA with Newman–Keuls multiple comparisons test. (*) $p < 0.001$ compared with "control"; (**) $p < 0.001$ compared with "GGT-stimulated"; (n.s.) not statistically different from "control".

B3.5: Mechanisms of GGT-mediated DNA damage

The mechanism by which GGT promotes DNA damage was further investigated in experiments performed in the presence of iron chelator DFO. As shown in Fig. 8, DFO completely prevented DNA damage, both in GGT-stimulated cells and in controls incubated in the absence of transpeptidation acceptor glycyl-glycine (Fig. 8A), confirming the participation of extracellular iron in the GGT-dependent damage. GSH consumption was unaffected by DFO, indicating that enzyme activity itself was not disturbed by DFO addition (Fig. 8B).

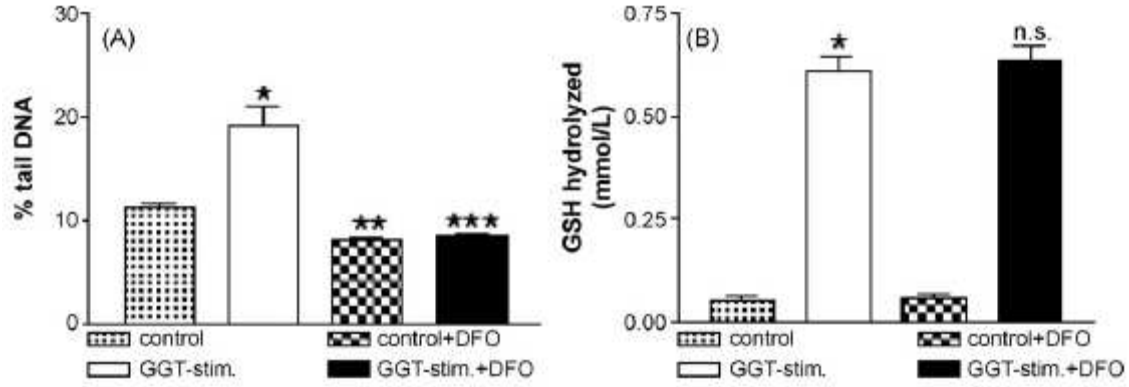

Fig. 8. Effects of iron-chelator DFO on GGT-induced DNA damage (A) and GSH hydrolysis (B) in c21/GGT clone. c21/GGT cellswere incubated in RPMImedium containing GSH, ADP-chelated $FeCl_3$ in the presence ("GGT-stimulated") or absence ("control") of transpeptidation acceptor glycyl-glycine. Where indicated the iron chelator DFO was added to incubation mixtures. Each value represents the mean±S.D. from three independent experiments. Data were analyzed by one-way ANOVA with Newman–Keuls multiple comparisons test. (*) $p < 0.001$, (**) $p < 0.01$ compared with "control"; (***) $p < 0.001$ compared with "GGT-stimulated"; (n.s.) not statistically different from "GGT-stimulated".

A marked decrease in DNA damage was also observed when cells were incubated in the presence of superoxide dismutase (SOD) and catalase (CAT), while GGT-mediated GSH hydrolysis remained unaffected (Fig. 9A and B). The same effects were observed when using the chain breaking antioxidants α-tocopherol (Fig. 9C and D), BHT or Trolox C (Fig. 9E and F).

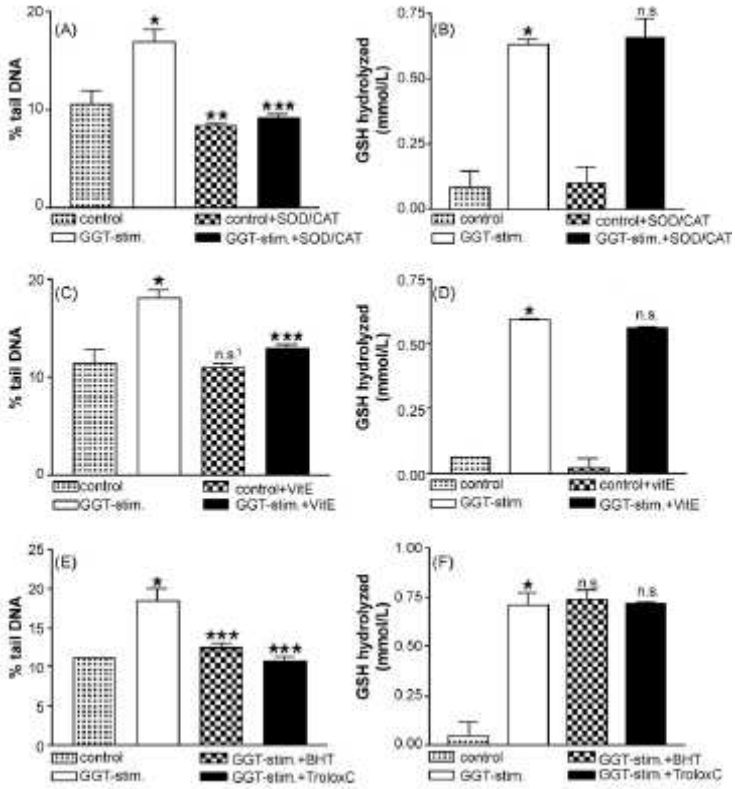

Fig. 9. Effects of antioxidants on GGT-induced DNA damage. c21/GGT cells were incubated in RPMI medium containing GSH, ADP-chelated $FeCl_3$ in the presence ("GGTstimulated") or absence ("control") of transpeptidation acceptor glycyl-glycine.Where indicated superoxide dismutase (SOD) and catalase (CAT),α-tocopherol (VitE), butylated hydroxytoluene (BHT) or Trolox C were added to incubation mixtures. Eachvalue represents the mean±S.D. fromthree independent experiments. (*) $p < 0.001$, (**) $p < 0.05$compared with "control"; (***) $p < 0.001$ compared with "GGT-stimulated"; (n.s.) not statistically different from "GGT-stimulated"; (n.s.1) not statistically different from "control".

Conclusion

Section A: Hsp90

In conclusion, the available evidence based on the biochemical, pharmacodynamic and cellular effects indicated that the class of natural compounds we tested may represent a novel series of Hsp90 inhibitors. It is evident that a major limitation of these compounds is the low potency in target inhibition, which requires micromolar concentrations to inhibit cell proliferation. Also considering the chemical features of these agents, we cannot rule out the possibility of interactions with other cellular components. If this is the case, these interactions may have a detrimental effect by limiting an effective inhibition of the primary target. However, our approaches aimed at modifying the basic structure of these agents provide evidence that specific variations may improve the Hsp90 inhibitory effect. In particular, compounds 16 and 17, containing a lipophilic chain linked to the azaphilone tricyclic ring system, brought about substantially increased binding to the enzyme, accompanied by relevant cytotoxic effects. Finally, we have documented the pharmacological interest of a representative compound of the novel series. Current efforts are directed toward optimization of the in vivo properties of selected analogues.

Curcumin has been shown to have multiple biological activities. The chemopreventive and anti-tumor effects of curcumin have been related to its ability to interfere with several signal transduction pathways which are involved in cell proliferation and/or apoptosis [30]. However, the underlying molecular mechanisms of these cellular effects are not well defined. In our study, we have provided evidence that curcumin at cytotoxic/anti-proliferative concentrations was able to directly inhibit Hsp90 function, thereby promoting the chaperone dissociation and the degradation of several Hsp90 client proteins. This finding may account for curcumin's ability to interfere with multiple signal transduction pathways, because Hsp90 plays a critical role in stabilization of several proteins implicated in the control of cell growth and malignant transformation [31, 32]. As compared with the geldanamycin derivative, 17-AAG, a well-established Hsp90 inhibitor, the potency of curcumin was substantially lower, because the inhibitory effects could be detected in the micromolar range of concentrations. This was consistent with lower antiproliferative potency and a weaker Hsp90 binding. The mechanism of curcumin-Hsp90 interaction remains to be defined. A lack of up-regulation of Hsp70 suggests a mechanism of interaction different from that of geldanamycin.

However, in preliminary limited proteolysis experiments, the proteolysis pattern observed on HSP90a indicated a protection of the N-terminal domain from the enzymatic hydrolysis.

Based on the observations that Hsp90 hyperacetylation by HDAC inhibitors disrupts its chaperone function [33-34], we have investigated the efficacy of curcumin in combination with wellknown pan-HDAC inhibitors. Our results provide evidence that the potentiation of the anti-proliferative/cytotoxic activity of both vorinostat and panobinostat by subtoxic concentrations of curcumin (~IC20) might be mediated by inhibition of Hsp90 function. Indeed, the combinations of curcumin and HDAC inhibitors, at concentrations which produced negligible effects when used alone, resulted in a marked induction of apoptosis. The cellular death could be related to a synergistic inhibition of Hsp90 activity, as under the same conditions, the combined treatment caused an almost complete depletion of several client proteins following 24 h exposure. The synergistic interaction of curcumin and HDAC inhibitor at target level was supported by co-immunoprecipitation experiment indicating an early (4 h) shift of the association of the Raf-1 from Hsp90 to Hsp70. Previous reports have shown that the shift in the chaperone association of the client proteins to the Hsp70-containing unstable multichaperone complex induces polyubiquitylation and degradation of the client proteins by the 26 S proteasome [35, 36, and 37].

The most striking finding of this study was the longlasting effect of the combination, which persisted even following removal of the drugs. As a consequence of the persistent inhibition, the enhancement of apoptosis did not required prolonged exposure. Thus, given the relatively rapid reversibility of cellular effects of HDAC inhibitors [38] and curcumin, these combinations may have therapeutic implications. Since Hsp90 acetylation may induce a modified conformation of the enzyme, a tentative explanation of the synergistic interaction between HDAC inhibitor and curcumin may be that, as a consequence of allosteric effects, changed conformation of the acetylated protein favors the curcumin–Hsp90 interaction. A synergistic interaction between HDAC inhibitors and standard inhibitors of Hsp90 (i.e. geldanamycin analogues) has already been reported in leukemia or sarcoma cells [39-40], and the sensitization has been ascribed to the modulation of Hsp90 chaperone function by its acetylation status [41].

In conclusion, our findings reveal a novel mechanism of action of curcumin, which is consistent with modulation of signaling pathways. The effects of curcumin described in this manuscript support previous observations indicating the ability of curcumin to down-regulate p210bcr/abl, a client protein

of Hsp90 [42]. Our obsvervations may be relevant to the therapeutic applications of both HDAC inhibitors and curcumin. Indeed, the therapeutic efficacy of these agents as single-agent therapy is still limited for pharmacological and pharmaco-dynamic reasons. Indeed, besides problems related to bioavailability and metabolism [43], the expected reversibility of target inhibition represents a major drawback of these target-specific agents.

Relevant to this point is the observation that the sensitization for drug-induced apoptosis could be produced by very low drug concentrations which are achievable in vivo and expected to be well tolerated. Both curcumin and HDAC inhibitors have been reported to enhance citotoxicity of various antitumor agents [44, 45-46]. The present study supports the potential interest of a novel combination which can be translated into the design of novel therapeutic approaches.

Conclusion

Section B: GGT

In the melanoma cell system used in our study, we found that overexpression of GGT was associated with a reduced sensitivity to oxidative stress caused by H2O2, as well as to cytotoxic effects of ascorbic acid. The GGT-overexpressing c21/GGT cells were markedly more resistant to H2O2 and AA treatments, approx. 50- and 2-fold more than the c21/basal clone. The ability of ascorbic acid to induce indirectly oxidant effects is a well established phenomenon, described in different cell types and different culture conditions, and likely related to AA interactions with trace levels of transition metal ions present in many incubation media. Thus, an increased resistance of c21/GGT clone to oxidative injury could explain both observations. Only moderate levels of ROS were indeed produced in c21/GGT cells following exposure to relatively high concentrations of H2O2, while paradoxically higher levels of ROS were produced in c21/basal clone exposed to substantially lower (equitoxic) H2O2 concentrations. Consistent with this finding, H2O2 treatment produced no DNA damage response in c21/GGT clone, i.e. neither histone γ–H2AX phosphorylation nor S phase checkpoint activation, wherease a typical DNA damage response was found in c21/basal clone, with S phase cell accumulation and phosphorylation of both histone γ–H2AX and p53. The increased catalase expression and activity observed in untreated c21/GGT cells (two times higher as compared to c21/basal) could account for the increased ability of this clone to tolerate oxidative stress, and likely reflects an adaptation phenomenon. In fact, GGT-mediated metabolism of extracellular GSH is known

to produce prooxidant effects, including production of H2O2.The occurrence of low but persistent oxidative stress in c21/GGT cells is consistent with a higher GSSG/GSH ratio. It is likely that the ongoing GGT-mediated production of prooxidants can induce activation of protective pathways, including catalase expression.

Anyway, a short-time exposure to cytotoxic concentrations of hydrogen peroxide or AA resulted in a significant induction of catalase activity, but not of its expression level. Thus it is conceivable that an acute oxidative stress causes an activation of the catalase already present in the cell, whereas a low persistent oxidative stress, present in the GGT-overexpressing cells as a consequence of GGT-mediated extracellular metabolism of GSH, results in modulation of protein expression.

Ascorbic acid was used in this study as a prooxidant agent to explore possible pharmacological implications of the features acquired by the GGT-overexpressing phenotype, because AA may have a therapeutic potential in melanoma. In spite of a comparable perturbation induced by AA on cell cycle with partial accumulation of cells in S-phase, the final outcome was substantially different in the two clones. In the more sensitive c21/basal clone, typical manifestations of oxidative stress were observed, including production of ROS, DNA damage response (γ–H2AX and p53 phosphorylation) and activation of cell death pathways (cytochrome C release and caspase activation). In contrast, following AA treatment the less responsive c21/GGT clone exhibited only marginal signs of genotoxic stress, with no evidence of apoptotic cell death. Such findings might be explained by the occurrence in c21/GGT clone of marginal, easily repairable DNA damage, and/or by a lack of recognition of DNA lesions. AA is known to induce prooxidant effects, and it was shown that the formation of H2O2 is a critical step in its cytotoxicity. In agreement with this interpretation, the addition of exogenous catalase provided a substantial protection in our experiments. Therefore, the increased resistance of c21/GGT cells to AA more likely reflects their increased ability to detoxify H2O2 following upregulation of cellular catalase activity.

It is well established that prooxidant rather than antioxidant effects of AA depend on its interactions with transition metal ions, in particular iron. Iron can also interact with H2O2 in the so-called Fenton reaction, leading to production of highly reactive and toxic hydroxyl radicals. Indeed, data reported indicate that free, redox-active iron is implicated in the phenomena observed. When the iron-chelating agent DFO was added to incubation mixtures, attenuation of citotoxicity of both H2O2 and AA was in fact observed, and even stronger protection was achieved using 2,2'-bipyridyl, an agent able to

permeate cells and hence to chelate both extracellular and intracellular free iron. Relevant to this point is the observation that, following exposure to an equimolar concentration (60 μM), the differential toxicity of AA between the two clones can be abolished by treating the c21/basal clone with 2, 2'-bipyridyl. The lower sensitivity of the GGT-expressing clone could thus support a lower content of intracellular free iron, required for the efficiency of redox-cycling processes, necessary to overdraw the inner oxidative burst. Indeed, free iron is known to participate in reaction resulting in free radical formation and oxidative stress leading to DNA damage and cell death. On the other hand, we have previously shown that iron-mediated oxidation of extracellular AA can favour its uptake by melanoma cells, and that this process is suppressed by iron chelation. Protection offered by DFO and bipyridyl against AA effects may also depend on this phenomenon.

In conclusion, our study provides evidence that overexpression of GGT in melanoma cells is associated with increased resistance to oxidative stress depending on the induction of protective mechanisms against reactive oxygen species. Such a resistance to oxidative stress can explain the decreased susceptibility of GGT-expressing cells to effects of ascorbic acid. The marked resistance of GGT-overexpressing cells to oxidative stress can thus have important pharmacological implications because production of oxidative stress is a relevant event in the apoptotic response to several cytotoxic agents. Figure beneath depicts our proposed mechanism of cellular stress induced by H2O2 or AA, and the possible defence mechanisms involved.

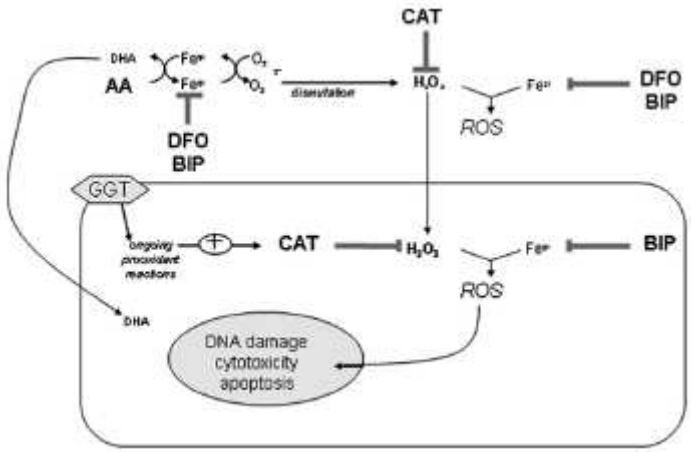

Catalase is responsible for degradation of endogeneous and exogenous H2O2. Previous studies showed an enhancement of catalase activity by repeated low-dose H2O2 exposure [47] and the increase enzyme activity was implicated as a resistance factor in response to oxidative stress-inducing agents and cisplatin [48].

Our results showed that single-agent treatment (ascorbic acid or arsenic trioxide) caused only a weak ROS induction in c21/GGT cells. Since the basal levels of catalase were unaffected by these drugs, it is conceivable that in these cells the basal catalase activity is an efficient protective system to fight oxidative stress triggered by these agents. On the other hand, since induction of enzyme activity in c21/basal cells was found after single-agent treatment, it is likely that these cells were more sensitive to drug-induced oxidative stress because little catalase activity was promptly available. This interpretation is consistent with the higher level of ROS found in c21/basal cells.

The combination of two stress-inducing agents, ascorbic acid and arsenic trioxide, resulted in a marked antiproliferative effect in c21/GGT cells, similar to that produced in the c21/basal cells. In spite of a differential effect of the single agents on the catalase activity of the two clones, the enzyme activity was similar after the combined treatment. Under these conditions, which resulted in a limitation of catalase activity, higher levels of ROS were detected. These results suggest that ascorbic acid and arsenic trioxide together inhibited catalase activity in the resistant clone and prevented enzyme induction in the basal one.

The lack of phosphorylation of p38 kinase could account for the modulation of catalase at least in the c21/GGT clone, because p38 activation has been implicated in catalase mRNA stabilization [47].

A comparison of the cellular response (apoptosis, DNA damage and cell cycle perturbation) in the two clones supports that the defense mechanisms developed by c21/GGT cells are efficient in protecting these cells against cellular injury induced by the single agents. When the same agents were used in combination the defense mechanisms of GGT-overexpressing cells were partially overcome, resulting in an increased DNA damage response and cell death. Again, the c21/basal clone which was already responsive to single-agent treatment, showed an enhanced stimulation of DNA damage response to the combination.

It has been shown that arsenic oxides can cause release of iron from ferritin, resulting in the formation of reactive oxygen species [48]. Ascorbic acid can produce the same effect and, when administered in combination, can greatly potentiate iron release and oxidative stress induced by arsenic [49]. The superoxide anion formed in the process can generate H2O2, either by spontaneous dismutation or by reaction with ascorbic acid itself [50]. H2O2 and iron together are well-known promoters of the formation of highly cytotoxic hydroxyl radicals through the Fenton reaction [51]. The stronger efficacy of the combined ascorbic acid and arsenic trioxide treatment could therefore be ascribed to a

stronger and more persistent oxidative stress, resulting from i) the synergic release of iron by arsenic trioxide and ascorbic acid from cellular stores, and ii) the promotion by ascorbic acid of iron-mediated production of superoxide anion and other cytotoxic oxygen species, leading to a burst of oxidative stress capable of impairing the cellular defense mechanisms. An additional explanation may be that the redox reactions initiated by ascorbic acid and iron may eventually help maintain arsenic in the more toxic As3+ form [52].

Mitochondria could play a crucial role in the decision of the cellular fate, such as the switch between apoptosis and recovery from oxidative injury including activation of autophagy, an event that depends on the cellular background and on the nature and strength of the stimulus. This protective process, activated in both clones, but more efficiently in GGT-overexpressing cells as indicated by LC-3 II induction, may contribute to cell survival.

Following the combined treatment, the protective mechanism was not activated, and the lack of activation is likely to favor apoptosis.

Consistent with this interpretation is the observed modulation of the ASK1/p38 pathway, which is known to be a cellular oxidative stress sensor that differentially activates intracellular pathways, resulting in apoptosis or survival depending on the cell ability to respond to oxidative stress [53]. As summarized in the figure below, ASK1, once activated, may phosphorylate a number of MAPKs, depending on the extent of cellular oxidative stress. In particular, activation of p38 is related to catalase stabilization and enhanced ability to fight ROS, resulting in cell protection; otherwise, if the oxidative stress is too strong, other MAPKs are involved, triggering apoptosis through p21 induction [53].

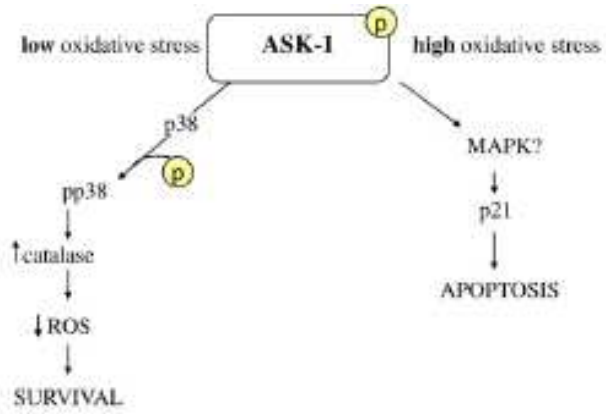

The stress-resistant clone showed a higher basal activation of p38 than the sensitive one and the phosphorylated form was already evident after single-agent treatment, suggesting that the moderate stress induced by the single agents can be tolerated at least in part. The activation of proapoptotic signals likely requires an overwhelming stress, resulting in ASK-1 activation and p21 induction. Since p38 may have a protective function in the stress response, it is conceivable that the lack of kinase activation in both clones reflects a cell decision towards cell death rather than recovery.

In conclusion, our study provides a cellular basis for overcoming the protective mechanisms implicated in the resistance of melanoma cells to oxidative stress. Indeed, although GGT-overexpressing cells were resistant to oxidative stress, cellular sensitization could be achieved by the appropriate combination of stress-inducing agents.

The prooxidant action of ascorbic acid might be exploited to enhance the activity of arsenic trioxide, a clinically available drug already proposed for the treatment of advanced metastatic melanoma [54].

Since the natural resistance of melanoma to conventional cytotoxic therapy likely reflects the cell ability to survive under oxidative stress conditions [55], our study supports the pharmacological interest of modulating the response to oxidative damage to improve antitumor efficacy. The ability of the subtoxic ascorbic acid concentrations to sensitize oxidative stress-resistant melanoma cells to arsenic trioxide may have therapeutic implications, and could be exploited to develop novel treatment approaches, based on this well-tolerated combination.

Early reports described the increase of GGT activity in cells and tissues exposed to carcinogenic treatments, a phenomenon often followed later on by increased cell proliferation and neoplastic growth. In recent years several studies have described alterations of GGT levels in a number of human tumors, and a new perspective has been forwarded proposing GGT as an “active” factor in development of a more aggressive and resistant phenotype of cancer cells [4].

Against this background, our data indicate that GGT overexpression in melanoma cells is per se associated with increased background levels of DNA damage and oxidized bases. The effect is magnified when ADP-chelated iron is exogenously added, confirming that the mechanism implicated includes metal ion redox-cycling reactions. Basing on this finding, genotoxicity could be thus included among the effects of the more pro-oxidant environment generated by GGT-overexpressing cells.

On the other hand, it has been suggested that the genome of cancer cells could be more prone to oxidative damage due to the higher rate of metabolism associated with increased cellular proliferation [56]. Several studies have documented a relationship between cell proliferative status and induction of DNA damage and repair capabilities, and differences of these parameters were observed in cells as they proceed along G1, S and G2 phases of the cell cycle [57, 58]. Moreover, some authors have proposed that apoptosis associated DNA fragmentation could also be detected by comet assay, and identified the apoptosis-type DNA fragmentation in the so-called 'hedgehog comets' [59, 60]. It has however been observed that 'hedgehog comets' are regularly produced by agents – e.g.H2O2– inducing DNA lesions that can be readily repaired, and therefore such comets probably do not represent a reliable indicator of apoptosis [5].

On the basis of the considerations above, we have investigated whether the higher DNA damage basally observed in GGT-overexpressing cells could be explained by differences in cell cycle distribution or by a higher apoptotic rate. No differences were observed between the two clones with respect to cell cycle distribution or apoptotic rate. Moreover, when the GGT-specific inhibitor ABBA was added to cell culture media, the difference in basal DNA damage was completely abolished, while no effect was produced on cell cycle distribution or apoptotic rate.

It is known that a source of endogenous ROS within the cell is represented by oxidative metabolism, and the question then arises, which can be the predominant mechanism operating in production of the observed DNA damage, i.e. whether the effect is promoted i) directly, through a GGT-mediated production of DNA-damaging reactive species, or ii) indirectly, through the upregulation by GGT activity of cellular processes involved in oxidative metabolism.

With respect to the "indirect" hypothesis, previous studies have shown that GGT expression may represent a growth advantage, insofar as GGT pro-oxidant effects can modulate the redox-sensitive transcription factors NF-kB and AP-1, involved in cell proliferation [61]. It is in fact well assessed that tumors obtained from c21/GGT cells transplanted in nude mice indeed grow faster than those derived from c21/basal cells [62]. A relationship was also documented between exposure to low grade oxidative stress and increased expression of GLUT1 glucose transporter, through the activation of AP-1 [63]. As shown by our results, a higher basal glucose transport is indeed present in c21/GGT cells as compared to c21/basal—an effect that was significantly decreased after 24 h preincubation with the specific GGT-inhibitor ABBA. GGT-rich cells appear thus to enjoy higher glucose

availability as compared to GGT-poor cells, a phenomenon likely leading to a higher metabolic rate and higher oxidative DNA damage.

On the other hand, potentially damaging reactive species are also directly produced by GGT pro-oxidant reactions ("direct hypothesis").

As mentioned above, these are able not only to modulate redox-sensitive signal transduction, but also to produce direct (metal ion-mediated) oxidative damage to biological molecules such as lipids and proteins. In agreement with previous data, our results demonstrate that conditions of stimulated GGT activity are also accompanied by increased DNA damage, and that such damage is indeed oxidative in nature. ABBA or serine–boric acid complex blocked GSH consumption and the corresponding DNA damage at the same time.

Moreover, when purified GGT was exogenously added to c21/basal cells, GSH hydrolysis and increased DNA damage were concomitantly observed. Also, a strong correlation was observed between net levels of GSH hydrolysis and DNA damage, further confirming a strict relationship existing between the two.

Metal ions redox cycling with production of reactive oxygen species is a critical step in the phenomena described. GGTdependent DNA damage was in fact completely inhibited in the presence of the extracellular iron chelator DFO, as well as in the presence of superoxide dismutase and catalase.

Previous reports described lipid peroxidation (LPO) among the prooxidant effects produced by GGT activity, both in a cellular [64] and cellular systems [65, 66, and 67]. Accordingly, increased production of malondialdehyde (MDA) was described as a consequence of GGT dependent lipid peroxidation of isolated LDL lipoproteins [68]. It is well established that LPO end-products (lipid peroxides, aldehydes, carbonyls) can damage DNA, either by reacting directly with bases, or by generating more reactive bifunctional intermediates forming exocyclic DNA adducts, DNA nicking and base substitutions [69].

Lipophilic antioxidants such as α-tocopherol or butylated hydroxytoluene were shown to exert strong protection against some types of such DNA damage [70]. Our results document a strong inhibition of GGT-dependent/iron-catalyzed DNA damage by α-tocopherol, butylated hydroxytoluene (a synthetic analogue of vitamin E) and Trolox C (a water-soluble vitamin E analogue). It is therefore conceivable that part of the observed GGT-dependent DNA damage may be mediated through the initiation of a

lipid peroxidation process, as previously observed in hepatoblastoma cells [71]; future studies will help elucidate this point.

Thus, continuous direct production of DNA damage through a GGT-dependent promotion of iron-dependent oxidative processes can represent a challenge to DNA-repair systems in GGT-expressing cancer cells, a condition likely leading to genomic instability and increased mutation risk. Modulating effects of pro-oxidants have also been reported with regards to DNA repair systems, such as, e.g. 8-oxoguanine DNA glycosylase (OGG1). An oxidative-mediated downregulation of DNA repair would indirectly exacerbate genomic instability; further studies are however needed on these aspects [72].

In conclusion, GGT-dependent DNA oxidative damage adds to previously described redox effects of this enzyme, such as direct oxidative damage to lipids and proteins, modulation of intracellular antioxidants, such as GSH [62] and catalase [27], and regulation of redox-sensitive molecular targets relevant to cell proliferation ability and cancer growth, like NF-kB and AP-1 [73, 61] and TNFR-1 [74].

The kidney represents an organ where initiation/progression of neoplastic transformation mediated through GGT-dependent redox processes may represent an important mechanism. The kidney is in fact very rich in GGT activity, expressed in tubular epithelial cells and participating in resorption of GSH from preurine, and it was repeatedly shown that treatment of animals with chelated iron results in lipid peroxidation and induction of kidney carcinomas [64, 75]. Moreover, it is known that oxidative conditions occurring during inflammation can induce the expression of GGT [76], and it has been recently shown that the pro-inflammatory cytokine TNF-alpha – implicated at several levels in cancer progression – induces GGT expression via NF-kappaB-dependent pathways [77].

It can thus be envisaged that GGT-dependent genomic instability might contribute to the pathogenesis of inflammation-related neoplasia.

References

1. Perego P, Cossa G, Zuco V, Zunino F.Modulation of cell sensitivity to antitumor agents by targeting survival pathways. Biochem Pharmacol. 2010 Nov 15;80(10):1459-65.
2. Trepel J, Mollapour M, Giaccone G, Neckers L. Targeting the dynamic HSP90 complex in cancer. Nat Rev Cancer. 2010 Aug;10(8):537-49.
3. Landriscina M, Maddalena F, Laudiero G, Esposito F. Adaptation to oxidative stress, chemoresistance, and cell survival. Antioxid Redox Signal. 2009 Nov; 11(11):2701-16.
4. Pompella A, Corti A, Paolicchi A, Giommarelli C, Zunino F. Gamma-glutamyltransferase, redox regulation and cancer drug resistance. Curr Opin Pharmacol. 2007 Aug;7(4):360-6.
5. M. Franzini, A. Corti, E. Lorenzini, A. Paolicchi, A. Pompella, M. De Cesare, P. Perego, L. Gatti, R. Leone, P. Apostoli, F. Zunino, Modulation of cell growth and cisplatin sensitivity by membrane γ-glutamyltransferase in melanoma cells, Eur. J. Cancer 42 (15) (2006) 2623–2630.
6. Zuco V, Zanchi C, Cassinelli G, Lanzi C, Supino R, Pisano C, Zanier R, Giordano V, Garattini E, Zunino F (2004) Induction of apoptosis and stress response in ovarian carcinoma cell lines treated with ST1926, an atipica retinoid. Cell Death Differ 11:280–289
7. Johnsson B, Lo¨fa°s S, Lindquist G (1991) Immobilization of proteins to a carboxymethyldextran-modified gold surface for biospecific interaction analysis in surface plasmon resonance sensors. Anal Biochem 198:268–277
8. Myszka DG (1999) Improving biosensor analysis. J Mol Recognit 12:279–284
9. Papalia GA, Leavitt S, Bynum MA, Katsamba PS, Wilton R, Qiu H, Steukers M, Wang S, Bindu L, Phogat S, Giannetti AM, Ryan TE, Pudlak VA, Matusiewicz K, Michelson KM, Nowakowski A, Pham-Baginski A, Brooks J, Tieman BC, Bruce BD, Vaughn M, Baksh M, Cho YH, Wit MD, Smets A, Vandersmissen J, Michiels L, Myszka DG (2006) Comparative analysis of 10 small molecules binding to carbonic anhydrase II by different investigators using Biacore technology. Anal Biochem 359:94–105
10. Birolo L, Dal Piaz F, Pucci P, Marino G (2002) Structural characterization of the M* partly folded intermediate of wild type and P138A aspartate aminotransferase fron Escherichia coli. J Biol Chem 277:17428–17437

11. N.E. Huseby, J.H. Strömme, Practical points regarding routine determination of gamma-glutamyl transferase (gamma-GT) in serum with a kinetic method at 37 degrees C, Scand. J. Clin. Lab. Invest. 34 (4) (1974) 357–363.
12. T.L. Duarte, G.M. Almeida, G.D. Jones, Investigation of the role of extracellular H2O2 and transition metal ions in the genotoxic action of ascorbic acid in cell culture models, Toxicol. Lett. 170 (1) (2007) 57–65.
13. A.R. Collins, M. Dusinská, C.M. Gedik, R. St˘etina, Oxidative damage to DNA: do we have a reliable biomarker? Environ. Health Perspect. 104 (Suppl. 3) (1996) 465–469.
14. M.A. Baker, G.J. Cerniglia, A. Zaman, Microtiter plate assay for the measurement of glutathione and glutathione disulfide in large numbers of biological samples, Anal. Biochem. 190 (2) (1990) 360–365.
15. Giommarelli, C.; Zuco, V.; Favini, E.; Pisano, C.; Dal Piaz, F.; De Tommasi, N.; Zunino, F. Cell. Mol. Life Sci. 2010, 67, 995.
16. Li, Y.; Zhang, T.; Jiang, Y.; Lee, H.-F.; Schwartz, S. J.; Sun, D. Mol. Pharmacol. 2009, 6, 1152.
17. Sharp SY, Prodromou C, Boxall K, Powers MV, Holmes JL, Box G, Matthews TP, Cheung KM, Kalusa A, James K, Hayes A, Hardcastle A, Dymock B, Brough PA, Barril X, Cansfield JE,Wright L, Surgenor A, Foloppe N, Hubbard RE, Aherne W, Pearl L, Jones K, McDonald E, Raynaud F, Eccles S, Drysdale M, Workman P (2007) Inhibition of the heat shock protein 90 molecular chaperone in vitro and in vivo by novel, synthetic, potent resorcinylic pyrazole/isoxazole amide analogues. Mol Cancer Ther 6:1198–1211
18. Mahalingam D, Swords R, Carew JS, Nawrocki ST, Bhalla K, Giles FJ (2009) Targeting Hsp90 for cancer therapy. Br J Cancer 100:1523–1529
19. An WG, Schulte TW, Neckers LM (2000) The heat shock protein 90 antagonist geldanamycin alters chaperone association with p210bcr–abl and v-src proteins before their degradation by the proteasome. Cell Growth Differ 11:355–360
20. Birolo L, Dal Piaz F, Pucci P, Marino G (2002) Structural characterization of the M* partly folded intermediate of wild type and P138A aspartate aminotransferase fron Escherichia coli. J Biol Chem 277:17428–17437
21. Atkinson RA, Joseph C, Dal Piaz F, Birolo L, Stier G, Pucci P, Pastore A (2000) Binding of alpha-actinin to titin: implications for Z-disk assembly. Biochemistry 39:5255–5264

22. Roe SM, Prodromou C, O'Brien R, Ladbury JE, Piper PW, Pearl LH (1999) Structural basis for inhibition of the Hsp90 molecular Curcumin and HDAC inhibitors 1003 chaperone by the antitumour antibiotics radicicol and geldanamycin. J Med Chem 42:260–266
23. Cooper MA (2003) Biosensor profiling of molecular interactions in pharmacology. Curr Opin Pharmacol 3:557–562
24. An WG, Schulte TW, Neckers LM (2000) The heat shock protein 90 antagonist geldanamycin alters chaperone association with p210bcr–abl and v-src proteins before their degradation by the proteasome. Cell Growth Differ 11:355–360
25. Nimmanapalli R, O'Bryan E, Bhalla K (2001) Geldanamycin and its analogue 17-allylamino-17-demethoxygeldanamycin lowers Bcr-Abl levels and induces apoptosis and differentiation of Bcr-Abl-positive human leukemic blasts. Cancer Res 61:1799–1804
26. Stancato LF, Silverstein AM, Owens-Grillo JK, Chow YH, Jove R, Pratt WB (1997) The Hsp90-binding antibiotic geldanamycin decreases Raf levels and epidermal growth factor signaling without disrupting formation of signalling complexes or reducing the specific enzymatic activity of Raf kinase. J Biol Chem 272:4013–4020
27. Giommarelli, C.; Corti, A.; Supino, R.; Favini, E.; Paolicchi, A.; Pompella, A.; Zunino, F. Cellular response to oxidative stress and ascorbic acid in melanoma cells overexpressing gamma-glutamyltransferase. Eur. J. Cancer 44:750–759; 2008.
28. Sen, P.; Chakraborty, P. K.; Raha, S. p38 mitogen-activated protein kinase (p38MAPK) upregulates catalase levels in response to low dose H2O2 treatment through enhancement of mRNA stability. FEBS Lett. 579:4402–4406; 2005.
29. R. Adelman, R.L. Saul, B.N. Ames, Oxidative damage to DNA: relation to species metabolic rate and life span, Proc. Natl. Acad. Sci. U.S.A. 85 (8) (1988) 2706–2708.
30. Reuter S, Eifes S, Dicato M, Aggarwal BB, Diederich M (2008) Modulation of anti-apoptotic and survival pathways by curcumin as a strategy to induce apoptosis in cancer cells. Biochem Pharmacol 76:1340–1351
31. Mosser DD, Morimoto RI (2004) Molecular chaperones and the stress of oncogenesis. Oncogene 23:2907–2918
32. Powers MV, Workman P (2007) Inhibitors of the heat shock response: biology and pharmacology. FEBS Lett 581:3758–3769

33. Bali P, Pranpat M, Bradner J, Balasis M, Fiskus E, Guo F, Rocha K, Kumaraswamy S, Boyapalle S, Atadja P, Seto E, Bhalla K (2005) Inhibition of histone deacetylase 6 acetylase and disrupts the chaperone function of heat shock protein 90: a novel basis for antileukemia activity of histone deacetylase inhibitors. J Biol Chem 280:26729–26734
34. Scroggins BT, Robzyk K, Wang D, Marcu MG, Tsutsumi S, Beebe K, Cotter RJ, Felts S, Toft D, Karnitz L, Rosen N, Neckers L (2007) An acetylation site in the middle domain of Hsp90 regulates chaperone function. Mol Cell 25:151–159
35. An WG, Schulte TW, Neckers LM (2000) The heat shock protein 90 antagonist geldanamycin alters chaperone association with p210bcr–abl and v-src proteins before their degradation by the proteasome. Cell Growth Differ 11:355–360
36. Nimmanapalli R, O'Bryan E, Bhalla K (2001) Geldanamycin and its analogue 17-allylamino-17-demethoxygeldanamycin lowers Bcr-Abl levels and induces apoptosis and differentiation of Bcr-Abl-positive human leukemic blasts. Cancer Res 61:1799–1804
37. Stancato LF, Silverstein AM, Owens-Grillo JK, Chow YH, Jove R, Pratt WB (1997) The Hsp90-binding antibiotic geldanamycin decreases Raf levels and epidermal growth factor signaling without disrupting formation of signalling complexes or reducing the specific enzymatic activity of Raf kinase. J Biol Chem 272:4013–4020
38. Pratt WB, Toft DO (2003) Regulation of signalling protein function and trafficking by the Hsp90/Hsp70-based chaperone machinery. Exp Biol Med 228:111–133
39. Rahmani M, Reese E, Dai Y, Bauer C, Kramer LB, Huang M,Jove R, Dent P, Grant S (2005) Cotreatment with suberanoylanilide hydroxamic acid and 17-allylamino 17-demethoxygeldanamycin synergistically induces apoptosis in Bcr-Abl? Cells sensitive and resistant to STI571 (Imatinib mesylate) in association with downregulation of Bcr-Abl, abrogation of signal transducer and activator of transcription 5 activity, and Bax conformational change. Mol Pharmacol 67:1166–1176
40. Nguyen A, Su L, Campbell B, Poulin NM Nielsen TO (2009) Synergism of heat shock protein 90 and histone deacetylase inhibitors in synovial sarcoma. Sarcoma 794901
41. Rao R, Fiskus W, Yang Y, Lee P, Joshi R (2008) HDAC6 inhibition enhances 17-AAG-mediated abrogation of Hsp90 chaperone function in human leukemia cells. Blood 112:1886–1893

42. Wu LX, Xu JH, Huang XW, Zhang KZ, Wen CX, Chen YZ (2006) Down-regulation of p210(bcr/abl) by curcumin involves disrupting molecular chaperone functions of Hsp90. Acta Pharmacol Sin 27:694–699
43. Anand P, Kunnumakkara AB, Newman RA, Aggarwal BB (2007) Bioavailability of curcumin: problems and promises. Mol Pharm 4:807–818
44. Kunnumakkara AB, Anand P, Aggarwal BB (2008) Curcumin inhibits proliferation, invasion, angiogenesis and metastasis of different cancers through interaction with multiple cell signaling proteins. Cancer Lett 269:199–225
45. Fulda S (2008) Modulation of TRAIL-induced apoptosis by HDAC inhibitors. Curr Cancer Drug Targets 8:132–140
46. Mai A, Altucci L (2009) Epi-drugs to fight cancer: from chemistry to cancer treatment, the road ahead. Int J Biochem Cell Biol 41:199–213
47. Sen, P.; Chakraborty, P. K.; Raha, S. p38 mitogen-activated protein kinase (p38MAPK) upregulates catalase levels in response to low dose H2O2 treatment through enhancement of mRNA stability. FEBS Lett. 579:4402–4406; 2005.
48. Bose Girigoswami, K.; Bhaumik, G.; Ghosh, R. Induced resistance in cells exposed to repeated low doses of H2O2 involves enhanced activity of antioxidant enzymes.Cell Biol. Int. 29:761–767; 2005.
49. Ahmad, S.; Kitchin, K. T.; Cullen, W. R. Arsenic species that cause release of iron from ferritin and generation of activated oxygen. Arch. Biochem. Biophys. 382:195–202; 2000.
50. Chatterjee, I. B.; Nandi, A. Ascorbic acid: a scavenger of oxyradicals. Indian J. Biochem. Biophys. 28:233–236; 1991.
51. Winterbourn, C. C. Toxicity of iron and hydrogen peroxide: the Fenton reaction. Toxicol. Lett. 82-83:969–974; 1995.
52. Kitchin, K. T.; Ahmad, S. Oxidative stress as a possible mode of action for arsenic carcinogenesis. Toxicol Lett. 137:3–13; 2003.
53. Matsuzawa, A.; Ichijo, H. Redox control of cell fate by MAP kinase: physiological roles of ASK1-MAP kinase pathway in stress signaling. Biochim. Biophys. Acta 1780:1325–1336; 2008.
54. Tarhini, A. A.; Kirkwood, J. M.; Tawbi, H.; Gooding, W. E.; Islam, M. F.; Agarwala, S. Safety and efficacy of arsenic trioxide for patients with advanced metastatic melanoma. Cancer 112:1131–1138; 2008.

55. Fruehauf, J. P.; Trapp, V. Reactive oxygen species: an Achilles' heel of melanoma?Expert Rev.Anticancer Ther. 8:1751–1757; 2008.

56. M.S. Cooke, M.D. Evans, M. Dizdaroglu, J. Lunec, Oxidative DNA damage: mechanisms, mutation, and disease, FASEB J. 17 (10) (2003) 1195–1214.

57. P.L. Olive, J.P. Banáth, Induction and rejoining of radiation-induced DNA single strand breaks: "tail moment" as a function of position in the cell cycle, Mutat. Res. 294 (3) (1993) 275–283.

58. P. Villani, P.L. Altavista, L. Castaldi, G. Leter, E. Cordelli, Analysis of DNA oxidative damage related to cell proliferation, Mutat. Res. 464 (2) (2000)229–237.

59. S. Wada, T.V. Khoa, Y. Kobayashi, T. Funayama, K. Yamamoto, M. Natsuhori, N. Ito, Detection of radiation-induced apoptosis using the comet assay, J. Vet. Med. Sci. 65 (11) (2003) 1161–1166.

60. P. Gopalakrishna, A. Khar, Comet assay to measure DNA damage in apoptotic cells, J. Biochem. Biophys. Methods 30 (1) (1995) 69–73.

61. A.R. Collins, A.A. Oscoz, G. Brunborg, I. Gaivão, L. Giovannelli, M. Kruszewski, C.C. Smith, R. Stetina, The comet assay: topical issues, Mutagenesis 23 (3) (2008) 143–151.

62. Paolicchi, S. Dominici, L. Pieri, E. Maellaro, A. Pompella, Glutathione catabolism as a signaling mechanism, Biochem. Pharmacol. 64 (2002) 1027–1035.

63. N. Kozlovsky, A. Rudich, R. Potashnik, Y. Ebina, T. Murakami, N. Bashan, Transcriptional activation of the Glut1 gene in response to oxidative stress in L6 myotubes, J. Biol. Chem. 272 (52) (1997) 33367–33372.

64. A.A. Stark, E. Zeiger, D.A. Pagano, Glutathione metabolism by gammaglutamyltranspeptidase leads to lipid peroxidation: characterization of the system and relevance to hepatocarcinogenesis, Carcinogenesis 14 (2) (1993)183–189.

65. A. Paolicchi, R. Tongiani, P. Tonarelli, M. Comporti, A. Pompella, gamma-Glutamyl transpeptidase-dependent lipid peroxidation in isolated hepatocytes and HepG2 hepatoma cells, Free Radic. Biol. Med. 22 (5) (1997) 853–860.

66. A.A. Stark, J.J. Russel, R. Langenbach, D.A. Pagano, E. Zeiger, E. Huberman, Localization of oxidative damage by a glutathione-γ-glutamyl transpeptidase system in preneoplastic lesions in sections of livers from carcinogen-treated rats, Carcinogenesis 15 (1994) 343–348.

67. A. Pompella, A. Paolicchi, S. Dominici, M. Comporti, R. Tongiani, Selective colocalization of lipid peroxidation and protein thiol loss in chemically induced hepatic preneoplastic lesions: the role of gamma-glutamyltranspeptidase activity, Histochem. Cell. Biol. 106 (3) (1996) 275–282.

68. A. Paolicchi, G. Minotti, P. Tonarelli, R. Tongiani, D. De Cesare, A. Mezzetti, S. Dominici, M. Comporti, A. Pompella, Gamma-glutamyl transpeptidase dependent iron reduction and LDL oxidation—a potential mechanism in atherosclerosis, J. Invest. Med. 47 (3) (1999) 151–160.

69. P.C. Burcham, Genotoxic lipid peroxidation products: their DNA damaging properties and role in formation of endogenous DNA adducts, Mutagenesis 13 (3) (1998) 287–305.

70. M.H. Yang, K.M. Schaich, Factors affecting DNA damage caused by lipid hydroperoxides and aldehydes, Free Radic. Biol. Med. 20 (2) (1996) 225–236.

71. A. Paolicchi, R. Tongiani, P. Tonarelli, M. Comporti, A. Pompella, gamma-Glutamyl transpeptidase-dependent lipid peroxidation in isolated hepatocytes and HepG2 hepatoma cells, Free Radic. Biol. Med. 22 (5) (1997) 853–860.

72. P. Mistry, K.E. Herbert, Modulation of hOGG1 DNA repair enzyme in human cultured cells in response to pro-oxidant and antioxidant challenge, Free Radic. Biol. Med. 35 (4) (2003) 397–405.

73. E. Maellaro, S. Dominici, B. Del Bello, M.A. Valentini, L. Pieri, P. Perego, R. Supino, F. Zunino, E. Lorenzini, A. Paolicchi, M. Comporti, A. Pompella, Membrane gamma-glutamyl transpeptidase activity of melanoma cells: effects on cellular H2O2 production, cell surface protein thiol oxidation and NF-kB activation status, J. Cell. Sci. 113 (2000) 2671–2678.

74. S. Dominici, L. Pieri, A. Paolicchi, V. De Tata, F. Zunino, A. Pompella, Endogenous oxidative stress induces distinct redox forms of tumor necrosis factor receptor-1 in melanoma cells, Ann. N. Y. Acad. Sci. 1030 (2004) 62–68.

75. S. Toyokuni, T. Mori, M. Dizdaroglu, DNA base modifications in renal chromatin of Wistar rats treated with a renal carcinogen, ferric nitrilotriacetate, Int. J.Cancer 57 (1) (1994) 123–128.

76. H. Zhang, H. Liu, D.A. Dickinson, R.M. Liu, E.M. Postlethwait, Y. Laperche, H.J.Forman, gamma-Glutamyl transpeptidase is induced by 4-hydroxynonenal via EpRE/Nrf2 signaling in rat epithelial type II cells, Free Radic. Biol.Med. 40 (2006)1281–1292.

77. S. Reuter, M. Schnekenburger, S. Cristofanon, I. Buck, M.H. Teiten, S. Daubeuf, S. Eifes, M. Dicato, B.B. Aggarwal, A. Visvikis, M. Diederich, Tumor necrosis factor alpha induces gamma-glutamyltransferase expression via nuclear factorkappaB in cooperation with Sp1, Biochem. Pharmacol. 77 (2009) 397–411.